

1991

# An evaluation of models for predicting fatigue crack initiation at notches

Hamid R. Azimi  
*Lehigh University*

Follow this and additional works at: <https://preserve.lehigh.edu/etd>



Part of the [Materials Science and Engineering Commons](#)

---

## Recommended Citation

Azimi, Hamid R., "An evaluation of models for predicting fatigue crack initiation at notches" (1991). *Theses and Dissertations*. 5489.  
<https://preserve.lehigh.edu/etd/5489>

This Thesis is brought to you for free and open access by Lehigh Preserve. It has been accepted for inclusion in Theses and Dissertations by an authorized administrator of Lehigh Preserve. For more information, please contact [preserve@lehigh.edu](mailto:preserve@lehigh.edu).

**An Evaluation Of Models For Predicting Fatigue  
Crack Initiation At Notches**

by

**Hamid R. Azimi**

**A Thesis**

**Presented to the Graduate Committee  
of Lehigh University  
in Candidacy for the Degree of Master of Science  
in  
Materials Science and Engineering**

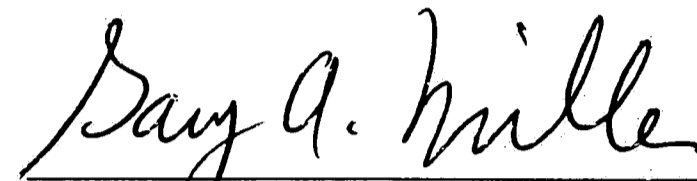
**Lehigh University**

**1991**

CERTIFICATE OF APPROVAL

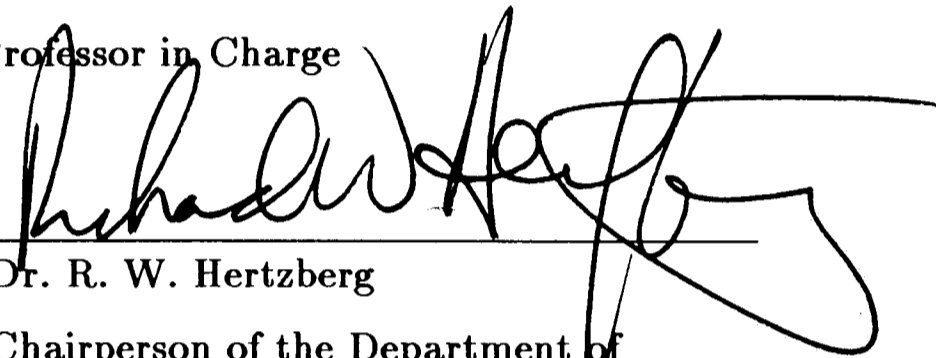
Approved and recommended for acceptance as a thesis in partial fulfilment of  
the requirements for the degree of Master of Science.

September 4, 1991



Dr. G. A. Miller

Professor in Charge



Dr. R. W. Hertzberg

Chairperson of the Department of  
Materials Science and Engineering

## *ACKNOWLEDGEMENTS*

The author would like to take this opportunity to thank some of the people who were of great help in reaching this goal. Firstly, I wish to thank my advisor Dr. Gary A. Miller for his patience, guidance, and encouragement. I have learned and accomplished much as a consequence of his efforts and guidance. Thanks also go to Dr. Clifford C. Haninen and my old friend Reza Bagheri for their many helpful discussions and suggestions. Similar thanks go to Tom Clark and Tom Pecorini for their helpful discussions and for instruction on the use of instruments. Grateful technical assistances from Gene Kozma, Jack Williams, and Arlan Bencoter are appreciated. The help of Dr. A. S. Voloshin and Mr. P. H. Tsao in performing the Moire fringe experiments are also sincerely appreciated.

Special thanks to the author's wife, Farzaneh, and child, Mohammad H., for their patience and understanding during the course of this study. My troubles were extended not only to them, but also to my youngest child who was born in the street when his dad was handing in his first thesis draft, and so my very special thanks go to him.

This work was sponsored by Iranian Ministry of Culture and Higher Education and NGK Metals Corporation and is gratefully acknowledged.

## Table of Contents

|  | <u>Page</u> |
|--|-------------|
| Title Page   | i           |
| Certificate of Approval                                    | ii          |
| Acknowledgements   | iii         |
| Table of Contents  | iv          |
| List of Figures  | vi          |
| List of Tables   | xi          |
| Abstract   | 1           |
| I. Introduction  | 2           |
| 1. 1- Fatigue Crack Initiation                             | 3           |
| 1. 2- Effect of Stress Concentrators                       | 4           |
| 1. 3- Effect of Tensile Strength and Stacking Fault Energy | 8           |
| 1. 4- Initiation Life Prediction At Notches                | 12          |
| 1. 4. 1- Fracture Mechanics Approach                       | 12          |
| 1. 4. 2- Local strain Approach                             | 17          |
| 1. 4. 3- $K_t$ -Based Approaches                           | 21          |
| II. Objective  | 23          |
| III. Experimental Procedure                                | 24          |
| 3. 1- Materials and Grain Size Measurements                | 24          |
| 3. 2- Mechanical Testing                                   | 25          |

|   |    |
|---|----|
| IV. Results and Discussion                                    | 33 |
| 4. 1- Nominal Stress  | 36 |
| 4. 2- Initiation Models                                       | 40 |
| 4. 2. 1- Fracture Mechanics Approach                          | 40 |
| 4. 2. 2- Local Strain Approach                                | 46 |
| 4. 2. 3- $K_t$ -Based Approaches                              | 53 |
| a) Maximum Elastic Stress ( $K_t \Delta S$ )                  | 53 |
| b) $K_{td}$ -Based Approach                                   | 56 |
| 4. 3- Initiation and Propagation Contribution to Fatigue Life | 69 |
| V. Conclusion   | 71 |
| References  | 72 |
| Appendix  | 79 |
| Vita  | 88 |

## List of Figures

| <u>Figure</u> |   | <u>Page</u> |
|---------------|---|-------------|
| Figure 1.1    | Schematic showing true and theoretical stress concentration.  | 5           |
| Figure 1.2    | Fatigue stress concentration factor as a function of life <sup>18,20</sup> .  | 6           |
| Figure 1.3    | Schematic showing the simulation of strain-controlled test specimen at notch root of a structure under stress control condition.  | 9           |
| Figure 1.4    | Fatigue strength as a function of hardness level. <sup>27</sup>   | 11          |
| Figure 1.5    | Elastic stress distribution near the tip of an elliptical notch for a structure under mode I deformation. <sup>41</sup>   | 13          |
| Figure 1.6    | Notched specimen geometries: (a) Center hole, (b) Compact, (c) Blunt double edge notch (DEN), and (d) Sharp double-edge notch. In each, $W=25.4$ mm; $t$ =thickness. <sup>2</sup> | 15          |
| Figure 1.7    | Fracture mechanics approach used to correlate fatigue crack initiation life for various notched specimens. <sup>2</sup>   | 16          |

|            |   |    |
|------------|---|----|
| Figure 1.8 | Estimation of fatigue crack initiation life based on Neuber's analysis and stress and/or strain-life curves.  | 19 |
| Figure 3.1 | Crack plane orientation code for rectangular sections. <sup>59</sup>  | 30 |
| Figure 3.2 | Crack plane orientation code for bar and hollow cylinder. <sup>59</sup>   | 31 |
| Figure 3.3 | Geometry and dimensions of compact tension specimens used in the present study.   | 32 |
| Figure 4.1 | Nominal stress normalized by ultimate tensile strength versus crack initiation life for Cu-Be and aluminum alloys. This Figure shows the effect of material strength on notch sensitivity and the effect of notch on initiation life. | 37 |
| Figure 4.2 | Nominal stress versus crack initiation life for brass with two different notches.   | 38 |
| Figure 4.3 | Nominal stress versus crack initiation life for copper with two different notches.  | 39 |
| Figure 4.4 | Fatigue crack initiation data for Al2024-T3 are correlated using fracture mechanics approach.   | 41 |
| Figure 4.5 | Correlating blunt and sharp notches data for Cu-Be alloy using fracture mechanics approach.   | 42 |



|             |  |    |
|-------------|--|----|
| Figure 4.6  | Correlating blunt and sharp notches data for brass using fracture mechanics approach.  | 43 |
| Figure 4.7  | Using fracture mechanics approach to correlate fatigue crack initiation life for blunt and sharp notched specimens of copper.                  | 44 |
| Figure 4.8  | Fracture mechanics approach used to correlate fatigue crack initiation data for different materials with two different notch radii.            | 45 |
| Figure 4.9  | Using local strain approach to compare fatigue crack initiation life for blunt keyhole- and sharp v-notch specimens of aluminum alloy 2024-T3. | 47 |
| Figure 4.10 | Using local strain approach to compare fatigue crack initiation life for blunt keyhole- and sharp v-notch specimens of Cu-Be alloy 25.         | 48 |
| Figure 4.11 | Using local strain approach to compare fatigue crack initiation life for blunt keyhole- and sharp v-notch specimens of brass.                  | 49 |
| Figure 4.12 | Using local strain approach to compare fatigue crack initiation life for blunt keyhole- and sharp v-notch specimens of copper.                 | 50 |

|                   |   |    |
|-------------------|---|----|
| Figure 4.13       | Using local strain approach to compare fatigue crack initiation life for blunt keyhole- and sharp v-notch specimens of materials used in the present study.   | 52 |
| Figure 4.14       | Elastic stress concentration factor versus notch sharpness calculated by finite element method for compact tension (CT) specimens. Notch sharpness, $R_n$ is defined as $r/(W-a)$ where $r$ , $W$ , and $a$ are notch radius, width, and crack length of CT specimens <sup>42</sup> . | 54 |
| Figure 4.15       | Elastic notch stress employed to correlate fatigue initiation life from blunt keyhole- and sharp v-notch specimens of materials used in the present study.  | 55 |
| Figure 4.16       | Residual compressive stress at the crack ( or notch ) tip. <sup>62,63</sup>   | 59 |
| Figures 4.17-4.20 | Using parameter $\Delta\epsilon = K_{td}\Delta S/2E$ determined for distances $d=50, 100, 150,$ and $200$ micron to correlate fatigue initiation life for blunt keyhole- and sharp v-notch specimens of 2024-T3 aluminum alloy.   | 60 |
| Figure 4.21       | Optimum distance from the notch root “ $d_{opt}$ ” versus yield strength for materials used in this study along with Ti-6Al-4V alloy with yield strength of 1007 MPa.   | 62 |

- Figure 4.22 Using parameter  $\Delta\epsilon=K_{td}\Delta S/2E$  to correlate fatigue initiation life from blunt keyhole- and sharp v-notch specimens of a Ti-6Al-4V alloy. Initiation life data obtained from Ref. 9. The quantity  $K_{td}$  was calculated for  $d_{opt}=20\ \mu\text{m}$  and for  $d=200\ \mu\text{m}$ . 63
- Figure 4.23 Parameter  $\Delta\epsilon=K_{td}\Delta S/2E$  used to correlate fatigue initiation life from blunt keyhole- and sharp v-notch specimens of materials investigated. The quantity  $K_{td}$  was calculated for  $d=d_{opt}$  as defined in Table 4.2. 64
- Figure 4.24 The parameter  $\Delta\epsilon=K_{td}\Delta S/2E$  normalized by the ratio  $YS/UTS$  to correlate fatigue initiation life for materials investigated.  $YS$  and  $UTS$  are yield and ultimate tensile strength of the materials, respectively. The quantity  $K_{td}$  calculated for  $d=d_{opt}$  as defined in Table 4.2. 65
- Figure 4.25 Strain amplitude determined from  $K_{td}\Delta S/2E$  used to correlate fatigue initiation life for the materials employed in the present study and for materials from References no. 1, 9, 11.  $K_{td}$  was calculated for  $d=d_{opt}$ . 68
- Figure 4.26 Plots of proposed initiation-propagation models along with data from present study. 70

## List of Tables

| <u>Table</u> |  | <u>Page</u> |
|--------------|--|-------------|
| Table 1.1    | Stress Concentration Factors for the Notches Shown<br>Figure 1.6. <sup>2</sup> | 14          |
| Table 3.1    | Chemical Composition of the Materials Investigated.                            | 27          |
| Table 3.2    | Grain Size of the Materials Tested.  | 28          |
| Table 3.3    | Average Tensile Properties of the Materials Investigated.                      | 29          |
| Table 4.1    | Fatigue Data for the Materials Investigated.                                   | 34          |
| Table 4.2    | Optimum Distance( $d_{opt}$ ) from the Notch Root.                             | 58          |
| Table 4.3    | Stacking Fault Energy “ $\gamma_{SF}$ ” for the Materials Investigated.        | 66          |

## ABSTRACT

Elastic stress concentration, fracture mechanics and local strain based approaches were evaluated in predicting fatigue crack initiation life at notches for materials 2024-T3 aluminum alloy, commercially pure copper, 70-30 brass, and Cu-Be alloy 25. Blunt keyhole and sharp V-notched compact tension specimens were subjected to cyclic loading in ambient laboratory air, at a stress ratio of  $R=0.1$ , and at frequency  $f=25$  Hz. Crack initiation was defined as the cycles to form a 1 mm long crack extending from the notch root. Maximum loads were selected to produce initiation in the range  $10^4$  to  $10^6$  cycles. The Moire' fringe technique was used to measure strains near the notch. Also, crack propagation tests were performed to evaluate initiation-propagation models and the fraction of life spent in initiation and propagation.

The results suggest that the best initiation model is based on computed estimates of strain at some distance ahead the notch root. This distance was shown to be inversely related to the materials' strength. This model properly described both the influence of material and geometry over the full range of initiation cycles. The models based on elastic notch stress and stress intensity factor did not lead to physically acceptable results, i.e., they predicted that initiation life for blunt notch specimens was shorter than that for sharp notch specimens. The strain-cycle fatigue model called local strain approach appeared to be somewhat better than approaches based on elastic stress or stress intensity factor but could not combine data for sharp and blunt notches for materials other than aluminum. In this case, estimating the fatigue notch factor,  $K_f$ , seemed to be the principal difficulty.

In the range  $10^4$ - $10^6$  cycles, about 30% of the total life is spent in initiating the crack for sharp notch specimens whereas for blunt notch specimens, initiation life covers about 75% of the total life of the specimen.

## I. INTRODUCTION

Materials failures are of particular importance in almost all aspects of human life. Of all types of mechanical failures, it is often stated that fatigue accounts for the majority of them and more importantly, fatigue failures almost always occur without any obvious warning. In order to prevent these insidious and catastrophic failures, and with the object of reducing both cost and time in designing a component, fatigue life prediction is an important process. It involves determining, for given service loadings, whether a crack will initiate, and then grow to such a size that catastrophic failure will occur.

The question of whether the initiation and propagation stages should be used independently in life prediction, or whether the results should be combined depends on the service conditions, component geometry, material fabrication processes, and the material itself. For instance, there are cases in which fabrication process produces crack-like flaws, or cases where a design engineer has to assume that crack already exists in the component. In such cases, life prediction logically uses only the crack propagation approach. On the other hand, there are many components that are produced by carefully controlled fabrication processes and are made of high quality materials or there are cases in which as soon as the crack initiates, the component is no longer allowed to be in service. In such cases, a component may spend most of its life in initiating cracks and in these cases, life prediction involves only the crack initiation stage. The relative importance of the two initiation and propagation phases may also depend upon loading conditions. Large proportions of the total cycles to failure are involved with propagation phase when stresses are high— low-cycle fatigue— whereas in long-life fatigue, where imposed stresses are low, initiation life is dominant.

Crack initiation, however, has proven to be the most complex, and the most difficult to characterize quantitatively. Some of the complexities include simply defining what constitutes a crack, measuring strain near the notch root, finding the

most appropriate initiation criteria, etc. Complexities notwithstanding, during the last three decades numerous initiation models have emerged. Previous work on several steels<sup>1</sup>, showed that models based on nominal stress<sup>1,3</sup>, or strain-cycle fatigue<sup>2,4-7</sup> were similar in their ability to predict crack initiation. Other evidence suggests that models based on the stress intensity factor may<sup>8,9</sup> or may not<sup>2</sup> provide better quantitative predictions. Finally, other work suggests that the strain at the notch root is the dominant parameter controlling crack initiation<sup>2,10,11</sup>.

A common feature of all models is the lack of influence of microstructural or metallurgical properties, excluding perhaps strength<sup>1</sup>, on crack initiation. Therefore, a better understanding of the complex fatigue crack initiation behavior from notches and in materials with a wide range in important metallurgical factors, particularly strength and stacking fault energy, is required for more precise prediction of fatigue life in designing a component.

#### •1.1- Fatigue Crack Initiation

For the first time in 1933, Gough<sup>12</sup> showed that the slip process is responsible for metal fatigue damage as it is in static deformation. The slip process in a material under cyclic deformation produces heavily distorted regions called slip bands. Among these slip bands, there are generally several which are more distorted and deepened than the rest. These are called persistent slip bands and are almost always the origins of fatigue cracks. Wood<sup>13</sup> showed that these persistent slip bands form at early stage of component fatigue life. For a design engineer, however, the question is when a deepened slip band should be called a crack. Should it be in the scale of micro-structural unit such as grain size as proposed by Wood<sup>13</sup>, or in the scale of Manson's criterion<sup>14</sup> -0.076 mm- or of the size suggested by Dowling<sup>15</sup>? Obviously, whatever size is selected, it should be within the range of the resolution of inspection equipment. Another problem is that initiation life,  $N_i$ , defined as the number of cycles to produce a crack of some size, depends on the component geometry.

In an attempt to eliminate the dependence of initiation life on specimen geometry, Dowling<sup>15</sup> has suggested that the crack length at initiation be less than or equal to the crack length at the transition,  $l_T$ , between short-crack- and long-crack-

controlled behavior. For a compact tension sample with sharp notch, he has shown<sup>15</sup> that  $l_T$  is on the order of  $r/5$ , where  $r$  is notch root radius. However, as mentioned previously, sometimes such a size might not be easily seen within the range of the resolution of practical equipment. In such cases, a larger crack length might be specified.

#### •1.2-Effect of Stress Concentrators

The presence of geometrical discontinuities such as keyholes, fillets, welds, etc. , is often unavoidable in engineering structures and machine parts. These discontinuities act as stress raisers and seriously reduce fatigue strength of the component. The theoretical maximum stress at the root of a discontinuity - notch can be calculated by elasticity theory. It can also be obtained through using handbook charts<sup>16</sup> showing the elastic stress concentration factor,  $K_t$ , for a wide range of components with different geometry.  $K_t$  is defined as the ratio of maximum elastic stress at the notch root to nominal stress. However, the actual stress at the notch root may be lowered due to local yielding as shown in Figure 1.1. This is the reason that the actual fatigue strength reduction of a notched component is less than that predicted on the basis of elastic stress concentration factor. In order to explain this discrepancy, the fatigue-notch factor or fatigue strength reduction factor,  $K_f$ , has been introduced and, at a given cycle defined as follows:

$$K_f = \frac{\text{fatigue strength of unnotched component}}{\text{fatigue strength of notched component}}$$

Since the fatigue strength of the notched component depends on the yield strength or on the extent of plastic deformation at the notch root,  $K_f$  is also expected to be dependent on material yield strength as well. Moreover, the results of several experimental investigations<sup>17,18,19</sup> show that  $K_f$  also depends on notch severity, stress state, and life. Figure 1.2<sup>18,20</sup> shows how  $K_f$  varies with cycles to failure.



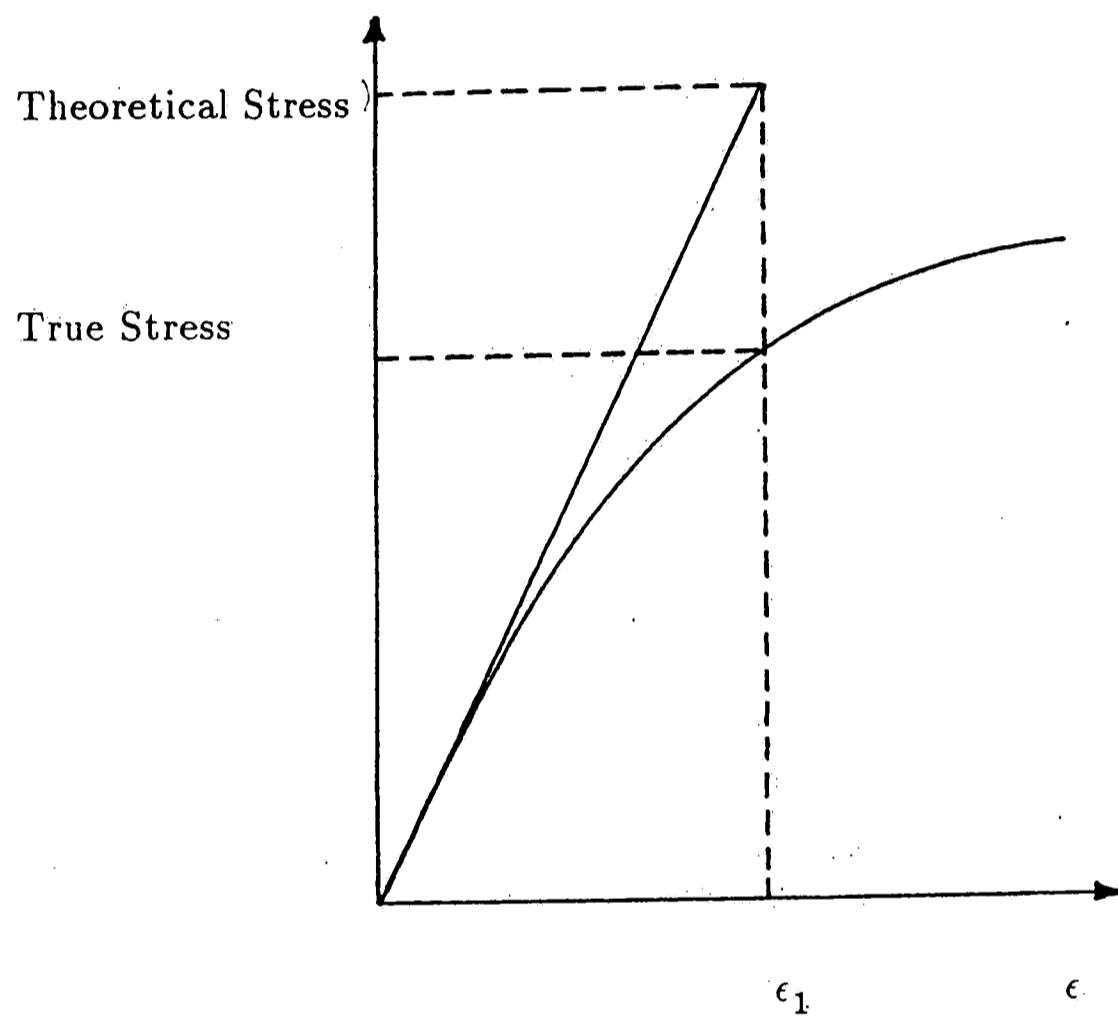


Figure 1.1- Schematic showing true and theoretical stress concentration.

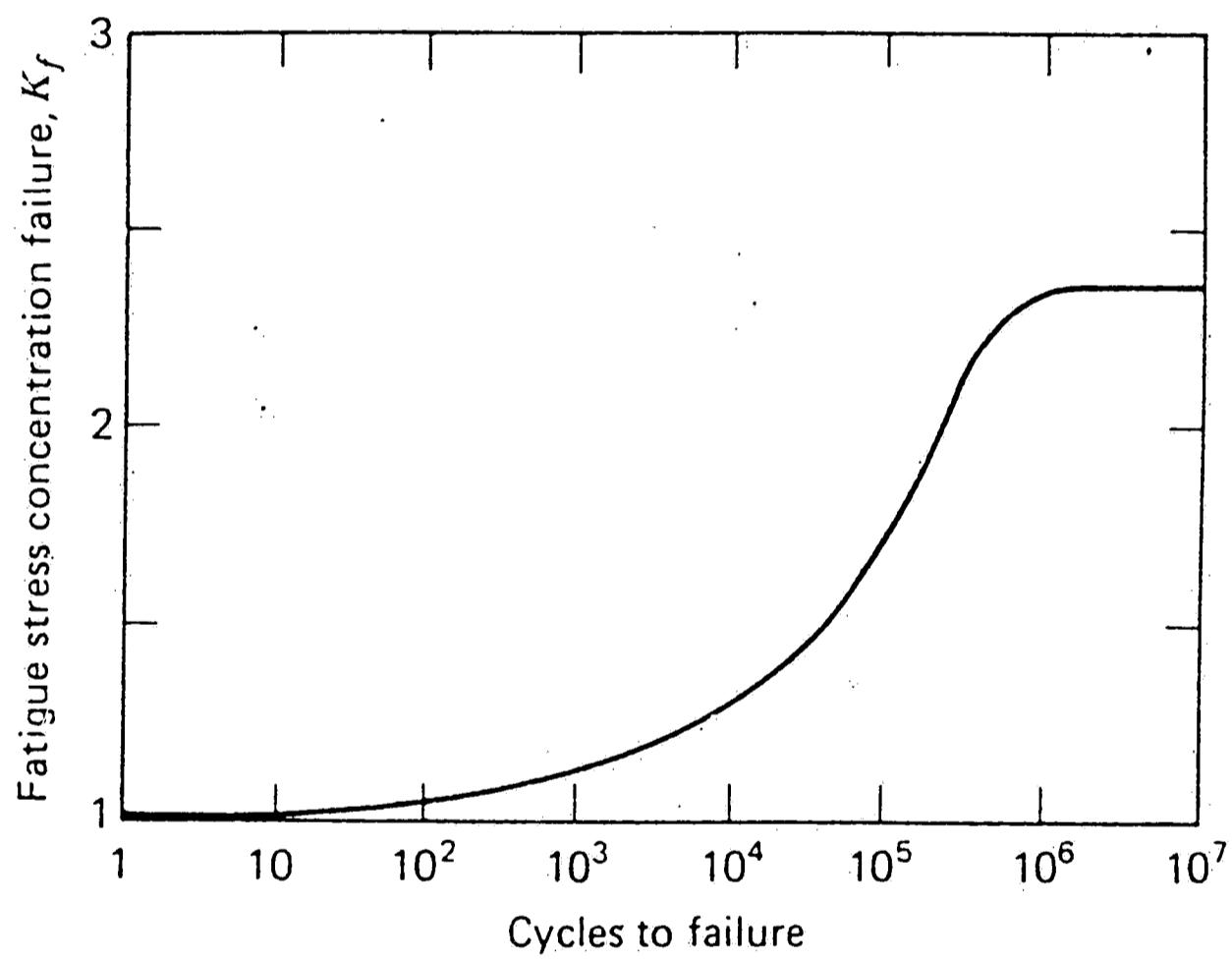


Figure 1.2- *Fatigue stress concentration factor as a function of life*<sup>18,20</sup>.

In order to be able to predict fatigue strength of a notched component from that of smooth specimens, many attempts have been made to correlate  $K_f$  with the elastic stress concentration factor,  $K_t$ . The following equation expresses this relationship based on Neuber's work.<sup>17,18,21</sup>

$$K_f = 1 + \frac{K_t - 1}{1 + \sqrt{\rho'/r}} \quad (1.1)$$

Where  $r$  is notch root radius and  $\rho'$  is related to the grain size of the material.  $K_f$  may also be determined by using plots of notch sensitivity<sup>18</sup>,  $q$ , versus notch root radius. The notch sensitivity factor is defined as

$$q = \frac{K_f - 1}{K_t - 1} \quad (1.2)$$

and may vary between 0 and 1 respectively for  $K_f = 1$  and  $K_f = K_t$ . When  $K_f = 1$ , the notch has no effect on the fatigue strength of the component and it has its maximum effect when  $K_f = K_t$ . It should be noted, however, that  $q$  is not a material property and depends on the same factors as  $K_f$  does.

One other equation has been given by Peterson<sup>22</sup> correlating  $K_f$  to  $K_t$  as follows:

$$K_f = 1 + \frac{K_t - 1}{1 + a/\rho} \quad (1.3)$$

Where  $\rho$  is notch root and  $a$  is empirically defined as  $a = 0.0254(2079/Su)^{1.8}$  where  $a$  and  $Su$ , ultimate tensile strength, are in mm and MPa, respectively. Peterson's equation seems to be a modified combination of Neuber's and notch sensitivity concept. Elsever<sup>17</sup>, it has been shown that  $K_f$  and  $K_t$  can be correlated with yield strength instead of ultimate tensile strength.

Some other general trends in  $K_t$  and  $K_f$  are as follow:

—As  $K_t$  increases,  $K_f/K_t$  ratio decreases. This means that for blunt notches,  $K_f$  is close to  $K_t$ . Moreover, there seems to be a critical notch root radius below which  $K_f$  does not increase.<sup>8,17,23-25</sup> This is the basis for the concept of the effective notch root radius.

—Different  $K_f$  values may be obtained for different geometries having the same  $K_t$ .<sup>17</sup> This arises from the fatigue size effect. Therefore,  $K_f$  accounts not only for plasticity but also for size effects.

— $K_f$  increases as grain size decreases.<sup>17,26</sup> This is consistent with the effect of yield strength on  $K_f$ .

—For similar geometries and at a given load, the higher the yield strength, the closer is  $K_f$  to  $K_t$ .

Notches can also introduce a state of triaxiality and develop residual stresses. When nominal stresses are within the elastic range, the local yielding can complicate the material behavior at the notch root by developing residual stresses. In such cases, the small specimen superimposed on the notch root, shown in Figure 1.3, undergoes cyclically strain-controlled conditions, whereas the rest of the material is under stress control. This concept which is an application of Neuber's rule has been used to determine fatigue initiation life at notches as will be explained later. Moreover, in low-cycle fatigue where the nominal stresses are high, the local stress can be fully reversed even though nominal stresses are tensile.

### •1.3 — Effect of Tensile Strength and Stacking Fault Energy

Besides mechanical factors such as stress raisers, and residual stresses, there are certain metallurgical factors which can affect the fatigue strength of any component. Among them, the tensile strength is frequently used to approximate fatigue properties of materials. For example, the fatigue limit of wrought alloy steels is usually stated to be approximately half of their tensile strength. On one hand, such general correlations may be expected since slip is more difficult in higher strength alloys. On the other hand, increasing the strength increases sensitivity to all kinds of stress raisers including inclusions, second phase particles, surface roughness, etc. and also it increases sensitivity to environmental attack and decreases fracture toughness of the material.

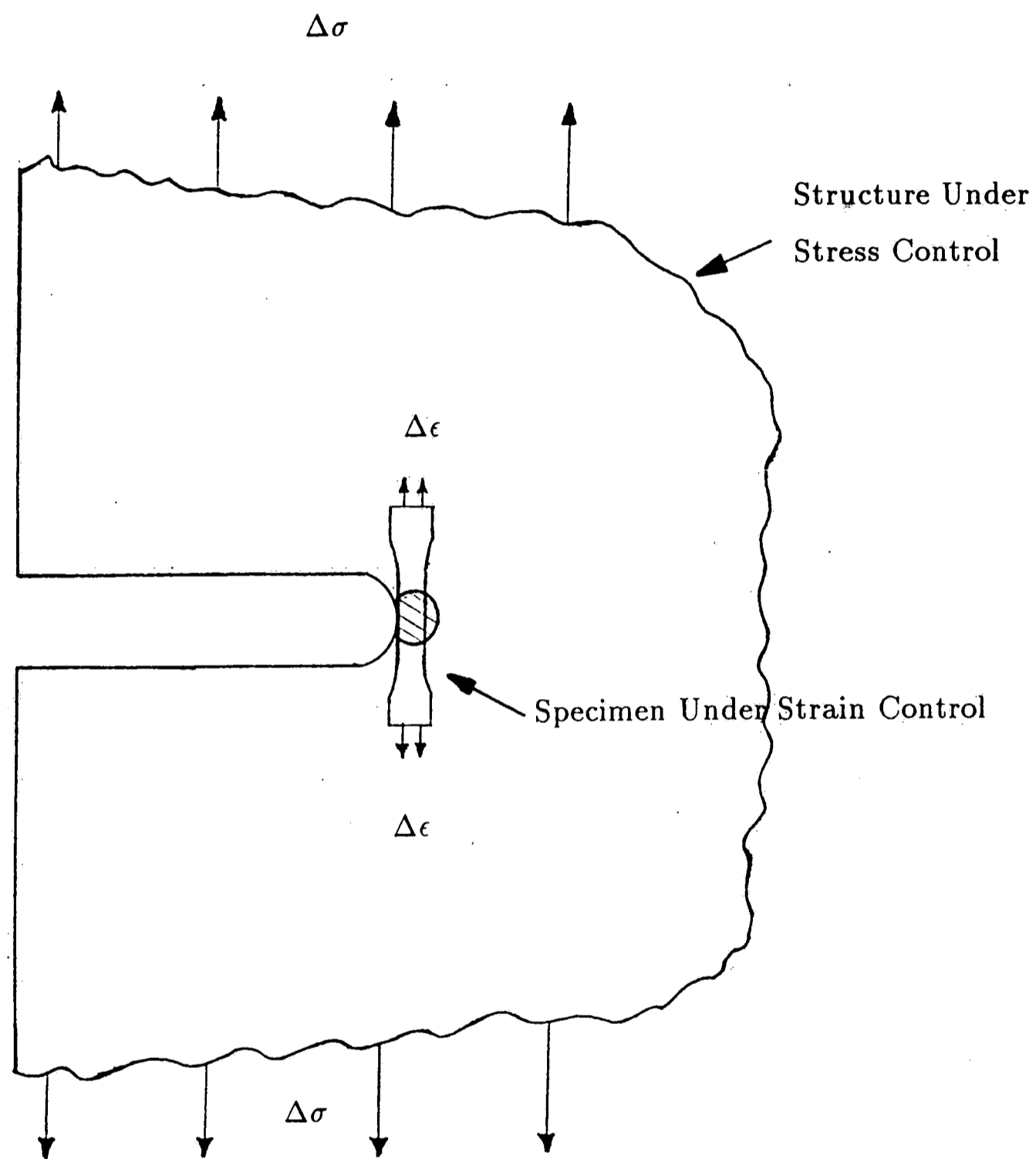


Figure 1.3- Schematic showing the simulation of strain-controlled test specimen at notch root of a structure under stress control condition.

Figure 1.4<sup>27</sup> shows the fatigue limits, as a function of hardness (or strength) for smooth specimens of different alloy steels under completely reversed stress tests at room temperature. As seen, the constant factor used to correlate fatigue limit to strength does not hold beyond a hardness of approximately 40 RC. Therefore, while approximate relations may be used for convenience, it should be noted that their use must be restricted to only certain circumstances such as smooth and highly polished specimens, up to a certain hardness range.

Fatigue strength can also be affected by the stacking fault energy which controls the ease of cross-slip as well as the mode of deformation.<sup>28-30</sup> In materials with high stacking fault energy, dislocations can cross slip easily around obstacles. As a result slip bands and plastically deformed zones can form which promote both crack initiation and propagation stages. Deformation mode in these materials is called wavy since the slip band appears to be wavy. Thompson and Backofen<sup>30</sup> have shown that in materials with high stacking fault energy, such as copper and aluminum, grain size does not affect fatigue strength of the materials tested over  $10^4$  -  $10^7$  cycles and under constant stress amplitude. This happens because dislocations cross slip easily and form cell structure which mask the effect of grain boundaries or grain size on fatigue life.<sup>30</sup> This concept is most meaningful for propagation. However, it is pertinent to mention it here because in this study, we define initiation life as the number of cycles to form a 1 mm long crack.

In materials with low stacking fault energy, partial dislocations are widely separated and recombination can be done only by applying large forces. Therefore, cross slip is not easy and barriers are effective in introducing strain hardening due to dislocation pile ups. In this case, transgranular slip bands are formed and the deformation mode is called planar. It has been shown<sup>30</sup> that in low-stacking-fault materials, grain size can affect fatigue strength through impeding crack near grain boundaries.

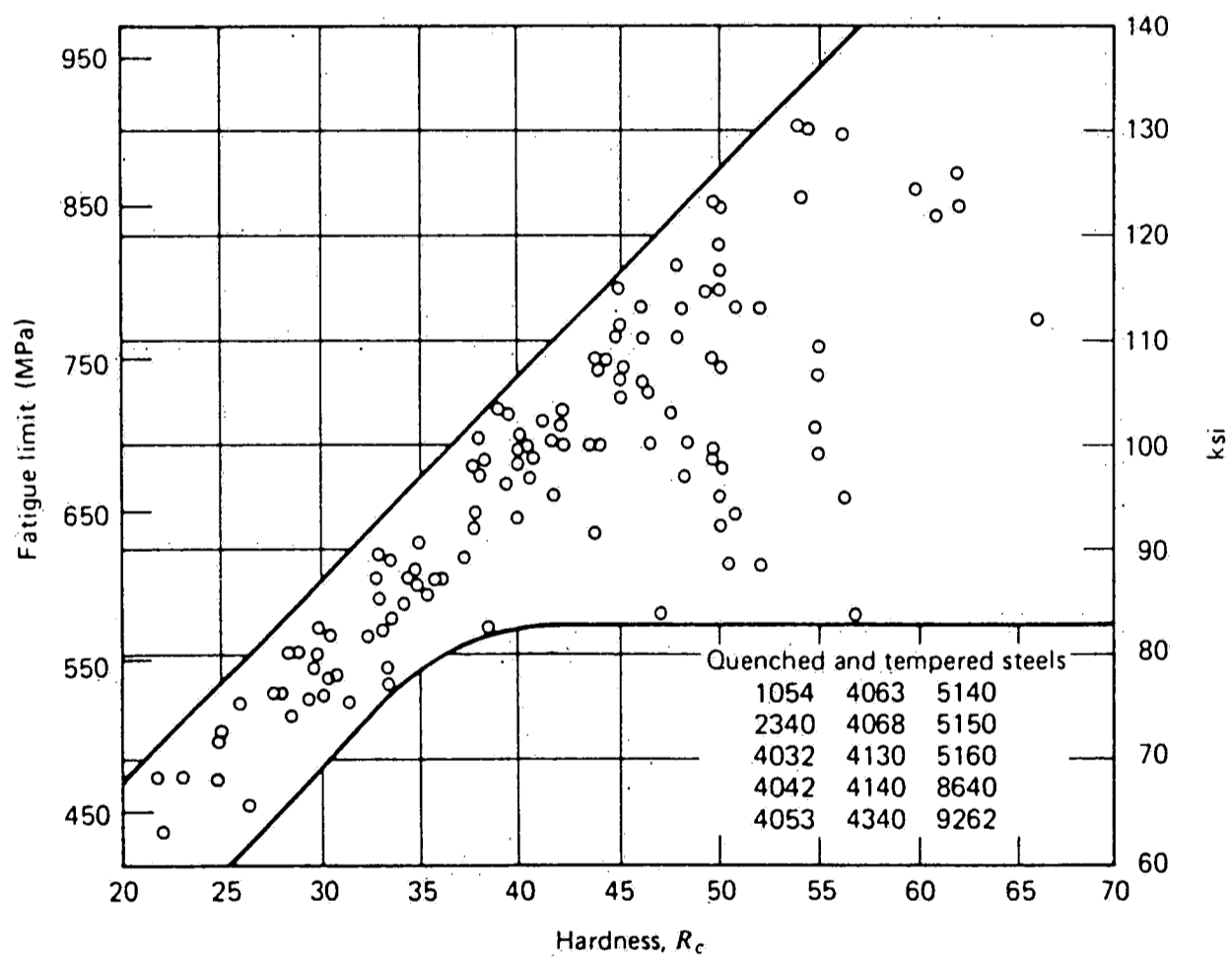


Figure 1.4- Fatigue strength as a function of hardness level.<sup>27</sup>

#### •1.4-Initiation Life Prediction At Notches

Prediction of fatigue crack initiation life from notches has been a subject of active interest during the last 30 years.<sup>1-11</sup> The principal reason is the need for a model by which a design engineer will be able to minimize the number of tests required to predict fatigue behavior for a notched component. Traditionally, nominal stresses and elastic stress concentration based approaches have been used. Recently, two more complicated methods—local strain and fracture mechanics based approaches— have been employed to predict crack initiation life in metals. In this part, fracture mechanics, local strain, and other approaches based on elastic stress concentration will be discussed.

##### •1.4.1—Fracture Mechanics Approach

Based on linear elastic analysis, this approach which has been used in several investigations<sup>8,9,24,31-38</sup> employs  $\Delta K/\sqrt{\rho}$  as a measure of maximum stress fluctuations at the root of the notch to predict initiation life for notched components.  $\Delta K$  represents the maximum range of stress intensity, which depends on applied load, component geometry, and crack length, and  $\rho$  is the notch root radius. The origin of this approach stems from Irwin<sup>39</sup> and Creager<sup>40</sup>. In 1966, Creager showed that elastic stress distribution around sharp elliptical or hyperbolic notches in a component subjected to mode I deformation can be calculated as a function of stress intensity from the following equations:

$$\sigma_x = \frac{K_I}{(2\pi r)^{1/2}} \cos \theta/2 [1 - \sin \theta/2 \sin 3\theta/2] - \frac{K_I}{(2\pi r)^{1/2}} \frac{\rho}{2r} \cos 3\theta/2 \quad (1.4a)$$

$$\sigma_y = \frac{K_I}{(2\pi r)^{1/2}} \cos \theta/2 [1 + \sin \theta/2 \sin 3\theta/2] + \frac{K_I}{(2\pi r)^{1/2}} \frac{\rho}{2r} \cos 3\theta/2 \quad (1.4b)$$

$$\tau_{xy} = \frac{K_I}{(2\pi r)^{1/2}} \sin \theta/2 \cos \theta/2 \cos 3\theta/2 - \frac{K_I}{(2\pi r)^{1/2}} \frac{\rho}{2r} \sin 3\theta/2 \quad (1.4c)$$

where  $r$ ,  $\theta$ , and  $\rho$  are shown in Figure 1.5<sup>41</sup>.



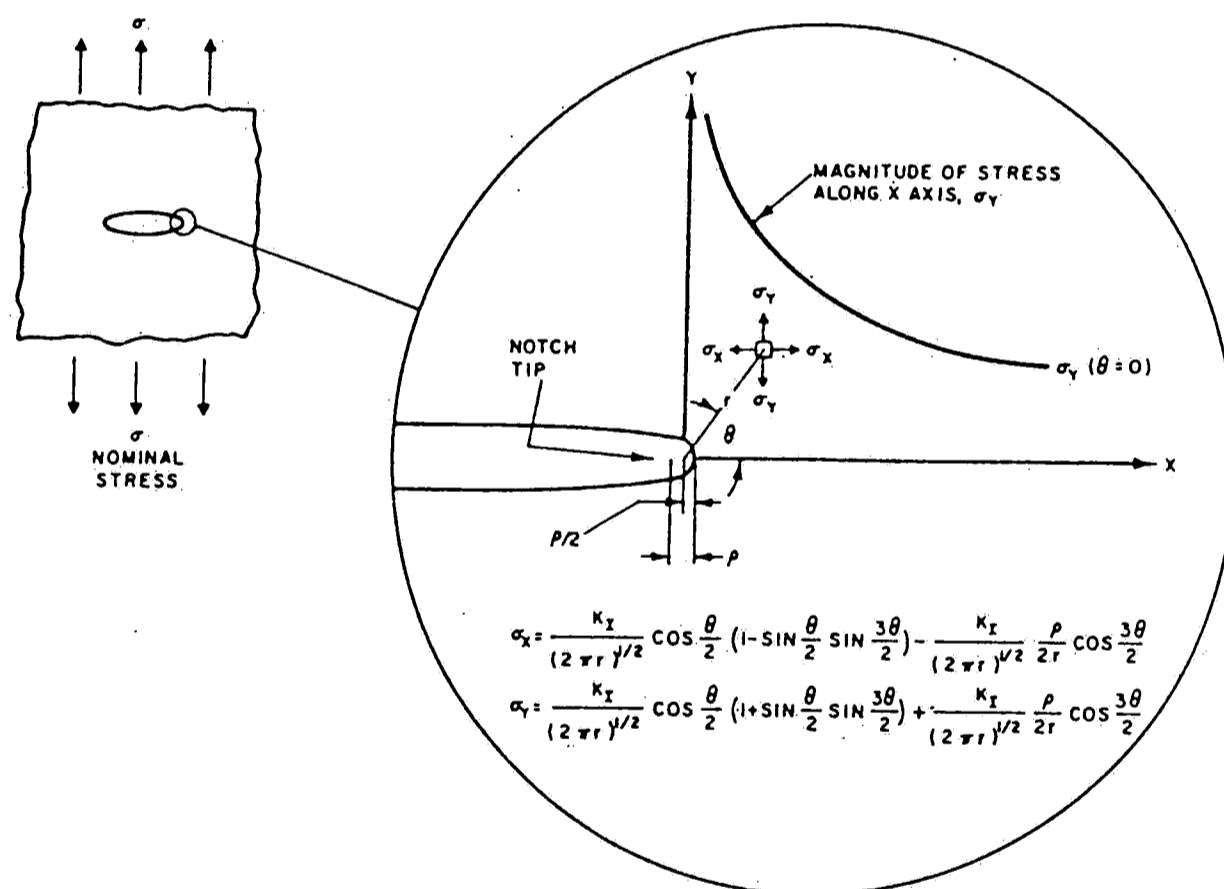


Figure 1.5- Elastic stress distribution near the tip of an elliptical notch for a structure under mode I deformation.<sup>41</sup>

When a structural component as in Figure 1.5 is cyclically loaded, maximum stress fluctuation at the notch root, i. e.,  $\theta=0$  and  $r=\rho/2$ , may be calculated by Eq. 1.4b as follows:

$$\Delta\sigma_{\max} = \frac{2}{\sqrt{\pi}} \left[ \frac{\Delta K}{\sqrt{\rho}} \right] \quad \text{when } \rho \rightarrow 0 \quad (1.5)$$

Also,  $\Delta\sigma_{\max}$  can be calculated using stress concentration factor as follows:

$$\Delta\sigma_{\max} = K_t \cdot \Delta S \quad (1.6)$$

As seen from the last two equations,  $K/\sqrt{\rho}$  is in fact equal to  $K_t \cdot \Delta S$  times a factor of  $\sqrt{\pi}/2$ . Therefore, an alternative stress concentration factor is defined<sup>2</sup> as  $K_{fm} = \frac{2 K}{S \cdot \sqrt{\pi \rho}}$  which is close to  $K_t$  only when notch has a crack-like geometry. Using finite element analysis for blunt compact-tension specimens, Wilson<sup>42</sup> has shown that Eq. 1.5 is accurate to within 10% for notch radius up to 5 mm. The accuracy of Eq. 1.5 has also been studied by Dowling<sup>2</sup> for notched specimens shown in Figure 1.6.<sup>2</sup> The results presented in Table 1.1 show a considerable difference between  $K_{fm}$  and  $K_t$  for the two blunt notches. The other limitation of this approach appears when there is significant plastic deformation at the notch root. In such cases when  $\Delta K/\sqrt{\rho}$  versus  $N_i$  is plotted for specimens with different notch geometry, data separation will be seen for low-cycle and high stress conditions. An example has been shown in Figure 1.7.<sup>2</sup>

Table 1.1- Stress Concentration Factors for the Notches Shown in Figure 1.6.<sup>2</sup>

| Specimen    | $K_t$ | $K_{fm}$ |
|-------------|-------|----------|
| Center Hole | 2.12  | 1.19     |
| Compact     | 2.62  | 2.41     |
| Blunt DEN   | 2.42  | 1.63     |
| Sharp DEN   | 10.7  | 10.3     |

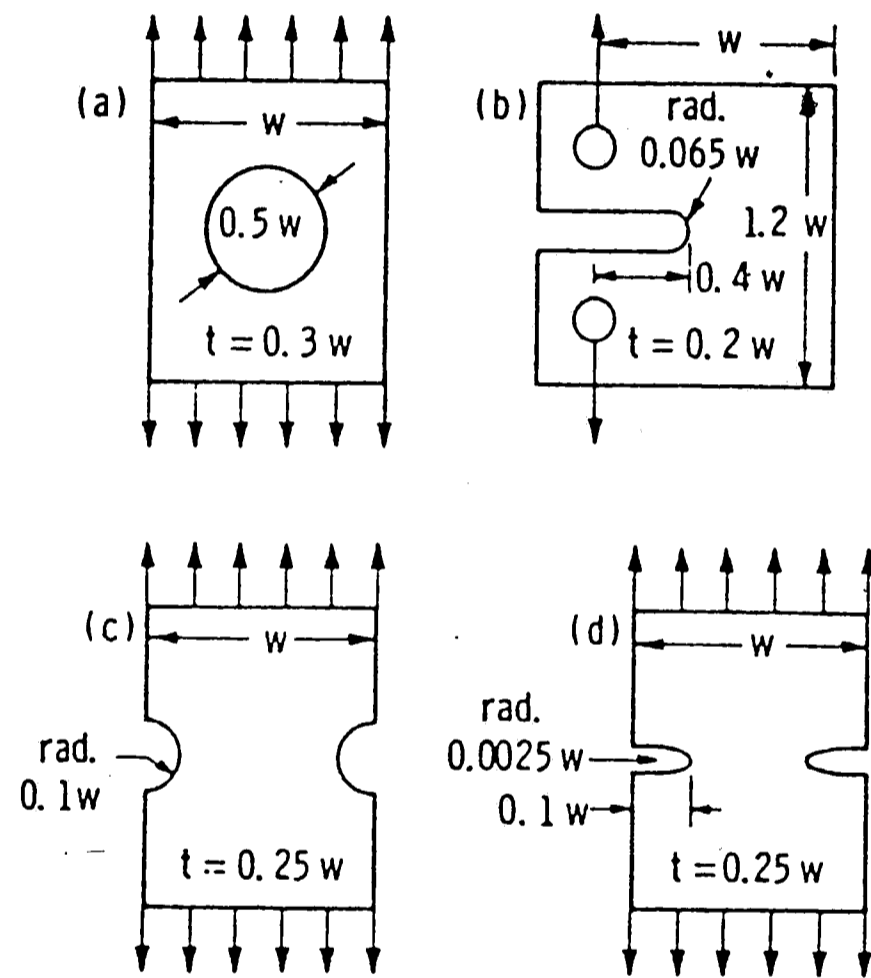


Figure 1.6- Notched specimen geometries: (a) Center hole, (b) Compact, (c) Blunt double edge notch (DEN), and (d) Sharp double-edge notch. For each geometry,  $W=25.4$  mm;  $t$ =thickness.<sup>2</sup>

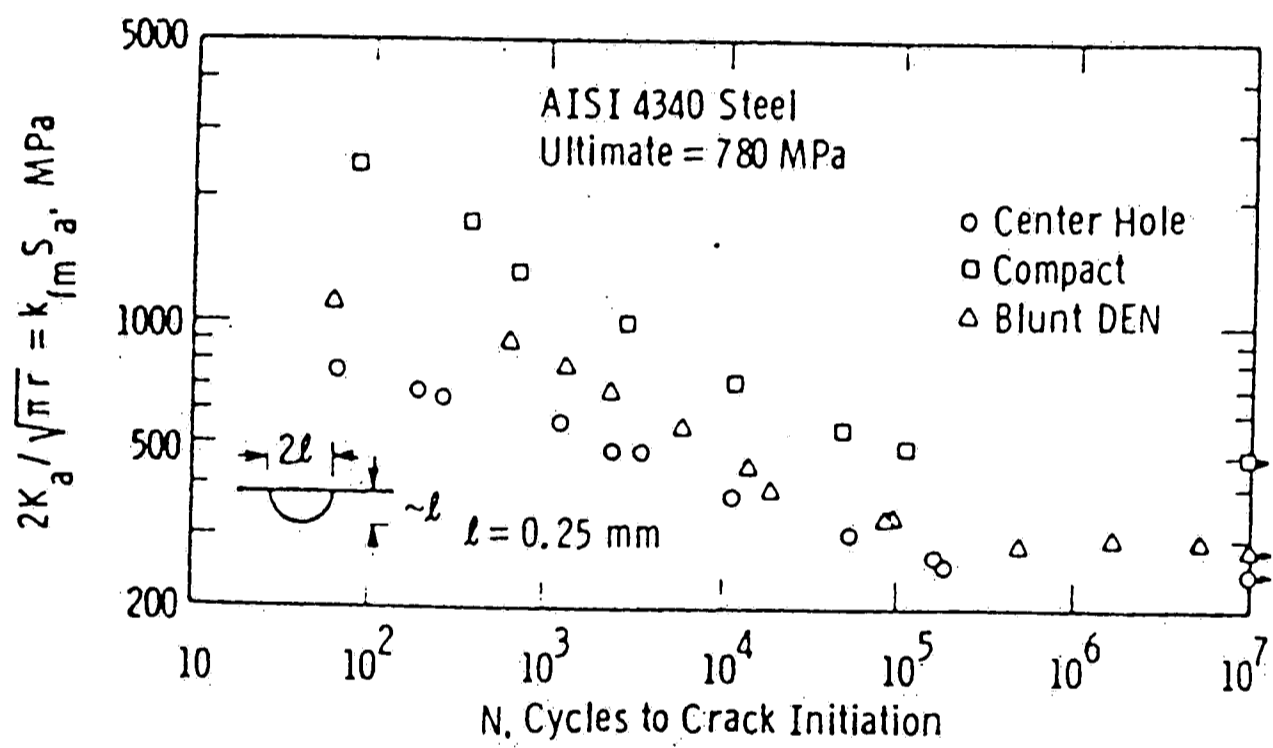


Figure 1.7- Fracture mechanics approach used to correlate fatigue crack initiation life for various notched specimens.<sup>2</sup>

#### •1.4.2—Local Strain Approach

Most problems of engineering interest in designing structural components and machine parts involve the case where nominal stresses are elastic while inelastic local stresses are developed at keyholes, welds, fillets, etc. In these cases, as would be expected, models based on elasticity theory are not able to predict the fatigue damage of the component. In order to account for plasticity effects at notches, the local strain approach has been introduced<sup>2,4-7,43-46</sup> which assumes that initiation at the notch occurs when a small smooth specimen located at the notch, shown in Figure 1.5, fails. This method then establishes the stress-strain history for this small specimen through experimental tests, hypotheses, or a finite element analysis. A rule proposed by Neuber<sup>47</sup> has been extended to fatigue problems by Topper et al.<sup>4</sup> to predict fatigue initiation life for notched components, as shown schematically in Figure 1.8.

Neuber studied the behavior of stress and strain concentration for notched shear-strained prismatic bodies and proposed a rule which can be used with stress-strain laws to correlate the nonlinear stress-strain behavior at the notch root to the nominal stress-strain applied to a component. He states<sup>47</sup> that "The geometrical mean value of the stress and strain concentration factors is equal to the Hookian stress-concentration factor,"<sup>47</sup> which means (The analysis has been developed by Topper et al.<sup>4</sup> and is repeated here for convenience):

$$K_t = (K_\sigma K_\epsilon)^{1/2} \quad (1.7) \quad \text{Neuber rule}$$

where  $K_\sigma$  and  $K_\epsilon$  are plastic stress and plastic strain concentration factors, respectively. Equation (1.7) states that the product  $K_\sigma K_\epsilon$  is constant. This is reasonably supported by the fact that  $K_\sigma$  decreases and  $K_\epsilon$  increases as yielding occurs. Substituting  $K_\sigma$  and  $K_\epsilon$  with a range of stress and strain gives:

$$K_t = \left( \frac{\Delta\sigma\Delta\epsilon}{\Delta s\Delta e} \right)^{1/2} \quad (1.8)$$

which is an important and useful equation because it correlates nominal factors to local factors or:

$$K_t(\Delta s\Delta e E)^{1/2} = (\Delta\sigma\Delta\epsilon E)^{1/2} \quad (1.9)$$

where  $\Delta s$  and  $\Delta e$  are nominal stress and strain ranges,  $\Delta\sigma$  and  $\Delta\epsilon$  are local stress and strain ranges, and  $E$  is the elastic modulus. When nominal stress and strain are elastic, using Hook's law Equation (1.9) may be rewritten as:

$$K_t \Delta s = (\Delta\sigma \Delta\epsilon E)^{1/2} \quad (1.10)$$

Since plasticity at the notch root can markedly lower the value of  $K_t$ ,  $K_f$  has been used in fatigue problems instead of  $K_t$ . Although  $K_f$ , as shown in Figure 1.2, varies over the life range, approximate equations like that of Peterson<sup>22</sup> may be used to determine  $K_f$ . Substituting  $K_t$  for  $K_f$ , Equation (1.10) becomes:

$$K_f \Delta s = (\Delta\sigma \Delta\epsilon E)^{1/2} \quad (1.11)$$

or

$$\Delta\sigma \Delta\epsilon = \frac{(K_f \Delta s)^2}{E} = \text{constant} \quad (1.12)$$

which is the equation of a rectangular hyperbola, shown in Figure 1.8, and is very important in most engineering designs where nominal stresses are essentially elastic and local stresses and strains might be plastic. When local stress and strain are also elastic, i.e., high-cycle fatigue, Equation (1.11) may be further simplified as:

$$K_f \Delta s = \Delta\sigma \quad (1.13)$$

It should be noted that when cyclic stress-strain curve is known, its intersection with Equation (1.12) will give the local stress and strain at the notch tip. Fatigue life can then be estimated using this strain with Manson<sup>48</sup> type strain-life equations (see Figure 1.8).

In summary, Equation (1.9), with  $K_t$  substituted by  $K_f$  may be used for all values of nominal stress even when general yielding occurs. In such cases, the cyclic stress-strain curve of the material should be used to obtain  $\Delta s$  and  $\Delta e$ . Equation (1.11) applies for  $\Delta s$  values less than the yield stress, and Equation (1.13) for  $\Delta s$  values less than the yield stress divided by  $K_t$ . This is the case when there is no plasticity even at notch root. However, Equation (1.13) is frequently used for initiation life estimates even in the presence of inelastic stress and strain at the notch.

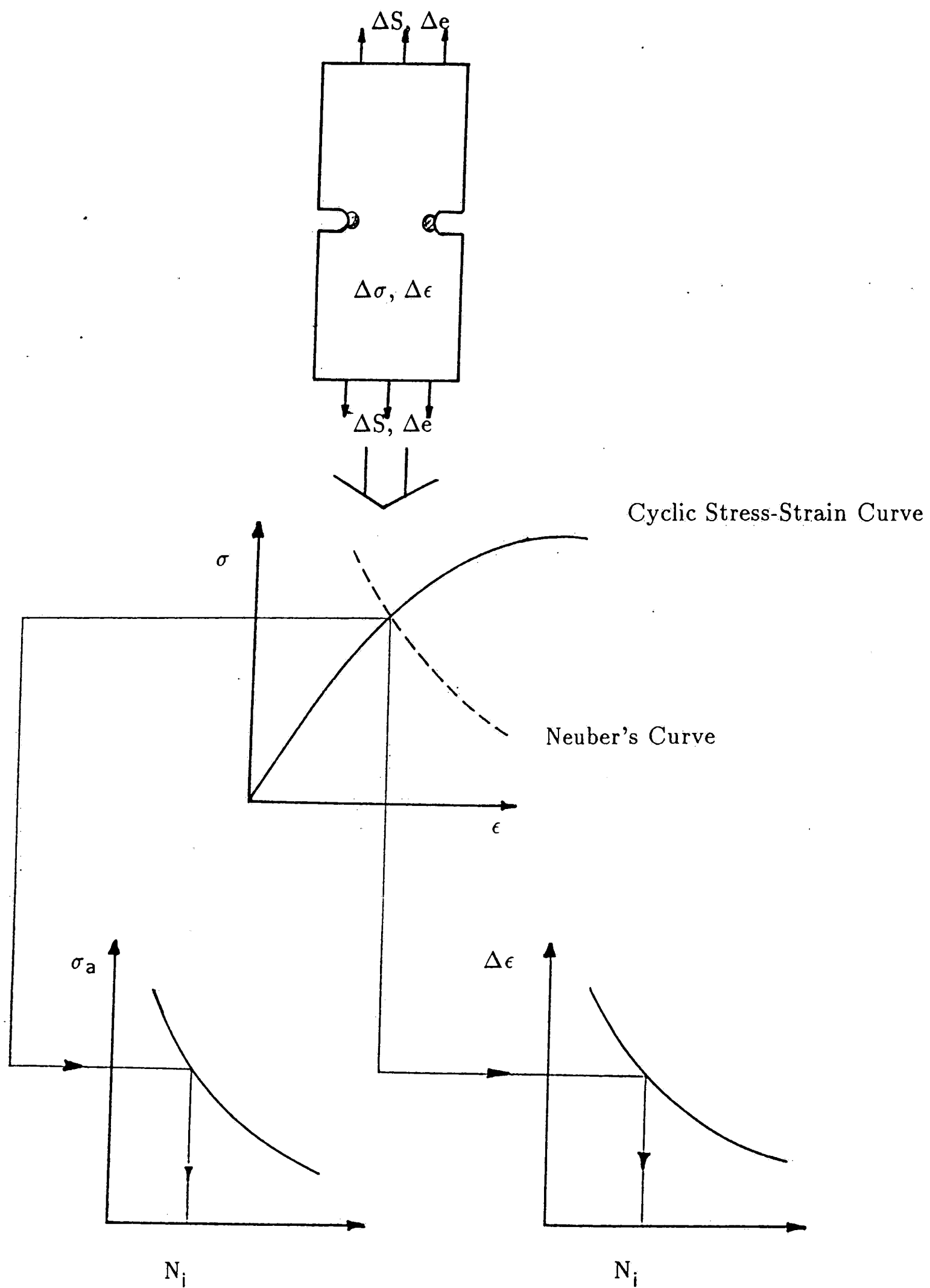


Figure 1.8- Estimation of fatigue crack initiation life based on Neuber's analysis and stress and/or strain-life curves.

This approach compared to fracture mechanics base approach has at least three advantages: it accounts for plasticity at notch root, notch geometry can be accounted for and life estimation using  $K_f \Delta s$  as a damage factor, is much easier since  $K_t$ , and therefore an estimate of  $K_f$ , is readily available for variety of geometries. Also, mean stress effects can be accounted for, using this approach, by subtracting the quantity  $\sigma_m$  from  $\sigma'_f$  in the following equation<sup>49,50</sup>.

$$\Delta\epsilon/2 = \frac{(\sigma'_f - \sigma_m)}{E} (2N)^b + \epsilon'_f (2N)^c \quad (1.14)$$

where

$\Delta\epsilon/2$  = total strain amplitude

$E$  = Young's modulus

$\sigma'_f$  = fatigue strength coefficient

$\sigma_m$  = mean stress

$2N$  = number of reversals to failure

$b$  = fatigue strength exponent ( the slope of elastic strain vs.  $2N$  line)

$c$  = fatigue ductility exponent ( the slope of plastic strain vs.  $2N$  line)

$\epsilon'_f$  = fatigue ductility coefficient

In notched members, local yielding induces either compressive or tensile residual stresses. These stresses may change the magnitude of the mean stress at the notch root. If the applied load is tensile, compressive mean stress develops and if it is compressive, tensile mean stress is developed around the notch root. Tensile mean stresses, if not being accounted for, may result in a nonconservative life estimates. However, since the material at notch root undergoes strain control, mean stresses will be relaxed after enough cyclic plastic strain is reached<sup>50-52</sup>. The effect of mean stress



becomes much more important when the component is under variable amplitude loading. In this case, load history must be known to predict the effect of mean stresses. Also, this approach accounts for hardening/softening effects through using cyclic stress strain data. Along with those advantages, there are some difficulties with this approach as follows:

—“Where the geometry or mode of loading differs drastically from cases for which Neuber's rule has been verified, it is advisable to use it (Neuber's rule) with caution.”<sup>2</sup>

—Material properties obtained either from literature or by testing specimens in laboratory may be very different from actual component properties due to fabrication related effects.<sup>2</sup> In the case where only local yielding occurs, the role of fabrication related effects may become more important since the properties of the material in a small zone at the notch root may differ drastically from those of laboratory tested specimens.

#### •1.4.3- $K_t$ -Based Approaches

Fatigue damage in this approach is defined by the product  $k_t \Delta s$ , where  $\Delta s$  is the maximum stress fluctuation at the notch tip and  $K_t$  is the elastic stress concentration factor. As stated before, when plasticity occurs, this approach leads to an unnecessarily conservative life estimates. When local plasticity occurs, the stress distribution in the notch vicinity is changed. Also, the damage factor may be maximized at some distance ahead of the notch. For this reason and the fact that in fatigue, sharp notches have less effect than predicted by  $K_t$ , historically  $K_t$  has been replaced by  $K_f$  is a function of material, loading condition and geometry as explained previously. The quantity  $K_f$  along with Neuber's equation were used to account for plasticity and geometry effects. The quantity  $K_f$  is treated as a constant whereas it was proved to be a function of life.

An alternative approach which uses  $K_{td}$  instead of  $K_f$  has been used by Bathias and Gabra, where  $K_{td}$  is  $k_t$  evaluated some distance ahead of notch.  $K_{td}$  is determined by Neuber<sup>21,53</sup> equation as follows:

$$K_{td} = K_t \left( \frac{\rho}{\rho + 4d} \right)^{0.5} \quad (1.14)$$

where  $\rho$  is notch root radius. Also, as mentioned previously, Neuber<sup>47</sup> has shown that

$$K_t = (K_\sigma K_\epsilon)^{0.5} \quad (1.7)$$

which can be applied at any distance ahead of notch. Combining equations 1.14 and 1.7 results in

$$K_{td} = \left( \frac{\Delta\sigma_d \Delta\epsilon_d}{\Delta s \Delta e} \right)^{0.5} \quad (1.15)$$

and thus

$$\Delta\epsilon_d = \frac{K_{td}^2 \cdot \Delta s \cdot \Delta e}{\Delta\sigma_d} \quad (1.16)$$

where far field stress is elastic, then  $\Delta e = \frac{\Delta s}{E}$ . Therefore,

$$\Delta\epsilon_d = \frac{K_{td} \cdot \Delta s}{E} \quad (1.17)$$

Note that  $K_{td} \cdot \Delta s = \Delta\sigma_d$ .

This approach accounts for plasticity and geometry, through utilizing  $K_{td}$  and Neuber analysis and is very similar to the local strain approach. However, the key question is "Is  $d$  a constant value as Bathias et al.<sup>12</sup> proposed?" They have calculated  $\Delta\epsilon_d$  at a distance  $d = 150 \mu\text{m}$  (grain size of the materials used) for prediction of fatigue crack initiation in two different aluminum alloys with yield strength of 328 and 410 MPa. They used compact tension specimens with notches ranging from 0.5 to 5 mm. The results of their work show that this approach may account for both notch effects and material properties. However, it seems that more work needs to be done to see if  $d$  has any correlation with material properties such as grain size, strength, etc.

## II-OBJECTIVE

Various modifications of the local strain and fracture mechanics approaches give conflicting predictions for initiation,<sup>2,8,41,54,55</sup> particularly in low-cycle region. Moreover, a common feature of all initiation models is the lack of influence of microstructural or metallurgical properties, excluding perhaps strength,<sup>1</sup> on crack initiation. *Therefore, the objective of the present study is to develop data on crack initiation at notches which can be used to compare the models while concurrently providing a range in both strength and stacking fault energy.* Strength controls the ease of slip whereas stacking fault energy controls the ease of cross-slip, as well as the type of deformation. For this purpose, the materials chosen were an aluminum alloy 2024-T3, commercial copper, 70-30 brass, and Cu-Be alloy 25. They provide ranges in strength and stacking fault energy from 300 to 850 MPa and from 15 to 120 mJ/m<sup>2</sup>, respectively. Minor objectives of this study are as follows:

1. Strain measurement at the notch root utilizing Moire-fringe technique to compare measured and computed strains.
2. Determining the relative importance of initiation cycles,  $N_i$ , versus total cycles to failure,  $N_f$ , for blunt and sharp notches.

### III. EXPERIMENTAL PROCEDURE

#### ●3.1-Materials and Grain-size Measurements

The materials tested in the present study were commercial copper (Bar 1/4-inch thick), 70-30 brass (1/4-inch thick plate), Cu-Be alloy 25\* (7-inch diameter hot forged bar), and 2024-T3 aluminum (3/8-inch thick bar). Chemical analysis and average grain size for all materials are shown in tables 3.1 and 3.2, respectively.

Grain size measurements were performed in accordance with ASTM standard E112 three circles method<sup>56</sup>, which is a grain boundary intercept technique, for both longitudinal and transverse orientations to the flow direction. For the aluminum alloy, the grain size was an average for three dimensions because the grains were not equiaxed. In the case of Cu-Be alloy 25, duplex grains were present in metallographic section. In measuring the average grain size,  $\bar{l}$ , for this alloy, both small and large grains were included. The etchants<sup>57</sup> used to reveal grain boundaries were: for aluminum, Keller's reagent; for Cu-2Be, 1 part ammonium persulfate hydroxide, 2 parts ammonium persulfate(2.5% in H<sub>2</sub>O); for brass, CrO<sub>3</sub>(saturated aqueous solution); for copper, 2 g K<sub>2</sub>Cr<sub>2</sub>O<sub>7</sub>, 4 ml NaCl (saturated solution), 8 ml H<sub>2</sub>SO<sub>4</sub>, 100 ml water, followed by Fe<sub>3</sub>Cl to increase grain boundary contrast.

---

\*Supplied by NGK Metals Corporation

### •3.2. Mechanical Testing

Tensile properties were obtained on an Instron screw driven tensile machine at a constant strain rate of 5 mm/min. Either button head or flat specimens were machined from longitudinal direction and tested according to ASTM E8-87a<sup>58</sup>. The results are shown in Table 3.3.

All fatigue experiments in this study were performed on an Instron servohydraulic closed-loop testing machine. Blunt and sharp keyhole notched compact tension (CT) type specimens were oriented in the longitudinal (LT) direction, except for Cu-Be specimens which were oriented in both (L- R) and (R- L) directions (see Figure 3.1 and 3.2<sup>59</sup>) were used. Specimen dimensions are shown in Figure 3.3.

The stress intensity solutions for these samples is as follows<sup>59</sup>:

$$K = \frac{P}{BW^{1/2}} f(a/W) \quad (3.1)$$

where

K=stress intensity factor

P=applied load

B=sample thickness

W=sample width

a=crack length

$$f(a/W) = \frac{(2+a/W)}{(1-a/W)^{3/2}} [0.886 + 4.64a/W - 13.32(a/W)^2 + 14.72(a/W)^3 - 5.6(a/W)^4]$$

The nominal stress at the root of the notch<sup>60</sup> for this geometry is:

$$S = \frac{P}{B(W-a)} \left[ \frac{3(W+a)}{W-a} + 1 \right] \quad (3.2)$$

The specimens were subjected to cyclic maximum loads ranging from 1500 to 15000N in ambient laboratory air (for additional details see Table 4.1). All waveforms were sinusoidal with stress ratio (min load/max load) of  $R=0.1$ , and all tests were conducted at a cyclic frequency of 25 Hz. Maximum loads were selected to produce initiation cycles in the range  $10^3$  to  $10^6$ . Crack initiation was defined as the cycles to form a 1 mm long crack extending from the notch root. Crack lengths, for both initiation and propagation were monitored via a compliance technique, with a 0.2 inch clip gage being attached to knife edges machined in the mouth of the notch. Visual verification of these readings were made at appropriate intervals on both sides of the samples with the aid of a traveling microscope. In order to facilitate crack observation, particularly for initiation period, all copper alloy and aluminum alloy specimens were electrolytically and mechanically polished, respectively.

Fatigue crack propagation data were also obtained under the same conditions and at constant load and constant stress ratio  $R=0.1$  utilizing an IBM XT computer and software developed by Fracture Technology Associates, Inc.

Table 3.1- Chemical Composition of the Materials Investigated\*.

| Element | Al2024-T3 | Copper | Brass  | Cu-Be |
|---------|-----------|--------|--------|-------|
| Zn      | —         | —      | 29.84  | —     |
| Cu      | 4.16      | 99.95  | 70.13  | Bal.  |
| Mn      | 0.57      | —      | —      | —     |
| Mg      | 1.37      | —      | —      | —     |
| Be      | —         | —      | —      | 1.85  |
| Co      | —         | —      | —      | 0.23  |
| Si      | 0.08      | —      | —      | —     |
| Sn      | —         | —      | <0.01  | —     |
| Fe      | —         | —      | 0.006  | —     |
| Pb      | —         | —      | <0.003 | —     |
| P       | —         | <0.001 | —      | —     |
| O       | —         | 0.034  | —      | —     |
| Al      | Bal.      | —      | —      | —     |

\* Wet Chemical and Gas Analysis; Weight Percent.

Table 3.2- Grain Size of the Materials Tested.

| Material   | Average Grain Size<br>$\bar{l}(\mu m)$ |
|------------|--|
| Copper     | 24                                     |
| Brass      | 22                                     |
| Cu-Be      | 40                                     |
| Al 2024-T3 | 162                                    |



Table 3.3- Average<sup>†</sup> Tensile Properties of the Materials Investigated.

| Material  | YS*<br>(MPa) | UTS**<br>(MPa) | Total Elongation<br>in 45mm, % |
|-----------|--------------|----------------|--------------------------------|
| Copper    | 336          | 337            | 10                             |
| Brass     | 365          | 436            | 39                             |
| Cu-Be     | 652          | 846            | 25                             |
| Al2024-T3 | 369          | 462            | 15                             |

† For Three Specimens; Standard Deviation  $\leq 2\%$  for Strength and  $\leq 10\%$  for Elongation.

\* Yield Strength at 0.2 % Offset

\*\* Ultimate Tensile Strength

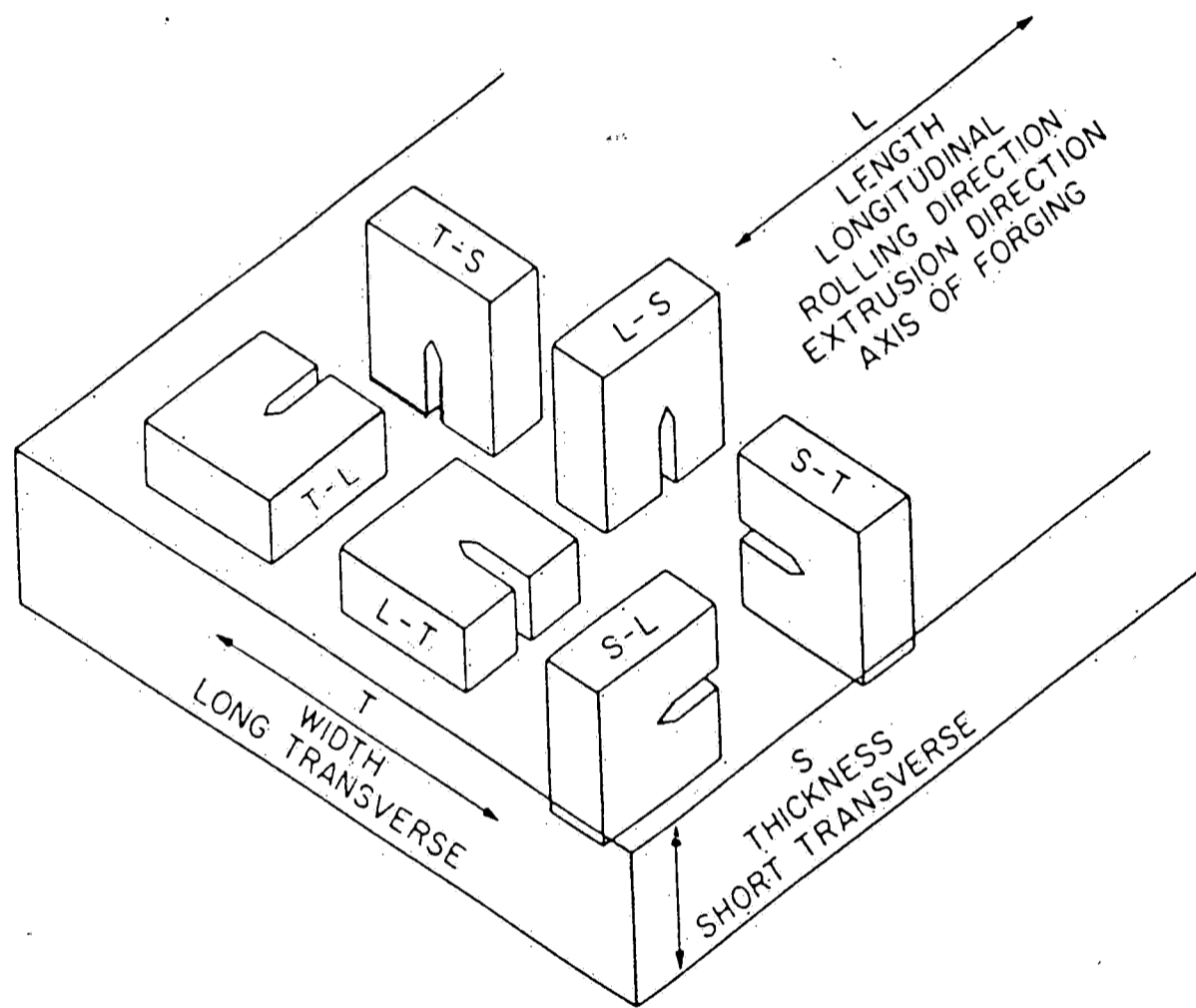


Figure 3.1- Crack plane orientation code for rectangular sections.<sup>59</sup>

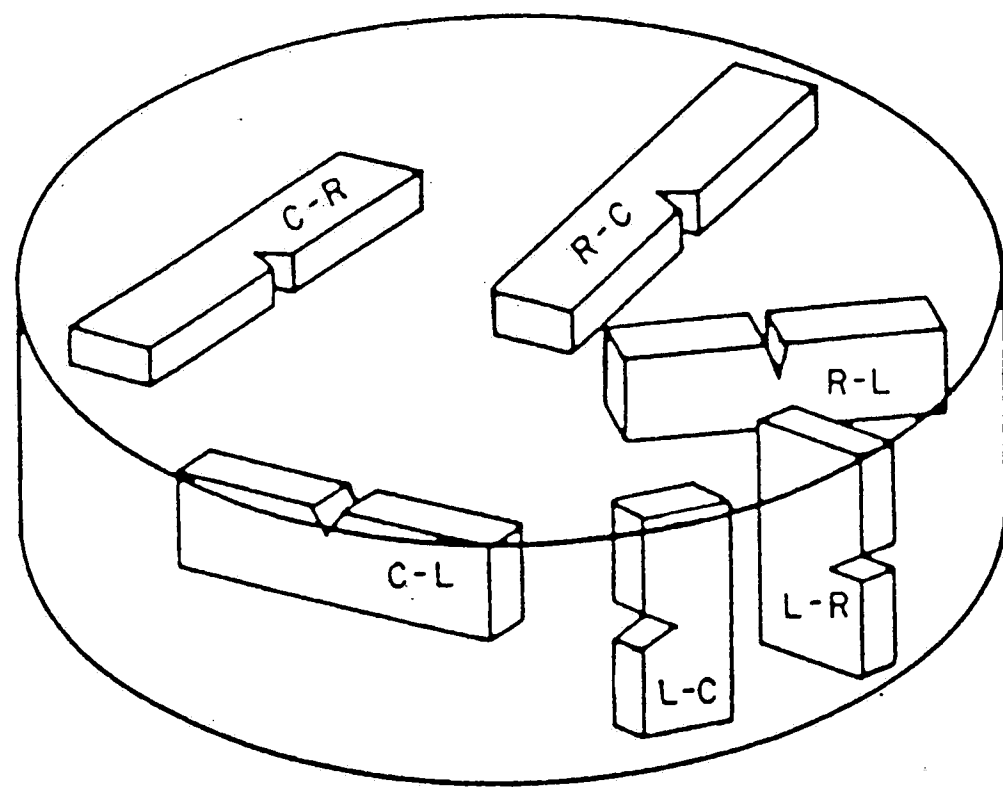
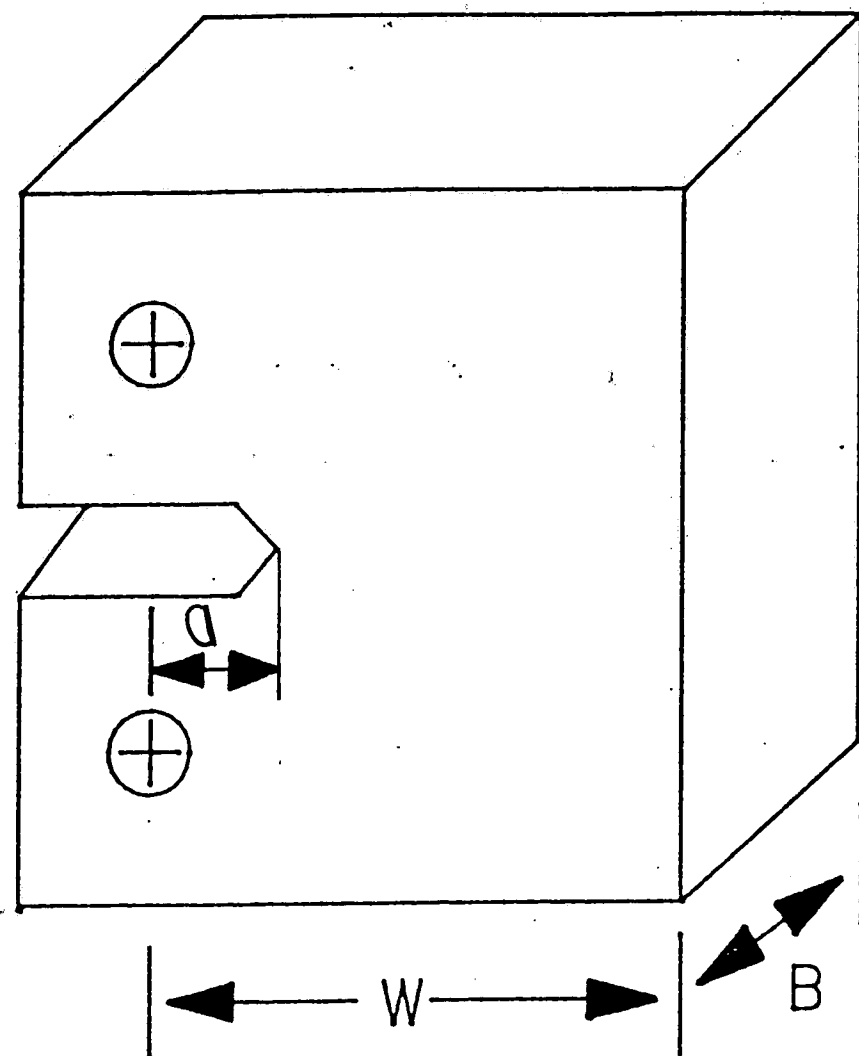


Figure 3.2- Crack plane orientation code for bar and hollow cylinder.<sup>59</sup>



| Material  | a<br>mm | W<br>mm | B<br>mm |
|-----------|---------|---------|---------|
| Copper    | 9.2     | 30.4    | 6.2     |
| Brass     | 12.2    | 40.6    | 6.3     |
| Cu-Be     | 15.2    | 50.8    | 12.6    |
| Al2024-T3 | 12.2    | 40.6    | 8.3     |

Figure 3.3- Geometry and dimensions of compact tension specimens used in the present study.

## IV-RESULTS AND DISCUSSION

In order to evaluate different fatigue—initiation—life models, fatigue experiments were performed on CT specimens with two different notch root radii for materials of 2024-T3 aluminum, commercial copper, 70-30 brass, and Cu-Be alloy 25. The results are shown in Table 4.1, whereas the symbols are defined as follows:

$\Delta S$ =maximum nominal fluctuating stress at the notch root,  
calculated from Equation 3.2.

$R$ =minimum nominal stress/maximum nominal stress

$\rho$ =notch root radius

$K_t$ =theoretical stress concentration factor,  
determined from Figure 4.14.<sup>42</sup>

$K_f$  =fatigue strength reduction factor,  
determined from Equation 1.3.

$N_i$ =number of cycles to initiate a 1 mm crack

$N_f$ =number of cycles to failure

Table 4.1- Fatigue Data for the Materials Investigated.

| Material | $\Delta S^*$<br>(MPa) | $\rho$<br>(mm) | $K_t$ | $K_f$ | $N_i$<br>(Cycles) | $N_f$<br>(Cycles) |
|----------|-----------------------|----------------|-------|-------|-------------------|-------------------|
| Copper   | 318                   | 1.59           | 3.1   | 2.5   | 4400              | 5900              |
| "        | 180                   | 0.13           | 9.9   | 2.4   | 8000              | 23100             |
| "        | 126                   | 0.13           | 9.9   | 2.4   | 41000             | 118500            |
| "        | 126                   | 0.13           | 9.9   | 2.4   | 61000             | 134300            |
| "        | 180                   | 1.59           | 3.1   | 2.5   | 70000             | 86800             |
| "        | 126                   | 1.59           | 3.1   | 2.5   | 235000            | 3054000           |
| "        | 68                    | 0.13           | 9.9   | 2.4   | 4010000           | *                 |
| Brass    | 180                   | 0.13           | 10.8  | 3.3   | 9500              | 37800             |
| "        | 168                   | 0.13           | 10.8  | 3.3   | 13500             | 48500             |
| "        | 263                   | 1.59           | 3.5   | 3.0   | 28800             | 36800             |
| "        | 231                   | 1.59           | 3.5   | 3.0   | 37600             | 51700             |
| "        | 126                   | 0.13           | 10.8  | 3.3   | 38500             | 116500            |
| "        | 126                   | 0.13           | 10.8  | 3.3   | 42000             | 127100            |
| "        | 180                   | 1.59           | 3.5   | 3.0   | 84000             | 113800            |
| "        | 126                   | 1.59           | 3.5   | 3.0   | 380000            | 474200            |
| "        | 84                    | 0.13           | 10.8  | 3.3   | 740000            | 1002300           |

Stress Ratio, R=0.1

\* Did not fail after  $4.01 \times 10^6$  cycles.

Table 4.1- (Continued)

| Material  | $\Delta S^*$<br>(MPa) | $\rho$<br>(mm) | $K_t$ | $K_f$ | $N_i$<br>(Cycles) | $N_f$<br>(Cycles) |
|-----------|-----------------------|----------------|-------|-------|-------------------|-------------------|
| Cu-Be     | 158                   | 0.07           | 16.5  | 6.5   | 11400             | 45000             |
| "         | 126                   | 0.07           | 16.5  | 6.5   | 18000             | 72100             |
| "         | 198                   | 1.59           | 3.9   | 3.7   | 85800             | 100800            |
| "         | 68                    | 0.07           | 16.5  | 6.5   | 130000            | 399800            |
| "         | 68                    | 0.07           | 16.5  | 6.5   | 133000            | 408600            |
| "         | 126                   | 1.59           | 3.9   | 3.7   | 405000            | 455900            |
| "         | 126                   | 1.59           | 3.9   | 3.7   | 440000            | 502100            |
| "         | 105                   | 1.59           | 3.9   | 3.7   | 665000            | 755100            |
| Al2024-T3 | 126                   | 0.13           | 10.8  | 3.8   | 11500             | 20300             |
| "         | 180                   | 1.59           | 3.5   | 3     | 14000             | 19300             |
| "         | 126                   | 1.59           | 3.5   | 3     | 37500             | 62400             |
| "         | 126                   | 1.59           | 3.5   | 3     | 38500             | 49500             |
| "         | 68                    | 0.13           | 10.8  | 3.8   | 138500            | 341100            |
| "         | 68                    | 0.13           | 10.8  | 3.8   | 149000            | 540400            |
| "         | 68                    | 1.59           | 3.5   | 3     | 335000            | 690100            |

Stress Ratio, R=0.1

#### •4.1-Nominal Stress

Fatigue initiation data for the 2024-T3 Al and Cu-Be alloys is plotted in Figure 4.1 as  $S_{nom}/UTS$  versus  $N_i$ . Nominal stresses were determined using Equation 3.2. As seen from this Figure, solid curves are spaced farther apart relative to broken curves. In other words, material with higher strength, i.e. the Cu-Be alloy, is more notch sensitive than the aluminum alloy which has lower strength.

From this Figure and Figures 4.2 and 4.3, it seems that for a given material, sharp and blunt notch data approach each other at long life. This happens because at long life, i.e.,  $10^5-10^6$  cycles, there is still some plastic deformation at notch root of sharp notch specimens whereas at the same cycles for blunt notch sample, the notch root stress is no longer plastic. Therefore,  $K_t$  for blunt notch keeps its full theoretical effect while the effect of  $K_t$  for sharp V-notch decreases due to plasticity and notch blunting. To verify the above hypothesis, consider the theoretical notch root stress ( $K_t \cdot \Delta S$ ) for aluminum alloy at its lowest applied stress ( $S=76$  MPa). For sharp V-notch,  $K_t \cdot \Delta S=739$  MPa, whereas for blunt keyhole notch,  $K_t \Delta S=239$  MPa. As seen from Table 3.3 the yield strength of this alloy is about 370 MPa and therefore, at nominal stress  $S=76$  MPa, plastic deformation at the notch root is expected only for sharp V-notch specimen. Also, from Figures 4.1 through 4.3, it may be concluded that at longer life, where notch root stress of both sharp and blunt notch specimens becomes elastic, all data approaches fatigue limit(i.e. fatigue strength at a given cycle) of smooth specimen divided by  $K_f$ . In other words, at long life,  $K_f$  becomes constant and the role of surface roughness left from machining the notch and the role of other flaws at the notch vicinity may become important.



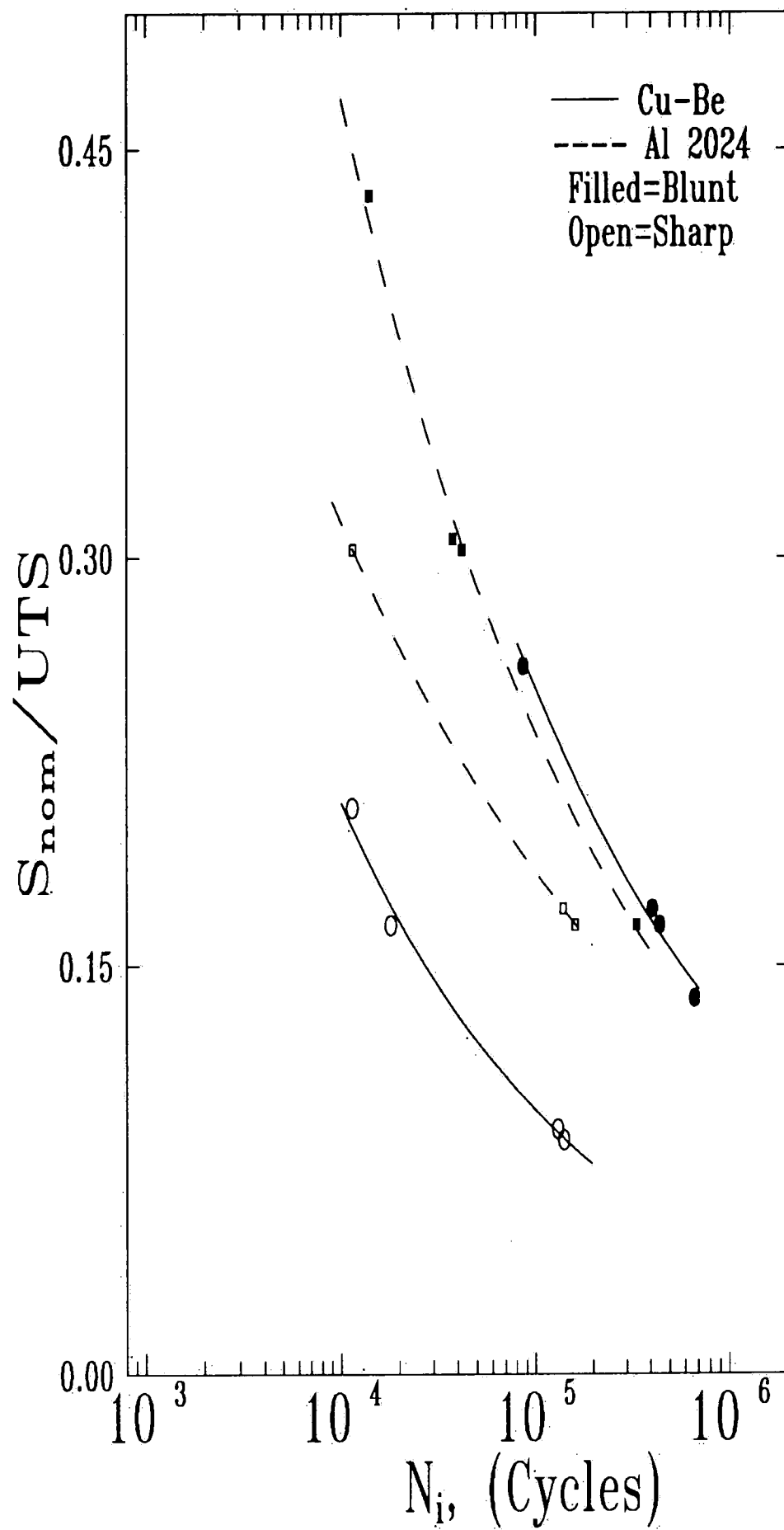


Figure 4.1- Nominal stress normalized by ultimate tensile strength versus crack initiation life for Cu-Be and aluminum alloys. This Figure shows the effect of material strength on notch sensitivity and the effect of notch on initiation life.

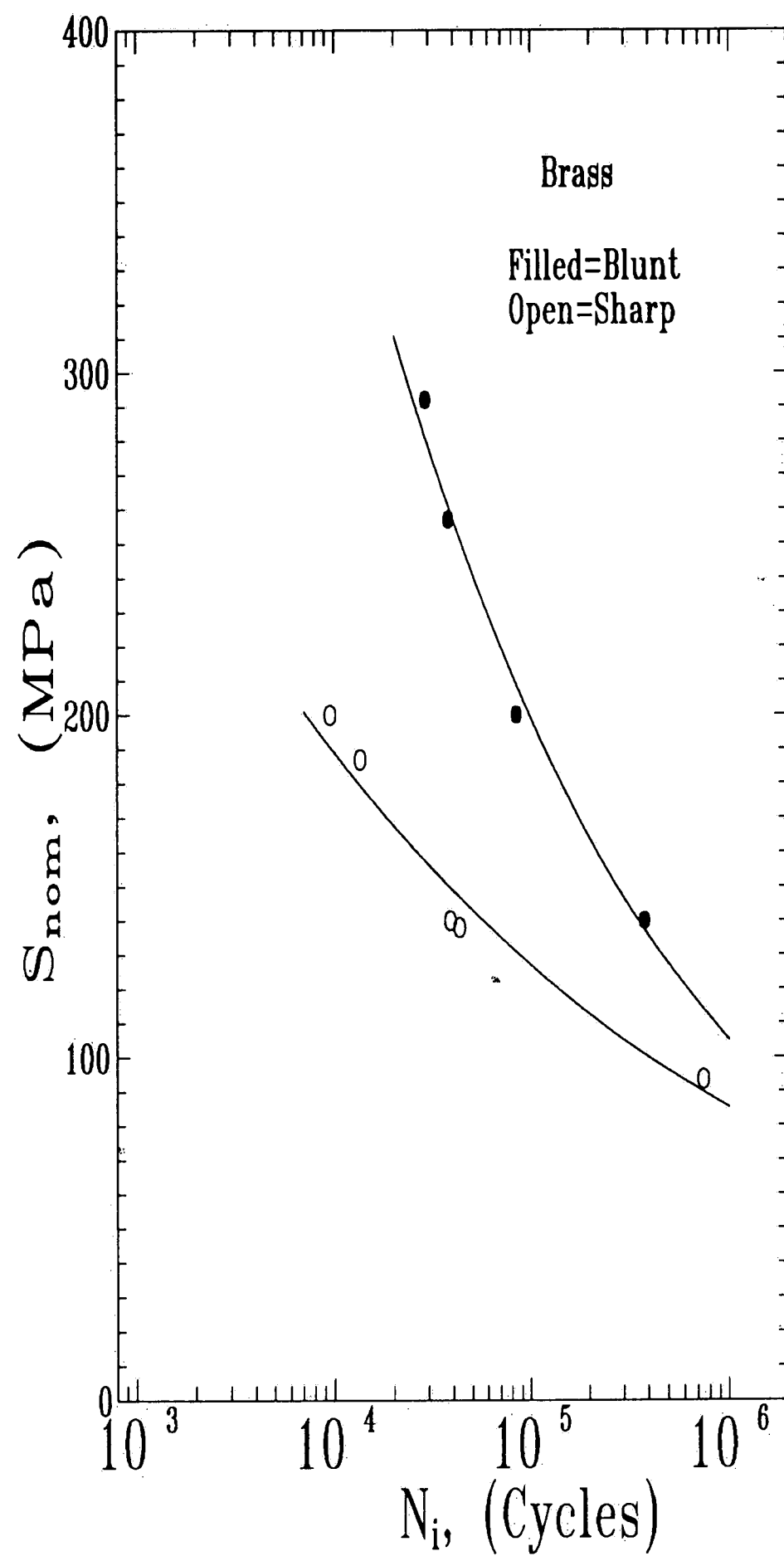


Figure 4.2- Nominal stress versus crack initiation life for brass with two different notches.

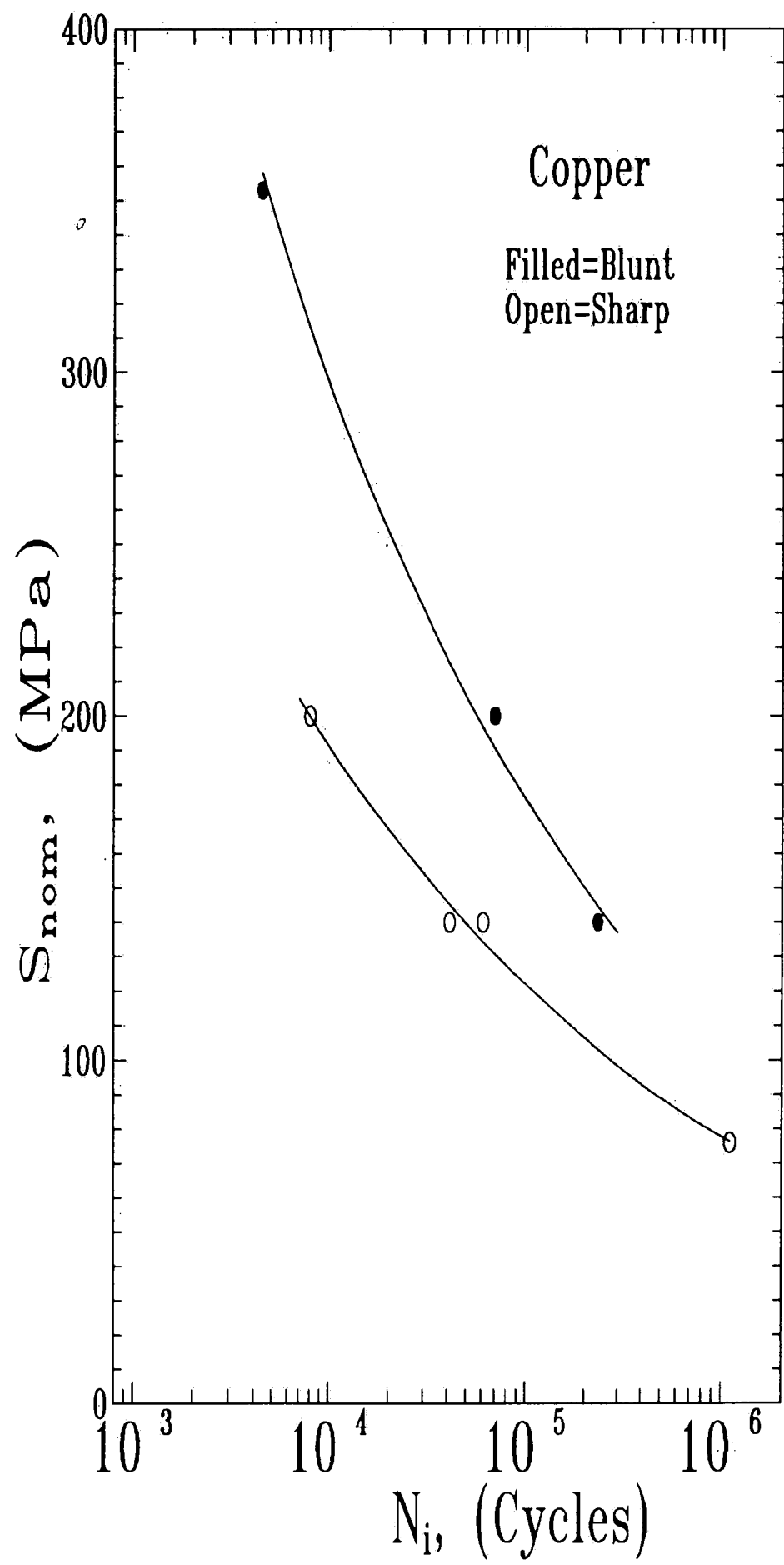


Figure 4.3- Nominal stress versus crack initiation life for copper with two different notches.

#### •4.2.1-Fracture mechanics approach

The  $\frac{\Delta K}{\sqrt{\rho}}$  factor which was employed as a model for predicting fatigue initiation life at notches by Barsom and McNicol<sup>8</sup> has been used in Figures 4.4–4.7 to correlate initiation data for blunt and sharp notch specimens. By combining the Equations 1.5 and 1.6, we saw that when notch root radius approaches zero, i.e., crack-like notch,  $\frac{\Delta K}{\sqrt{\rho}}$  becomes equal to  $\frac{\sqrt{\pi}}{2} \cdot K_t \cdot \Delta S$  or  $\approx 0.85 K_t \cdot \Delta S$ . Therefore, choosing such a factor as a representative for maximum local stress at notch root is expected to give too conservative results particularly for sharp V-notch specimens and also in the low-cycle regime where there is considerable plastic deformation in the notch vicinity. This result is clearly shown in Figures 4.4–4.7. Initiation data from all materials are plotted together in Figure 4.8.

If  $\Delta K/\sqrt{\rho}$ -type models properly accounted for notch geometry, one would expect blunt and sharp notch results to follow a common trend. However, as seen, not only do the blunt and sharp notch results not follow a common trend, but also fatigue crack initiation data for sharp V-notched specimens of all materials lies above data for blunt-keyhole notched specimens. In fact, the data in Figures 4.4 through 4.7 suggest that initiation requires more cycles for sharp than blunt notches at the same  $\frac{\Delta K}{\sqrt{\rho}}$ . In other words, this model does not lead to physically plausible results. In summary, this approach does not account for either notch-root plasticity or notch geometry.

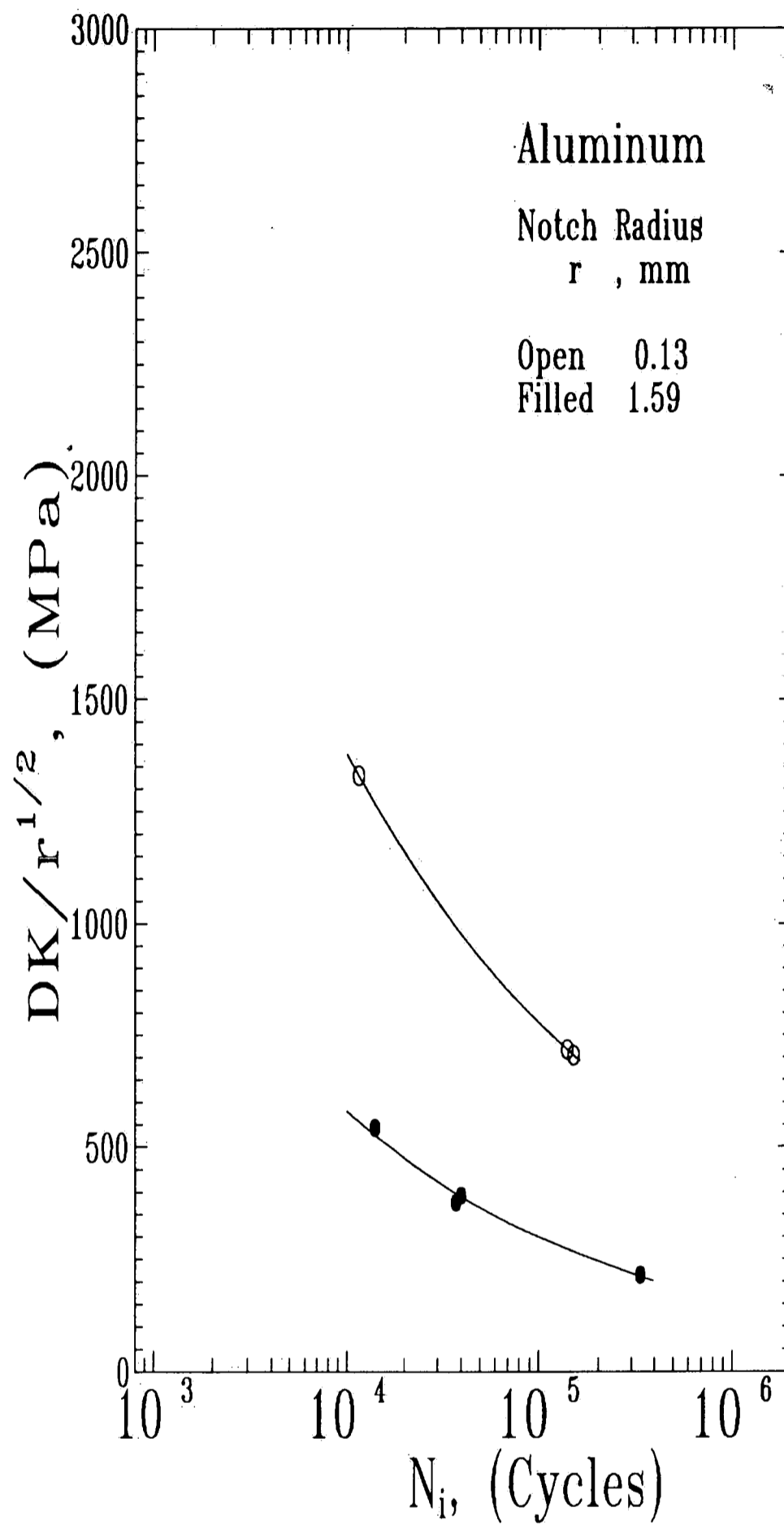


Figure 4.4- Fatigue crack initiation data for 2024-T3 aluminum are correlated using fracture mechanics approach.

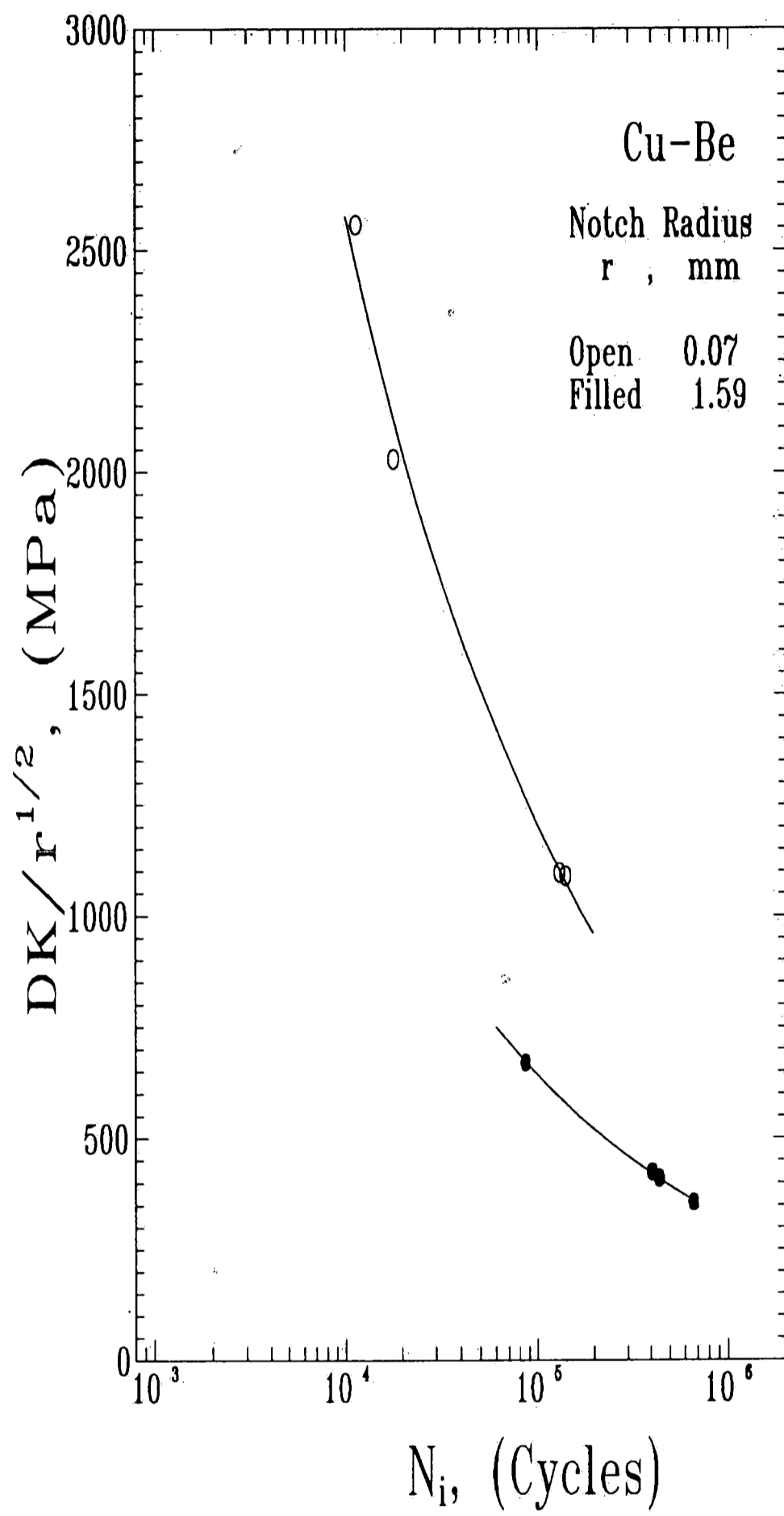


Figure 4.5- Correlating blunt and sharp notches data for Cu-Be alloy using fracture mechanics approach.

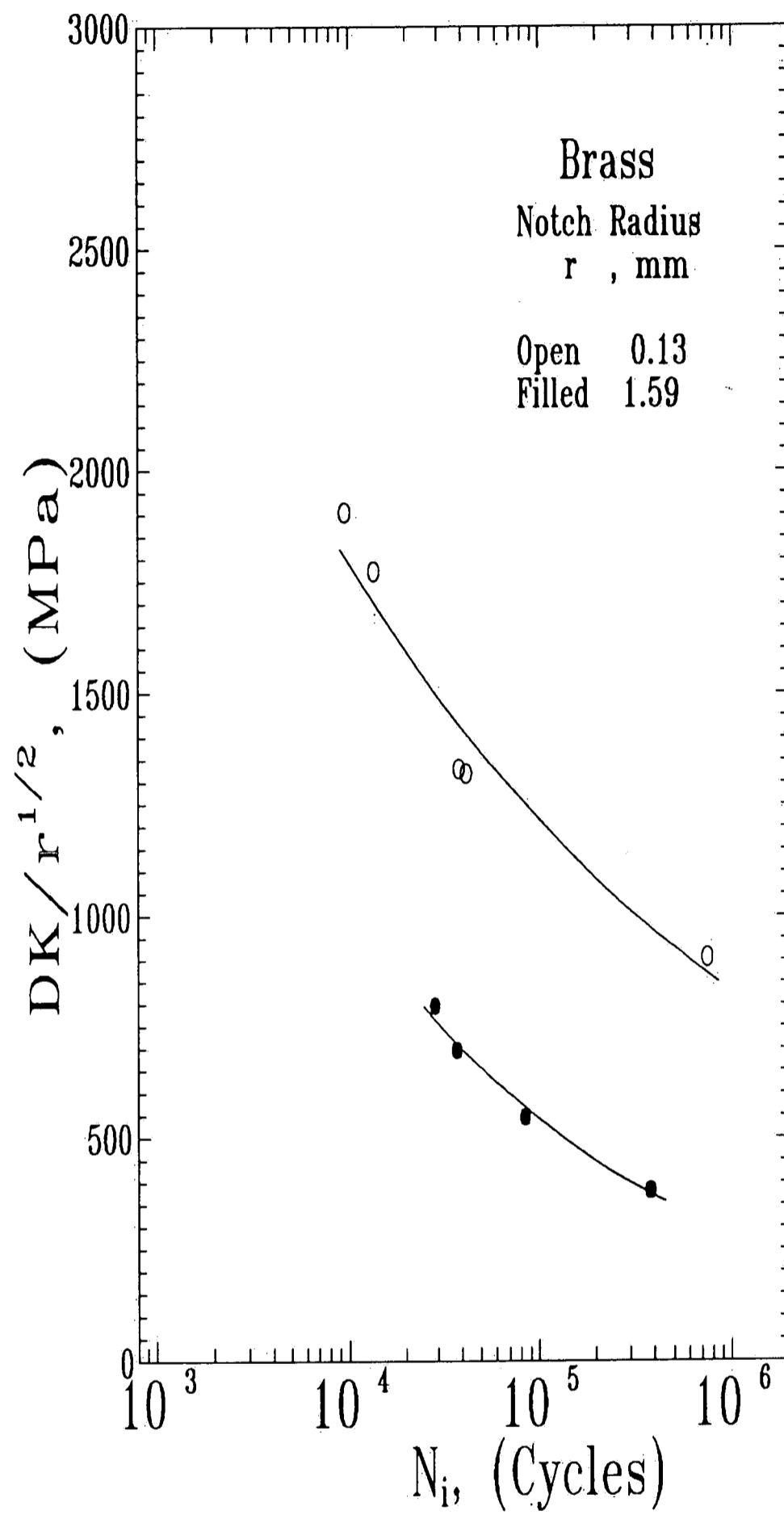


Figure 4.6- Correlating blunt and sharp notches data for brass using fracture mechanics approach.

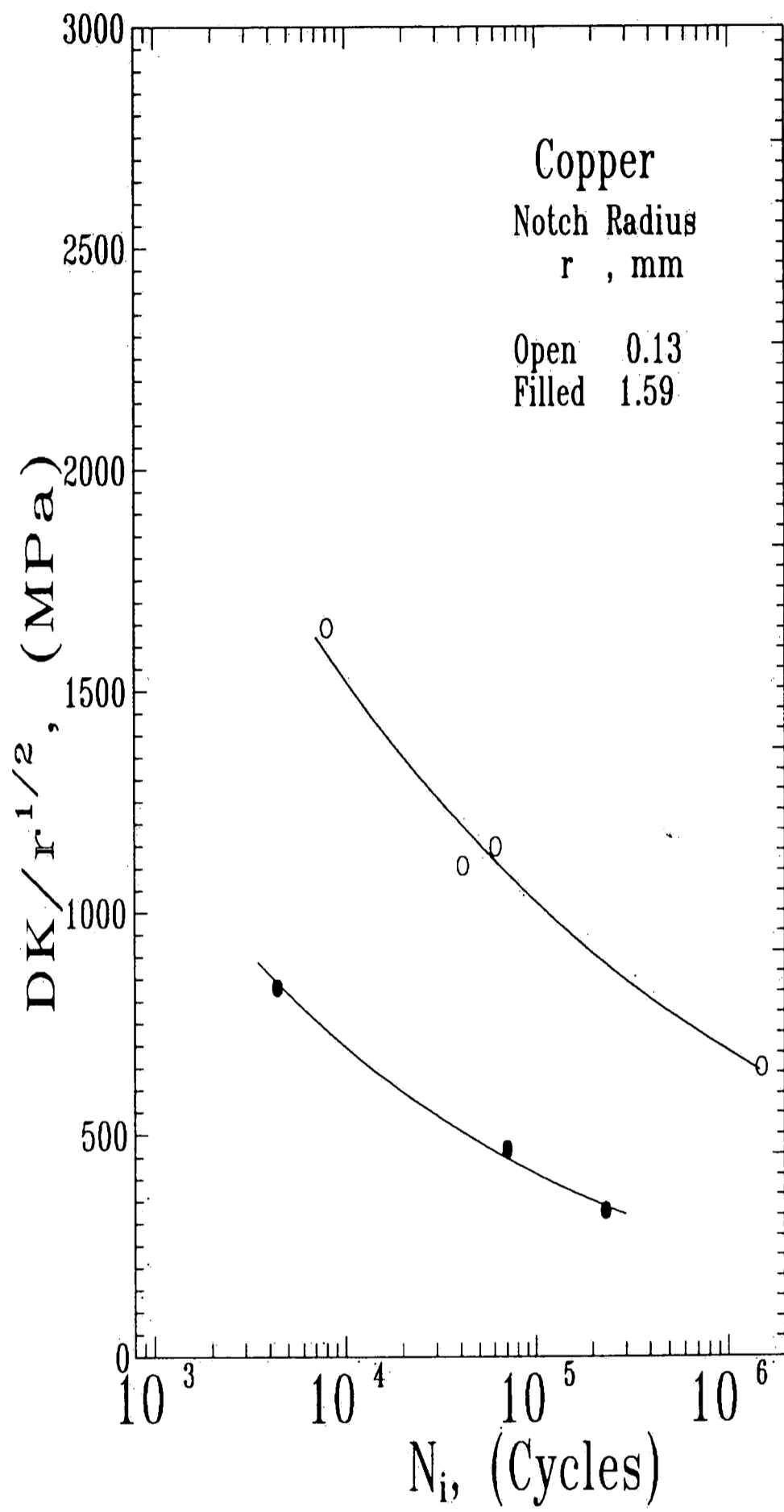


Figure 4.7- Using fracture mechanics approach to correlate fatigue crack initiation life for blunt and sharp notched specimens of copper.



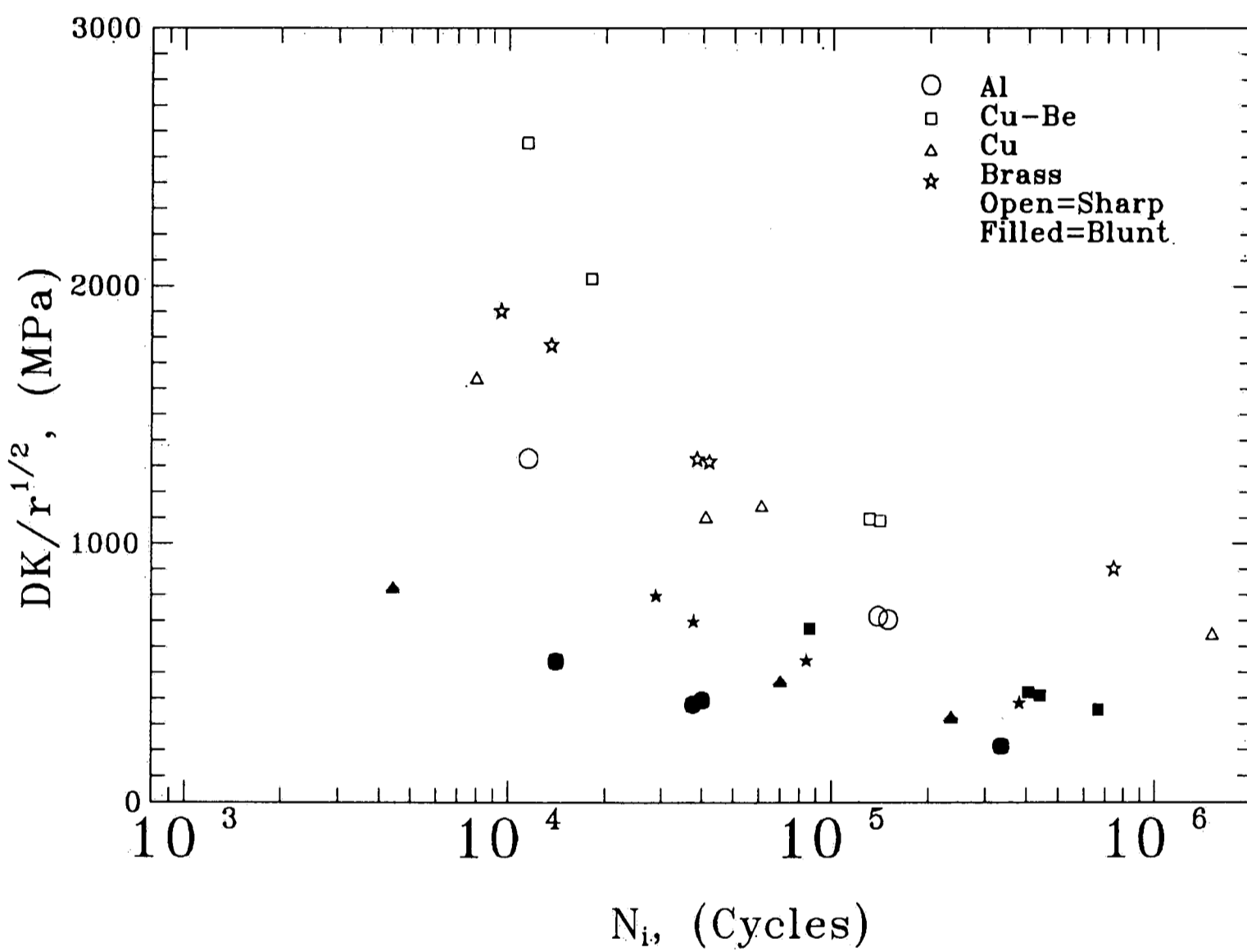


Figure 4.8- Fracture mechanics approach used to correlate fatigue crack initiation data for different materials with two different notch radii.

Assuming that general yielding did not occur in present experiment, the simplified form of Neuber's<sup>47</sup> equation, which has been developed for fatigue problems by Topper et al.<sup>4</sup>, has been employed in Figures 4.9 through 4.12 to correlate fatigue crack initiation data. As discussed in section 1.4.2, the quantity  $K_f \Delta S$  has been derived through simplifying Equation 1.7 and is taken to be equal to  $(\Delta \sigma \Delta \epsilon E)^{1/2}$ . Therefore,  $K_f \Delta S$ , if calculated properly, is a measure of local stress and strain at the notch root.

As shown in Figures 4.9 through 4.12, only fatigue crack initiation data for aluminum alloy appears to be independent of notch root radius, whereas for the other materials the data obtained for the blunt keyhole notch geometry lies above that for the sharp notch data. The quantities  $K_f$  and  $\Delta S$  were determined using Equations 1.3 and 3.2, respectively. In order to evaluate the accuracy of Equation 1.3,  $K_f$  was obtained from handbook of military standards<sup>61</sup> for different types of aluminum alloys with different notch root radii and for lives from  $10^4$  to  $10^6$  cycles, and then was compared with  $K_f$  determined by Equation 1.3. Also, the results were compared with actual data obtained from plots of notch sensitivity index versus notch radius for aluminum alloy<sup>18</sup>. The results were satisfactory and showed that the various ways to estimate  $K_f$  were within -10 to +10 percent.

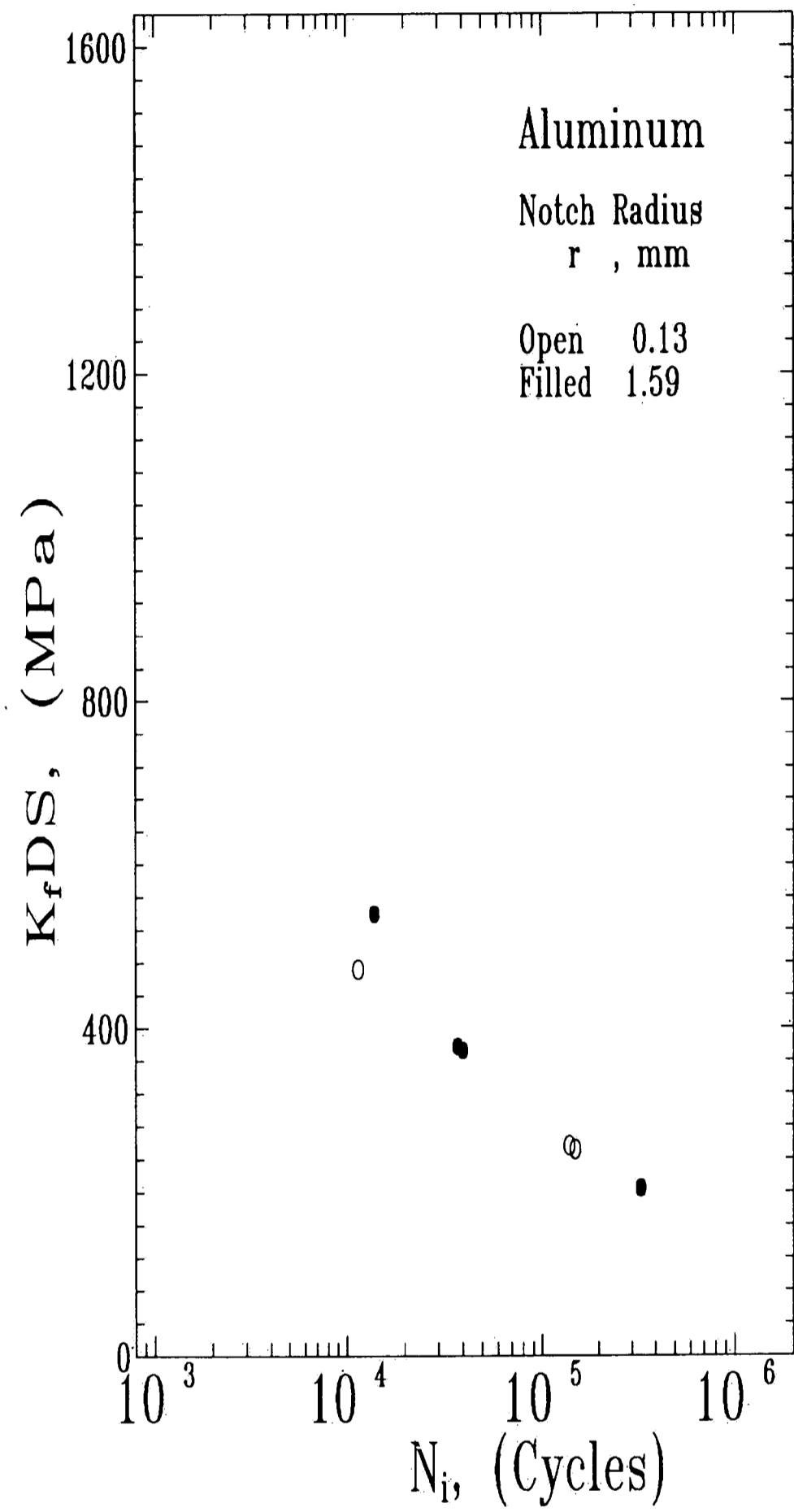


Figure 4.9- Using the local strain approach to compare fatigue crack initiation life for blunt keyhole- and sharp v-notch specimens of aluminum alloy 2024-T3.

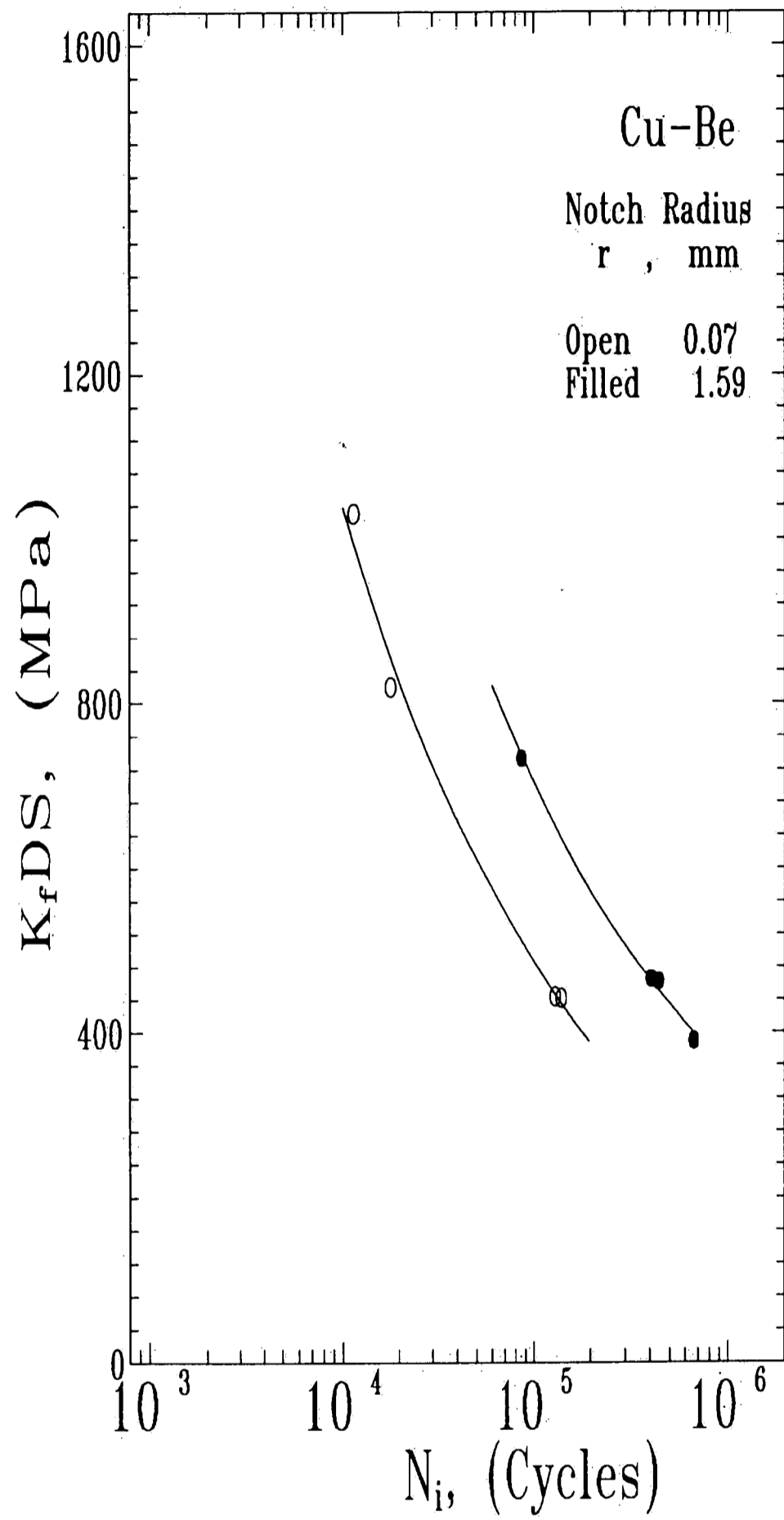


Figure 4.10- Using the local strain approach to compare fatigue crack initiation life for blunt keyhole- and sharp v-notch specimens of Cu-Be alloy 25.

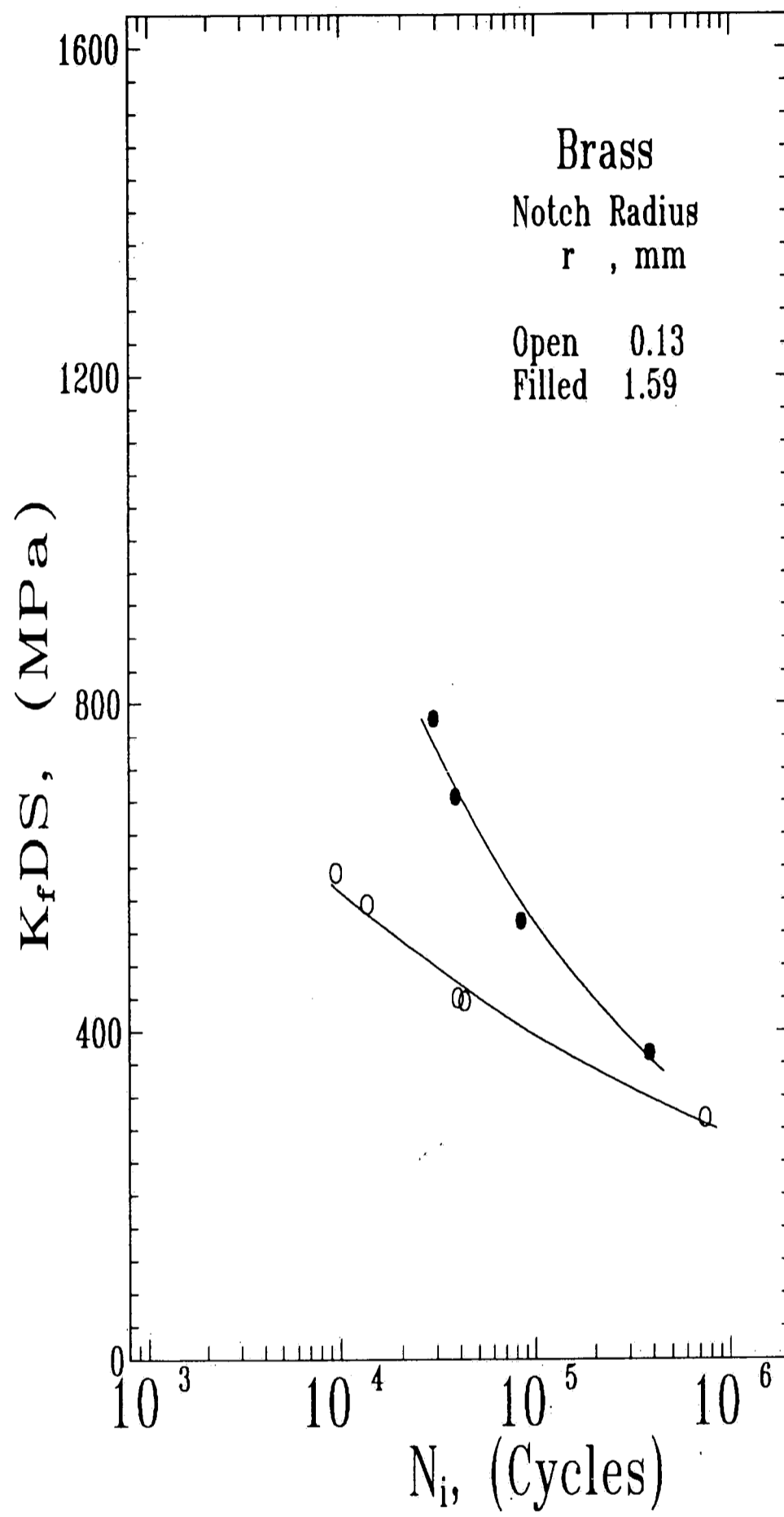


Figure 4.11- Using the local strain approach to compare fatigue crack initiation life for blunt keyhole- and sharp v-notch specimens of brass.

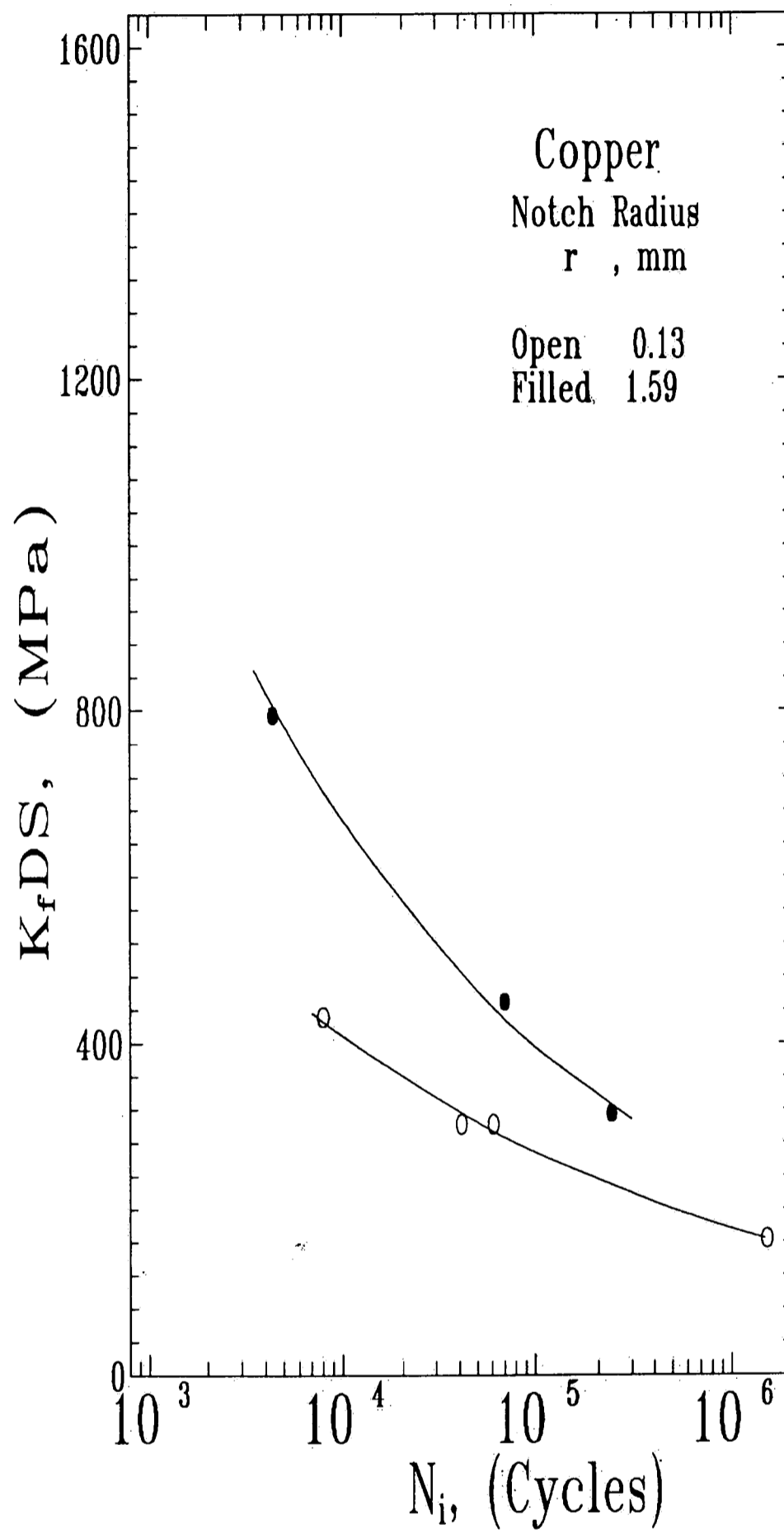


Figure 4.12- Using the local strain approach to compare fatigue crack initiation life for blunt keyhole- and sharp v-notch specimens of copper.

As shown in Figures 4.9 through 4.12, only the aluminum fatigue crack initiation data appears to be independent of notch root radius whereas for all the other materials the blunt notch data lies above the sharp notch data. This discrepancy may arise from the following reasons:

—Equation 1.3 used to determine  $K_f$  may not be valid for Cu-Be alloy, brass and copper.

—As discussed in §1.2, the quantity  $K_f$  varies with life, i.e.,  $K_f=f(N)$ , whereas in the present analysis, a constant value has been used for  $K_f$  for the whole fatigue life range.

—In low-cycle region, where the sample experiences large tensile loads, the plastically deformed material at the notch vicinity may go under compressive mean stresses. This, even for a rather short period of time, may affect the initiation life. This effect is not accounted for by this approach.

In order to compare this approach with fracture mechanics approach, all data have plotted in Figure 4.13 and in the same scale as in Figure 4.8. As shown in Figure 4.13, using this approach, blunt and sharp data falls together to a much greater extent compared with fracture mechanics results in Figure 4.8. However, as can be seen, the overall slope of  $K_f \cdot \Delta S$  versus  $N_i$  plot is low. In the other words,  $N_i$  appears to be quite insensitive to  $K_f \cdot \Delta S$ . The advantages and disadvantages of this approach were explained in §1.4.2.

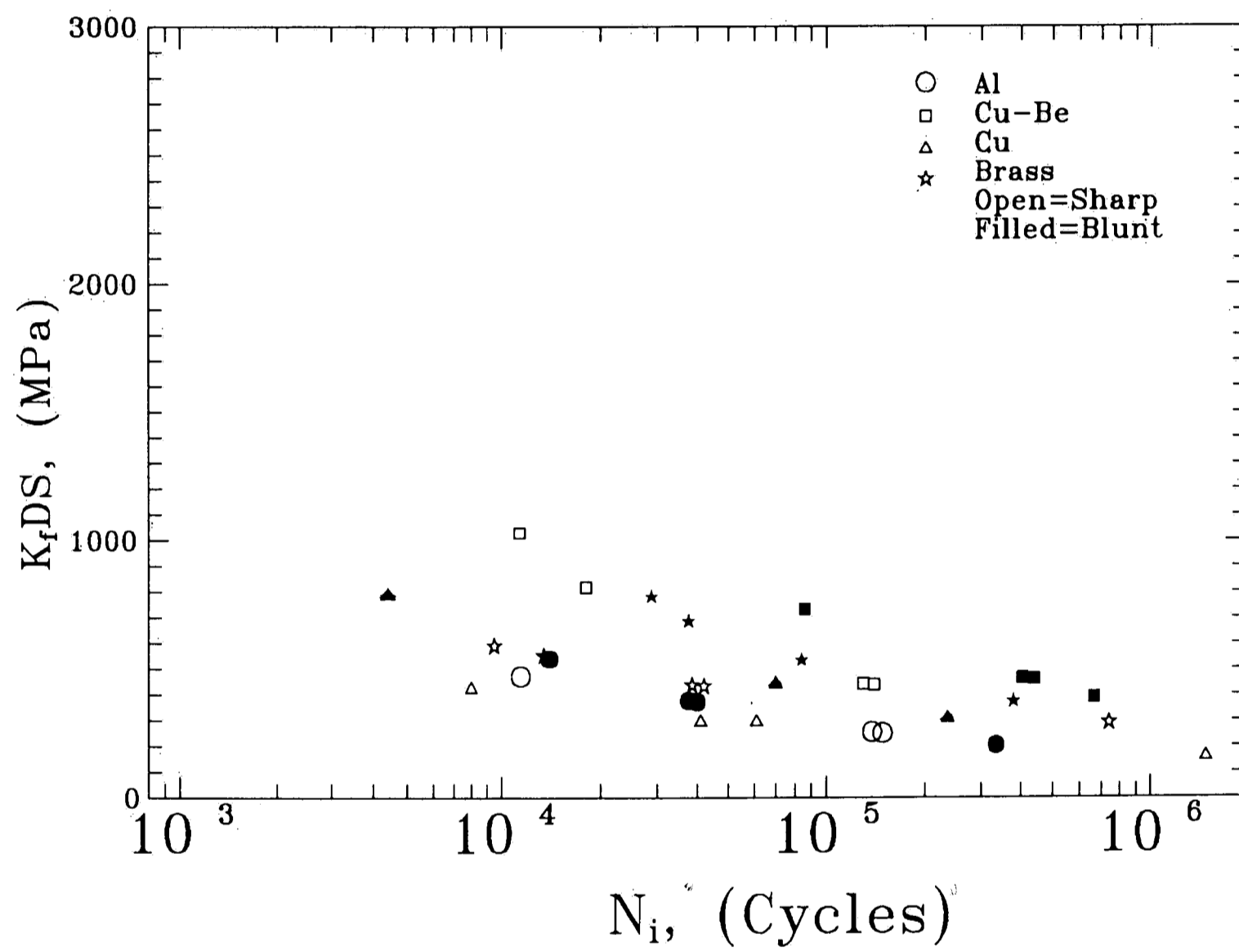


Figure 4.13- Using the local strain approach to compare fatigue crack initiation life for blunt keyhole- and sharp  $v$ -notch specimens of materials used in the present study.



#### •4.2.3— $K_t$ —Based Approaches

##### a) Maximum Elastic Stress ( $K_t\Delta S$ )

In this approach, the elastic notch stress,  $\sigma=K_t\Delta S$ , has been calculated and plotted versus fatigue crack initiation data. The quantity  $K_t$  has been calculated using the results of Wilson's<sup>42</sup> finite element analysis (Figure 4.14) and the nominal stress  $S$  from Equation 3.2. The results are shown in Figure 4.15 where, as was true for the fracture mechanics approach, the fatigue crack initiation data for sharp V-notched specimens of all materials lies above the data for blunt keyhole-notched specimens. Here again, the parameter  $K_t\Delta S$  leads to the physically unsatisfactory result that initiation occurs sooner in blunt than sharply notched specimens. The individual plots for this approach are almost the same as Figures 4.4-4.7, as explained previously.

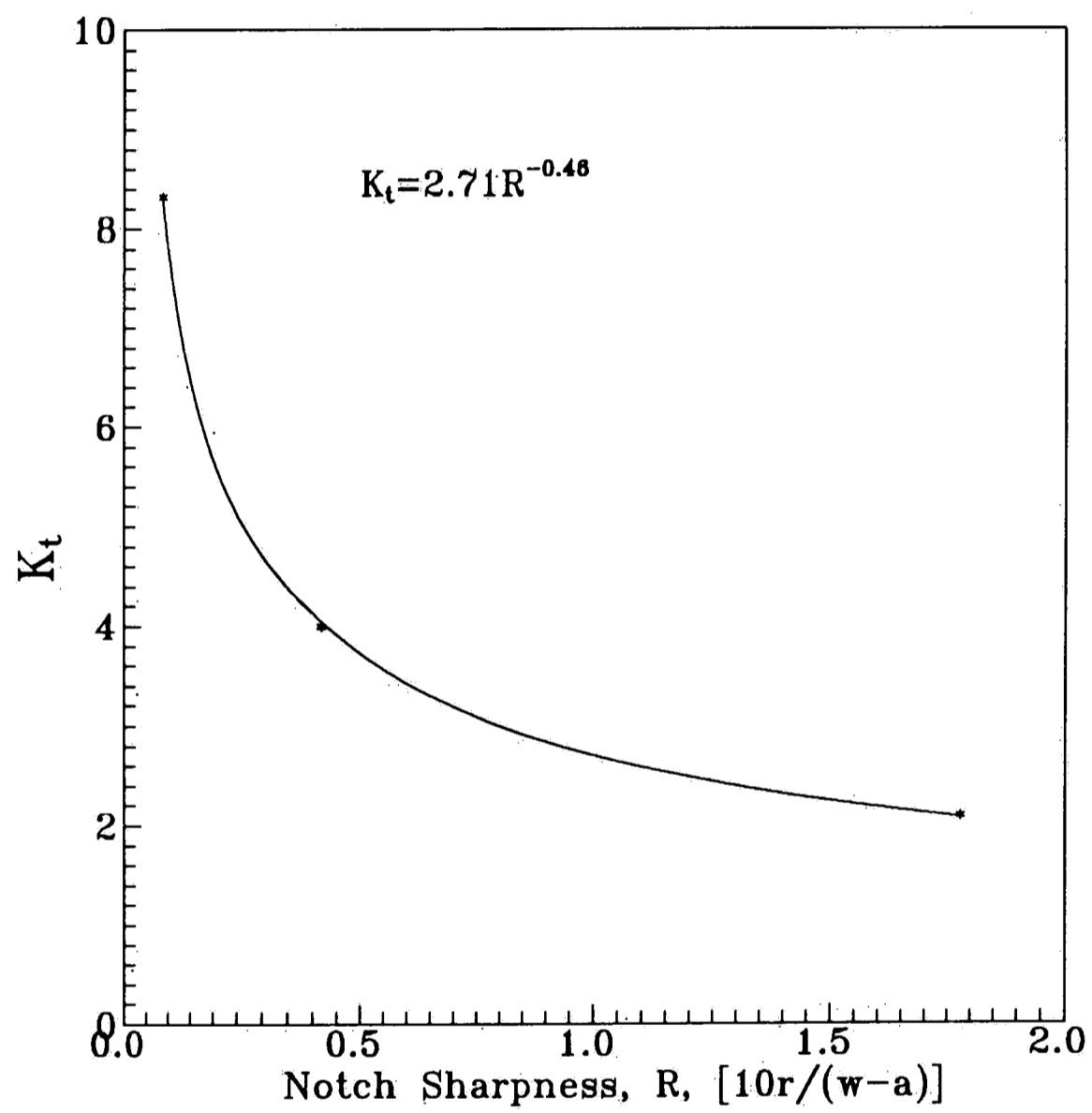


Figure 4.14.- Elastic stress concentration factor versus notch sharpness calculated by finite element method for compact tension (CT) specimens. Notch sharpness,  $R$ , is defined as  $r/(W-a)$  where  $r$ ,  $W$ , and  $a$  are notch radius, width, and crack length of CT specimens<sup>42</sup>.

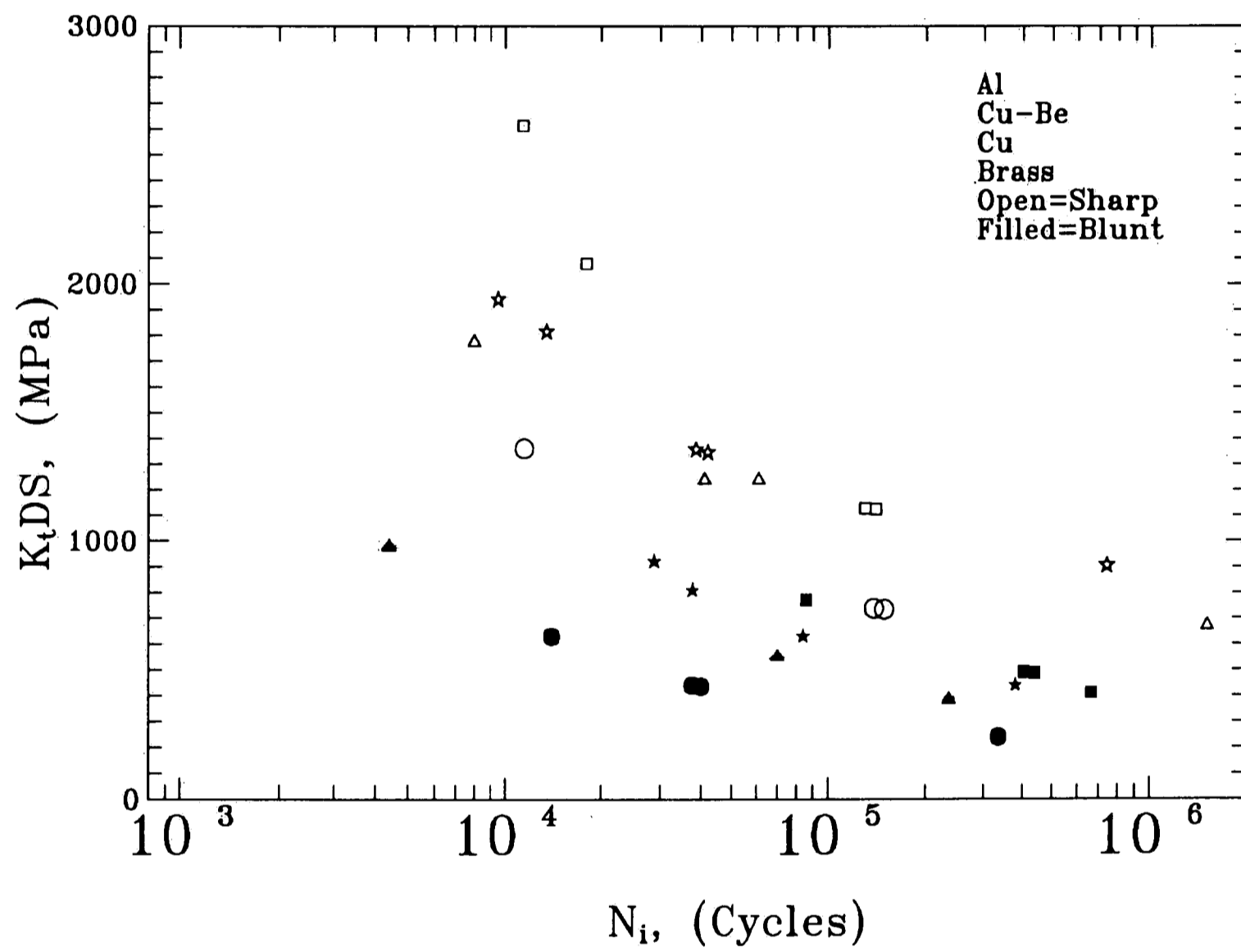


Figure 4.15- Elastic notch stress employed to correlate fatigue initiation life from blunt keyhole- and sharp v-notch specimens of materials used in the present study.

## b) $K_{td}$ Based Approach

As a result of local plasticity, approaches based on maximum theoretical stress at notch root resulted in unnecessarily conservative results, particularly for sharp notches. Also, they were not able to account for notch geometry. For this reason, Neuber's equation and  $K_f$  were employed in local strain approach to account for plasticity and geometry effects. Although  $K_f$  has been proven to be a function of life, it is used as a constant which may represent a source of error. Moreover, we saw that different  $K_f$  might be obtained for components with different geometries but with equal  $K_t S$ . In order to alleviate these problems, an alternative approach is warranted. Perhaps such an approach can be based on  $K_{td}$  where  $K_{td}$  is  $K_t$  evaluated some distance ahead of notch. This approach, as discussed previously, employs the ratio  $\frac{K_{td} \Delta S}{2E}$  to determine strain amplitude at some distance ahead of notch. It then correlates this value with fatigue crack initiation data.

Here an important question is what distance "d" ahead of the notch should be selected. Bathias and Gabra<sup>11</sup> have used the  $K_{td}$  approach to correlate fatigue crack initiation data from different notch geometries for two aluminum alloys. In their study, they have calculated the strain at distance  $d=150 \mu\text{m}$ . The reason for the choice of  $d=150 \mu\text{m}$  was stated simply that this value gave the minimum scatter of initiation data and was about the same as the grain size.

An alternative and a new rationale for distance "d" is proposed here. The idea is that fatigue damage factor defined by the  $(\Delta\sigma \cdot \Delta\epsilon)$  product may be maximized ahead of the notch root whereas the strain itself is maximized at the notch root. This can be explained by stress redistribution at notch root due to local yielding. When the applied load is reduced to its minimum level, compressive stresses are developed at the notch vicinity, as shown in Figure 4.16<sup>62,63</sup>. This stress redistribution process may cause the product  $\Delta\sigma \cdot \Delta\epsilon$  to be maximized at some distance ahead of the notch. The fact that the product  $\Delta\sigma \cdot \Delta\epsilon$  is mainly responsible for controlling fatigue damage, is reasonably

supported by the fact that this product is a measure of the strain energy density. Consequently, if the proposed rationale is correct, one might expect "d" to be dependent on both specimen geometry and material strength both of which control the extent and the magnitude of deformation.

As mentioned, Bathias' results suggest that "d" is a constant. To assess whether d is a constant, we studied the effect of the choice of d for different materials and judged the optimum value, "d<sub>opt</sub>", as being that which best describes data for both blunt and sharp notches resulting in a common dependence of  $\frac{K_{td}\Delta S}{2E}$  on N<sub>i</sub>. As an example, consider the data for 2024-T3 aluminum alloy shown in figures 4.17-4.20.

As d increases toward 200 μm, data for blunt and sharp notches approach each other and get farther apart when d exceeds 200 μm. Therefore, the optimum value is taken to be d<sub>opt</sub>=175 μm. Similar analyses have been done for the copper alloys and the optimum values are tabulated in Table 4.2. One should note that "d<sub>opt</sub>" is not actually a single value but generally falls within ± 25 μm of the values presented in Table 4.2.

Table 4.2- Optimum Distance( $d_{opt}$ ) From The Notch Root.

| Material  | $d_{opt}, \mu\text{m}$ |
|-----------|------------------------|
| Copper    | 200                    |
| Al2024-T3 | 175                    |
| Brass     | 125                    |
| Cu-Be     | 50                     |

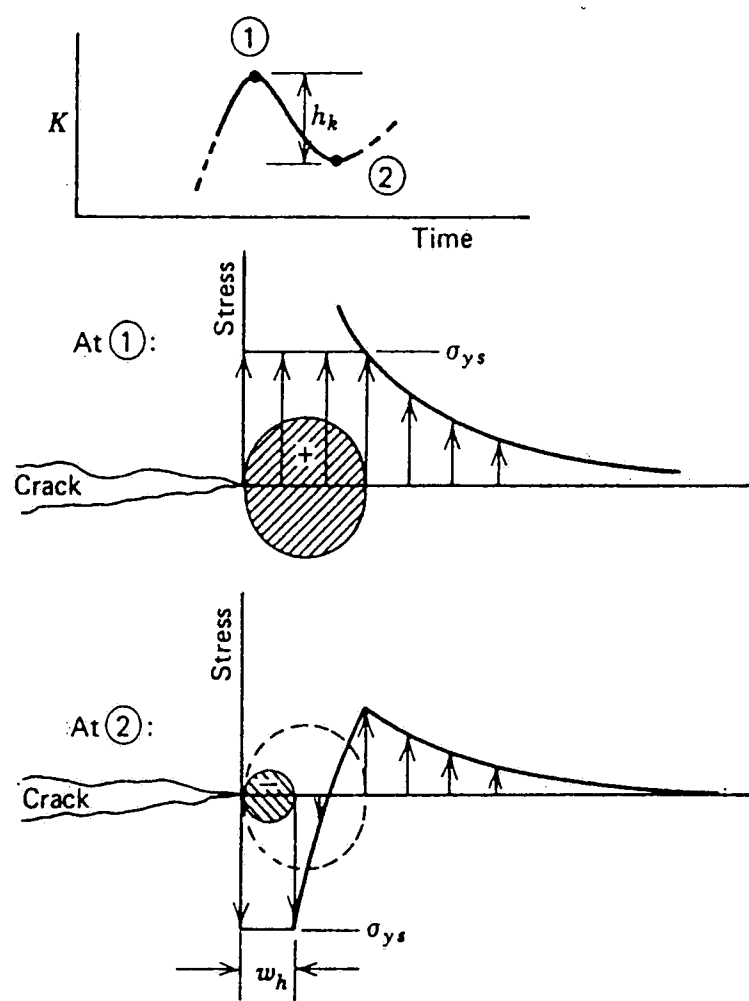
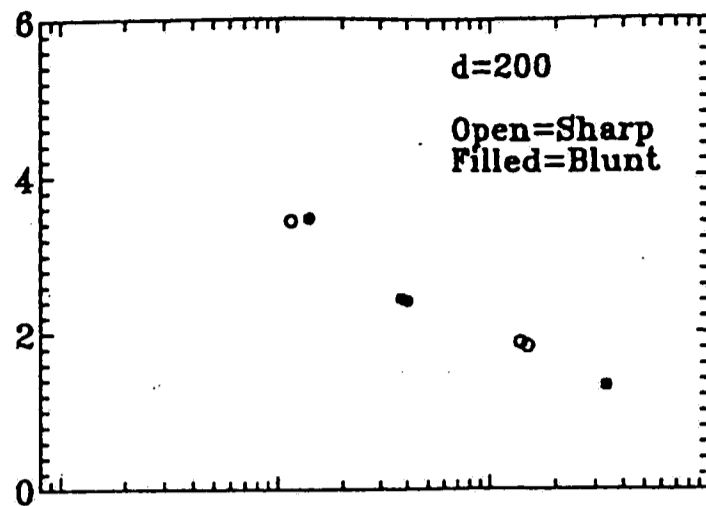
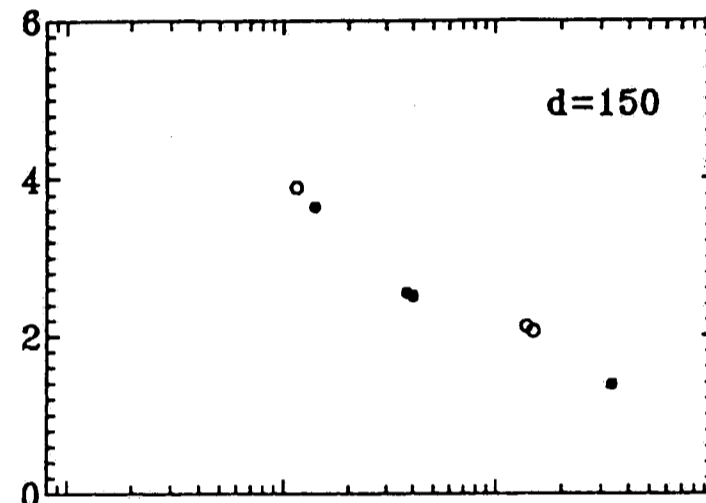


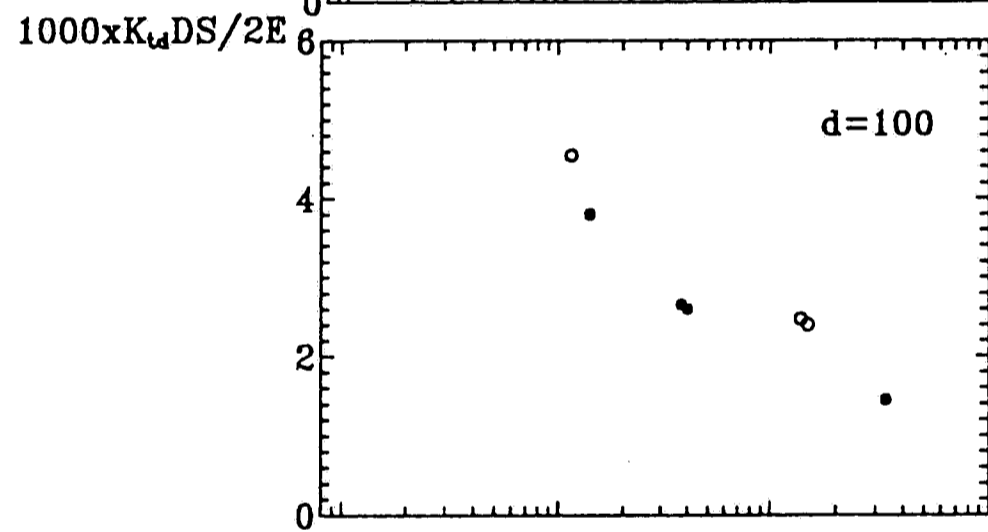
Figure 4.16- Residual compressive stress at the crack (or notch) tip.<sup>62,63</sup>



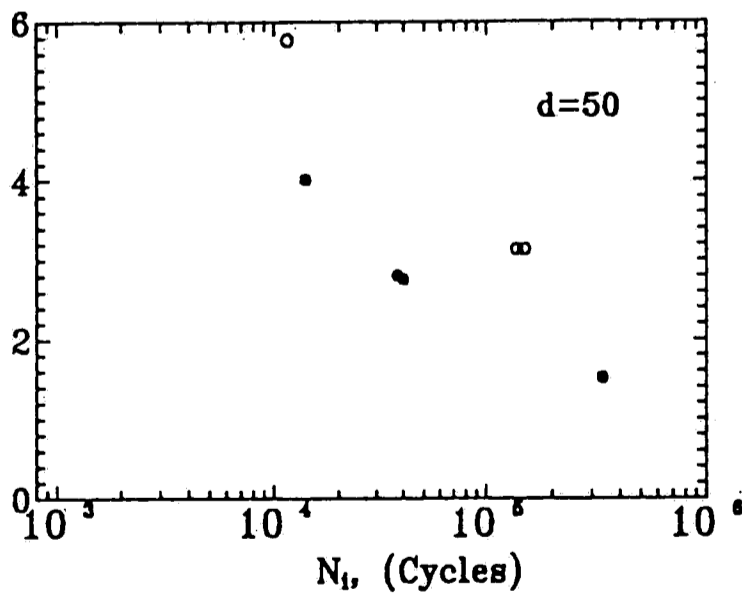
(4.17)



(4.18)



(4.19)



(4.20)

Figures 4.17-4.20- Using parameter  $\Delta\epsilon = K_{td}\Delta S/2E$  determined for distances  $d=50$ , 100, 150, and 200 micron to correlate fatigue initiation life,  $N_i$ , for blunt keyhole- and sharp  $v$ -notch specimens of aluminum alloy 2024-T3.



Since  $d_{opt}$  is not constant, and since it is expected to be a function of plastic zone size and/or yield strength, we studied its relationship to these and other material properties. The results suggest that " $d_{opt}$ " is inversely proportional to the strength (either yield or tensile) of the material. There was no relation between  $d_{opt}$  and other material properties such as grain size, stacking fault energy, modulus of elasticity, and true fracture strain. Figure 4.21 shows the inverse relation between  $d_{opt}$  and yield strength which suggests that  $d_{opt}$  relates to notch sensitivity. This relationship can be tested by using data reported in Ref. 9 for a Ti-6Al-4V alloy. This material has yield strength of 1007 MPa. Using the best fit plot in Figure 4.21, dashed line to the filled symbol,  $d_{opt}$  is determined to be about 20  $\mu\text{m}$ . Fatigue initiation data<sup>9</sup> for this alloy for blunt and sharp notched specimens with  $K_t=4.1$  and 12.6 has been plotted in Figure 4.22 employing the quantity  $\frac{K_{td}\Delta S}{2E}$ , where  $K_{td}$  is determined for  $d=20 \mu\text{m}$  where data from blunt and sharp notched specimens falls together in a common trend. As can be seen from this figure, the data from blunt and sharp notched specimens are separated for  $d=200 \mu\text{m}$  which is very different from  $d_{opt}$ .

In Figure 4.23, this model is utilized to correlate fatigue crack initiation data for both blunt and sharp notches for the materials used in the present study. All data has been determined at a distance  $d=d_{opt}$  as defined in Table 4.2. In contrast to  $\Delta K/\sqrt{\rho}$  and  $K_f\Delta S$ , this model correctly accounts for notch and nearly for material effects. In order to more properly account for material effects, the data is normalized using the ratio YS/UTS, where YS and UTS are yield and ultimate tensile strength of material, as shown in Figure 4.24. The role of another metallurgical factor which affects the fatigue life of the component is appearing in this Figure since for a given life, there is a stratification of the results with low stacking fault energy materials lying at the highest positions on the ordinate compared with the high stacking fault energy materials. The values of stacking fault energy are shown in Table 4.3. It should be noted that values for copper, brass, and aluminum alloy have been obtained directly from Ref. 64, whereas the value for Cu-Be alloy has been indirectly determined using Refs. 64 and 65. As mentioned previously, stacking fault energy controls the ease of cross-slip, as well as the type of deformation topography observed during fatigue<sup>28</sup>.

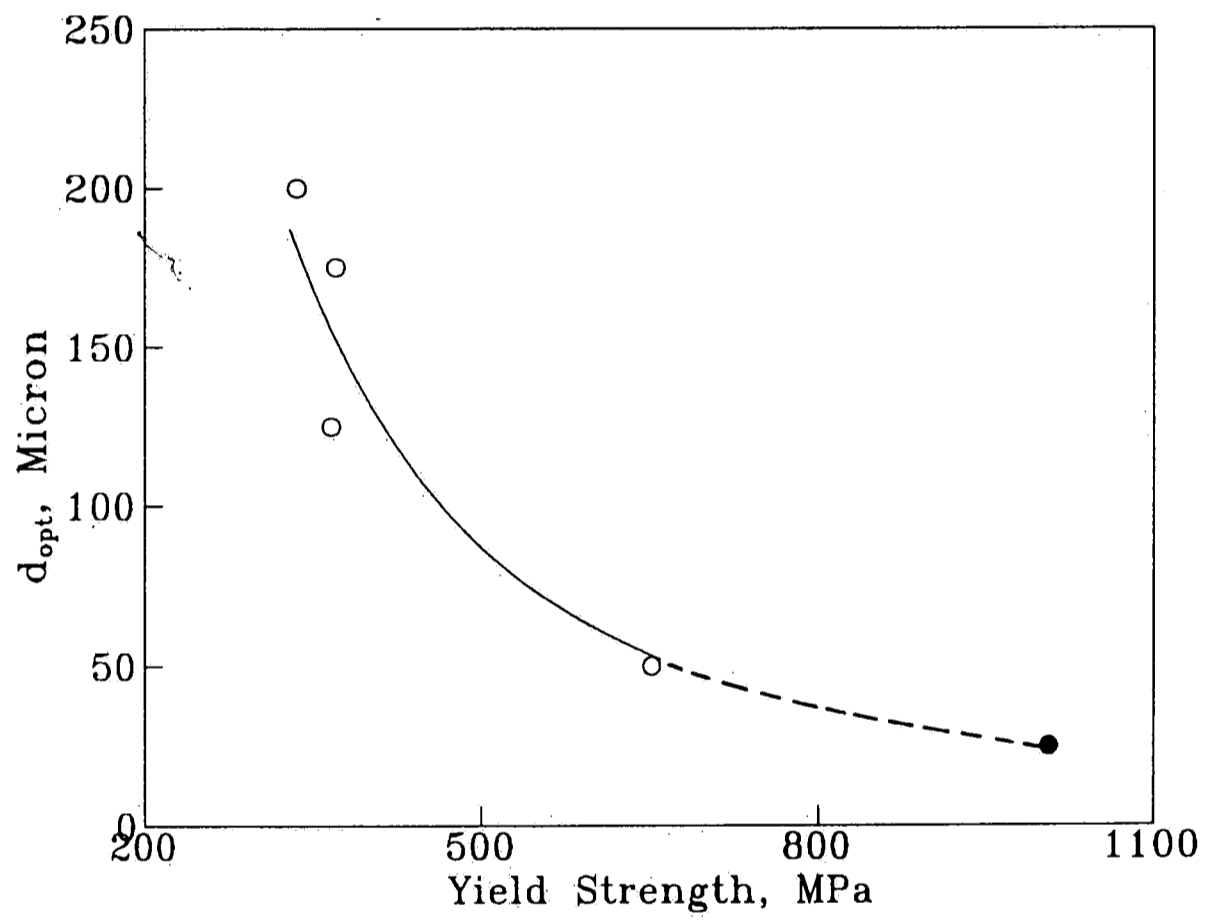


Figure 4.21- Optimum distance from the notch root " $d_{opt}$ " versus yield strength for materials used in this study along with Ti-6Al-4V alloy<sup>9</sup> with yield strength of 1007 MPa.

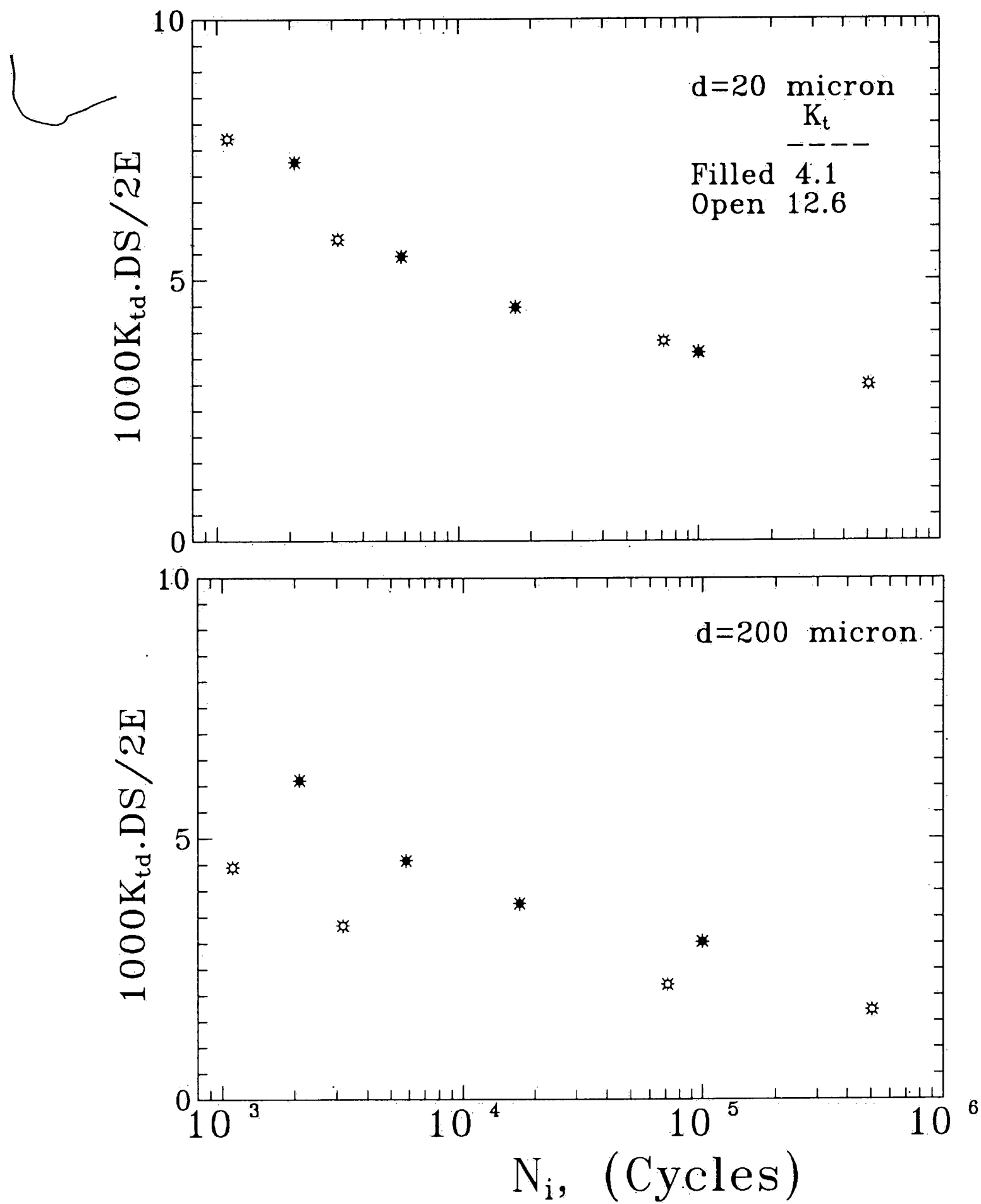


Figure 4.22- Using parameter  $\Delta\epsilon = K_{td}\Delta S/2E$  to correlate fatigue initiation life from blunt keyhole- and sharp v-notch specimens of a Ti-6Al-4V alloy. Initiation life data obtained from Ref. 9. The quantity  $K_{td}$  was calculated for  $d_{opt} = 20$  and  $d = 200\mu m$ .

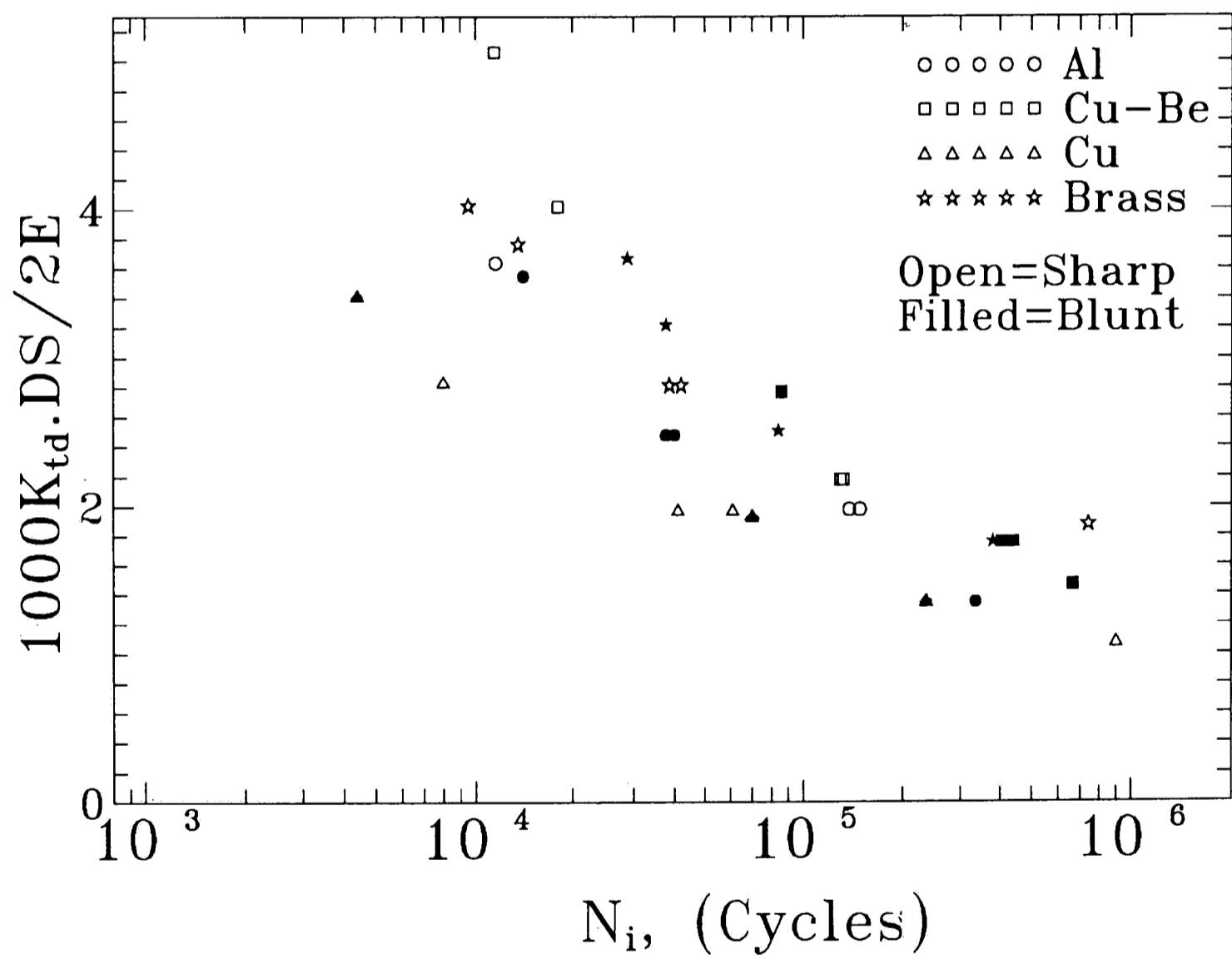


Figure 4.23- Parameter  $\Delta\epsilon = K_{td}\Delta S/2E$  used to correlate fatigue initiation life from blunt keyhole- and sharp v-notch specimens of materials investigated. The quantity  $K_{td}$  was calculated for  $d = d_{opt}$  as defined in Table 4.2.

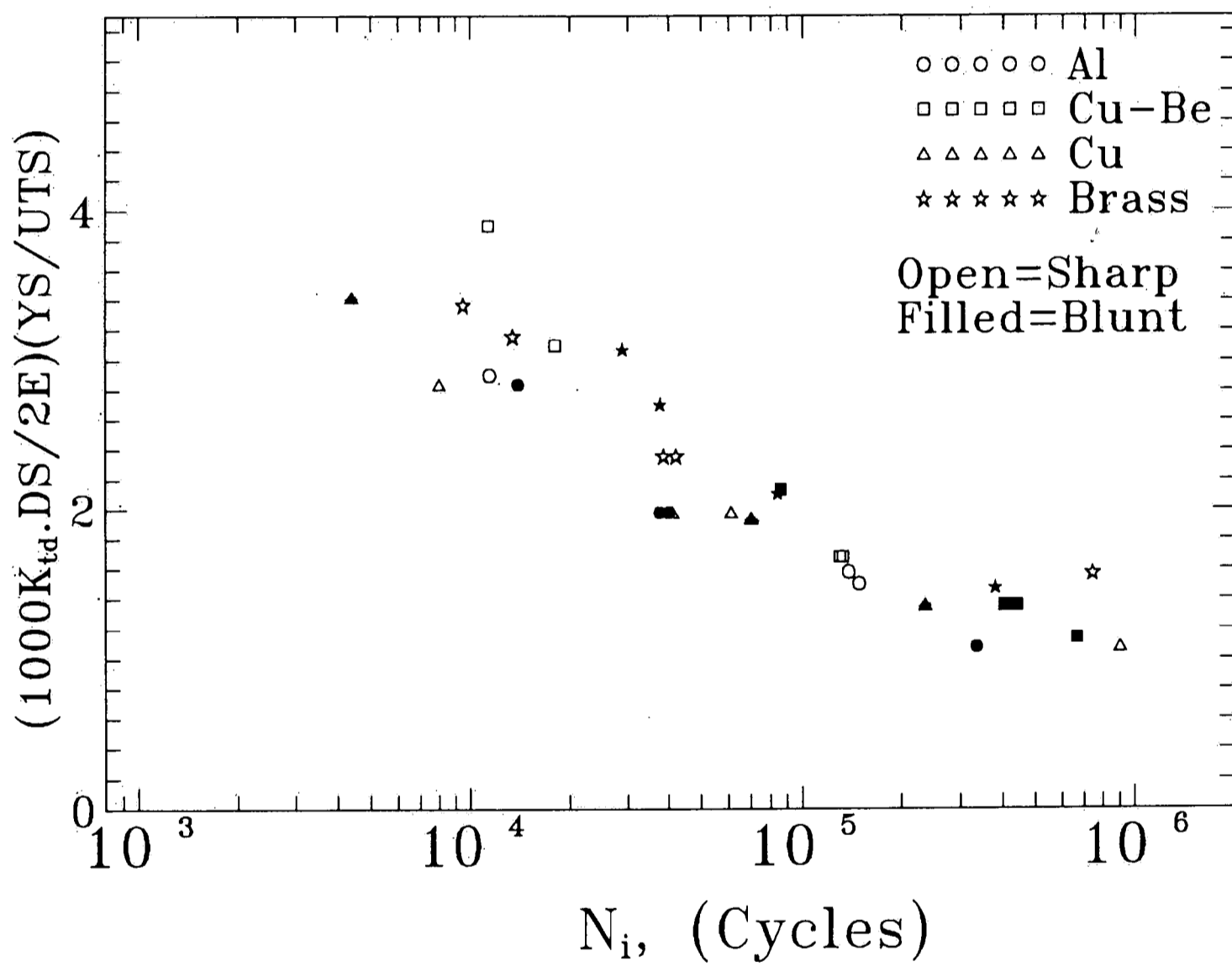


Figure 4.24- The parameter  $\Delta\epsilon = K_{td}\Delta S/2E$  normalized by the ratio  $YS/UTS$  to correlate fatigue initiation life for materials investigated.  $YS$  and  $UTS$  are yield and ultimate tensile strength of the materials, respectively. The quantity  $K_{td}$  calculated for  $d=d_{opt}$  as defined in Table 4.2.

Table 4.3- Stacking Fault Energy " $\gamma_{SF}$ " for the Materials Investigated.

| Material       | $\gamma_{SF}$<br>mJ/m <sup>2</sup> | Temperature<br>C° | Ref. # |
|----------------|------------------------------------|-------------------|--------|
| Cu-Be alloy 25 | 10-20                              | 25                | 66, 67 |
| Brass(70-30)   | ≈14                                | 25                | 66     |
| Copper         | ≈78                                | 25                | 66     |
| Aluminum       | ≈120                               | 25                | 66     |

The lower and upper limit of the fatigue crack initiation data obtained from this study along with other data from literature have been correlated using this model, as shown in Figure 4.25. The data for aluminum alloys are well within the range predicted by present work. These data has been obtained from compact tension specimens with  $K_t=2.1$  and  $K_t=6.7$  at stress ratio  $R=0.01$ . However, it seems that this model underestimates initiation life for Ti alloy whereas it overestimates initiation life for the steel alloys. These discrepancies might be related to several factors such as geometry and mean stress effects.

In summary, this model more correctly explains both material and notch effects when compared with the local strain or  $\Delta K/\sqrt{\rho}$  approaches. This is especially evident when the data are normalized by the ratio of  $YS/UTS$ . The quantity  $K_{td}$  determined for an optimum distance from the notch root appears to work much better than  $K_f$  calculated from the empirical equations. The strength of the material can be used to estimate the optimum distance by utilizing the relation given in Figure 4.21.

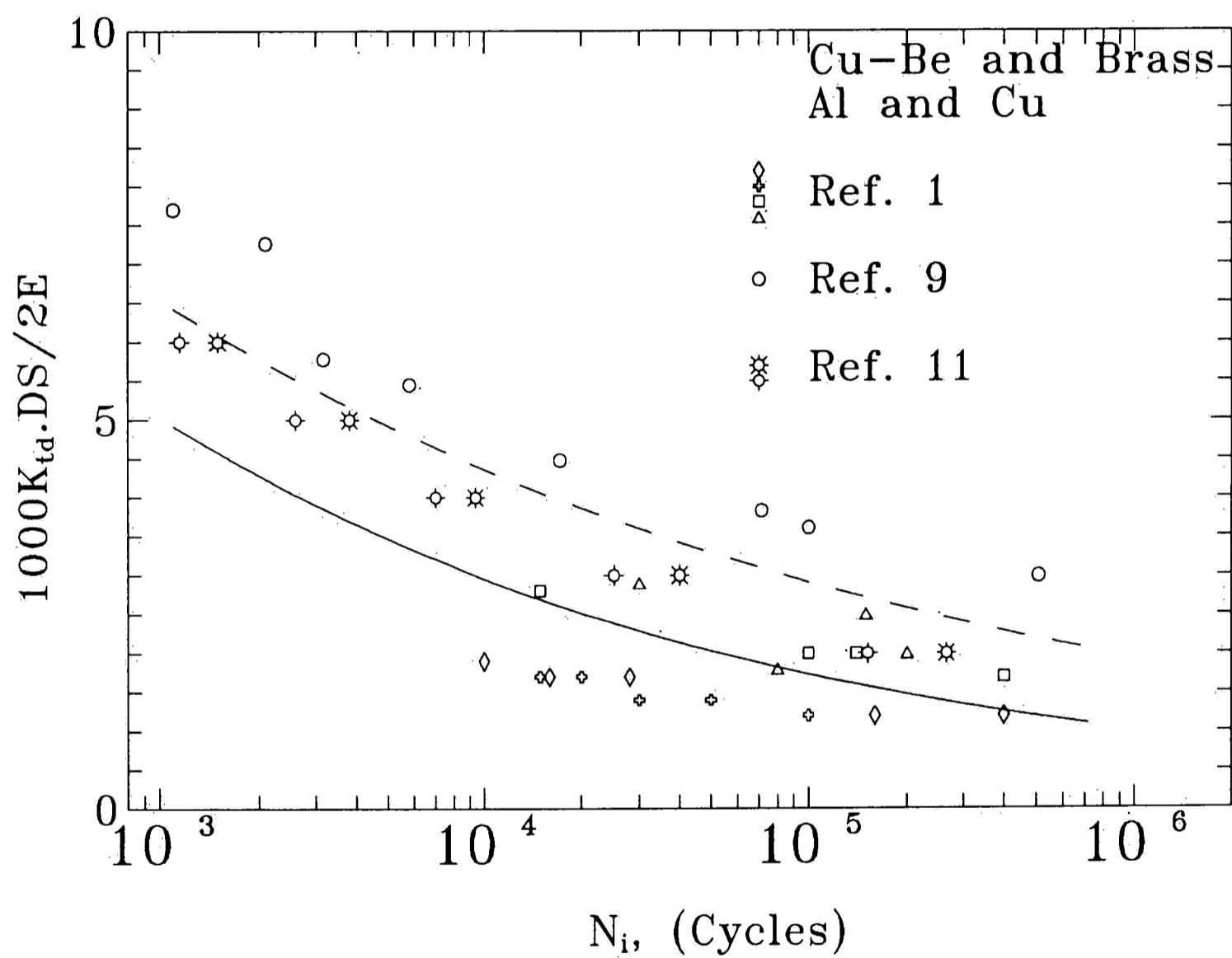


Figure 4.25- Strain amplitude determined from  $K_{td} \Delta S / 2E$  used to correlate fatigue initiation life for the materials employed in the present study and for materials from References no. 1, 9, 11.  $K_{td}$  was calculated for  $d=d_{opt}$ .



#### •4.3-Initiation and Propagation Contribution to Fatigue Life

An important question from a fatigue design viewpoint is how much of life is spent in the initiation and propagation components. In other words, the question is whether these two stages should be used independently for life prediction, or the results should be combined. The answer, as described previously, is that it depends on the service condition, component geometry, material fabrication process, and material itself. Several models<sup>48,66-73</sup> have been proposed during the past three decades to describe how these two components depend on the total life. The plots of some of these models along with the blunt and sharp data from present study are shown in Figure 4.26. As seen data from blunt notches appears to follow model number (4.1), whereas the sharp notch data seems to be consistent with model numbers (4.2) and (4.3). Model number (4.1) proposed by Manson<sup>48</sup> gives the following relation between  $N_i$  and  $N_f$ .

$$N_i = N_f - 14N_f^{0.6} \quad (4.1)$$

Models number (4.2)<sup>72</sup> and (4.3)<sup>73</sup> describe the relation between  $N_i$  and  $N_f$ , respectively, as follows:

$$N_i = 0.016N_f^{1.31} \quad (4.2)$$

$$N_i = 0.0014N_f^{1.42} \quad (4.3)$$

For both groups of data, i.e. blunt and sharp notches,  $N_i/N_f$  appears to be quite independent of  $N_f$  in range  $10^4$  to  $10^6$  cycles. As can be seen from this Figure, about 30% of the total life is spent in initiating the crack for sharp notch specimens whereas for blunt notch specimens, initiation life covers about 75% of the total life of the component.

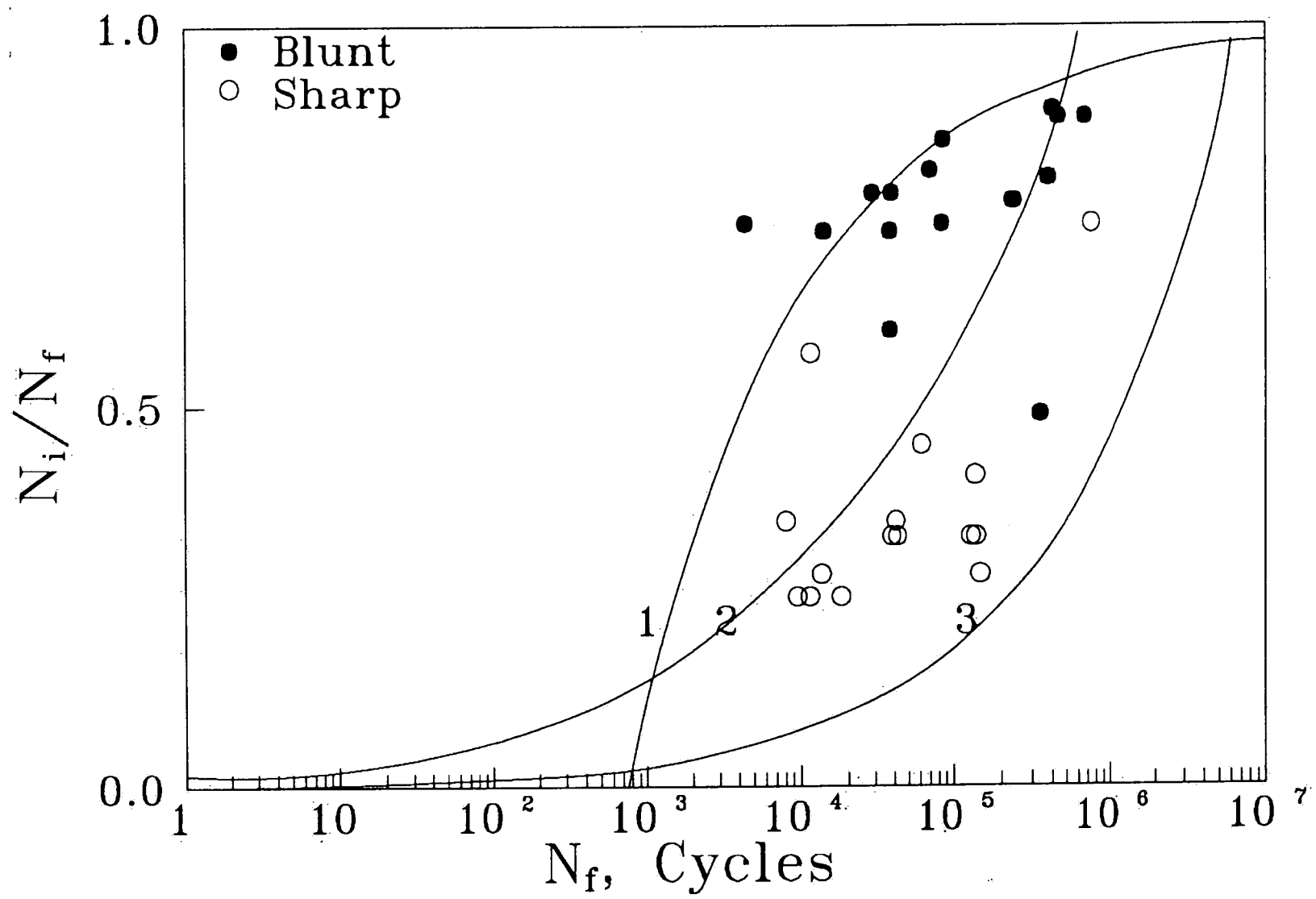


Figure 4.26- Plots of proposed initiation-propagation models along with data from present study.

## V-CONCLUSION

Fatigue crack initiation was studied for 2024-T3 aluminum, 70-30 brass, Cu-Be alloy 25, and commercially pure copper. Blunt-keyhole and sharp-V notch compact tension specimens were loaded with a minimum to maximum stress ratio of 0.1. Based on the results of these tests, the conclusions are:

1. The parameter  $\Delta\epsilon = \frac{K_{td} \cdot \Delta S}{2E}$  was used to correlate fatigue initiation data from blunt and sharp notches and appears to be a better descriptor than the other approaches for explaining for both notch and material effects.  $K_{td}$  is the elastic stress concentration factor,  $K_t$ , evaluated at a distance  $d_{opt}$  ahead of the notch. The distance " $d_{opt}$ " is shown to be inversely related to material strength. A further modification of this approach by the  $\frac{YS}{UTS}$  improves the correlation with cycles to crack initiation.
2. The local strain approach did not combine data for blunt and sharp notches for materials other than aluminum. The principal difficulty seems to stem from the fact that the utility of this approach depends on the accuracy of  $K_f$ .  $K_f$  is not always available in literature and empirical relations are not necessarily valid for all materials.
3. The parameter  $\frac{\Delta K}{\sqrt{\rho}}$  may be used to estimate  $K_t$  only for crack-like notch geometries. For blunt notches, this approach does not lead to physically acceptable results, i.e., it predicts that initiation life for blunt notches is shorter than that for sharp notches.
4. In the range  $10^4$ - $10^6$  cycles, about 30% of the total life is spent in initiating the crack for sharp notch specimens whereas for blunt notch specimens, initiation life covers about 75% of the total life of the component.
5. Using  $\epsilon = \frac{K_{td} \cdot S}{E}$ , the strain was calculated for blunt copper for  $d=160 \mu\text{m}$  ahead of the notch. For nominal stresses  $S=140, 200, 350 \text{ MPa}$ , the computed strain appeared to be consistent with Moire fringe measurements within  $\pm 10\%$  (Figure 4 in Appendix).

## REFERENCES

- (1). G. A. Miller and H. S. Reemsynder, "Strain-Cycle Fatigue of Sheet and Plate Steels III: Tests of Notched Specimens," SAE paper no. 830176, Society of Automotive Engineers, Warrendale, PA, 1983, pp.43-53.
- (2). N. E. Dowling, "A Discussion of Methods for Estimating Fatigue Life," in "Proceedings of the SAE Fatigue Conference, P-109," Society of Automotive Engineers, Warrendale, PA, 1982, pp. 161-174.
- (3). D. V. Nelson and H. O. Fuchs, "Predictions of Cumulative Fatigue Damage using Condensed Load Histories," in "Fatigue Under Complex Loading: Analyses and Experiments," R. M. Wetzel, ed., Society of Automotive Engineers, Warrendale, PA, 1971, pp. 163-188.
- (4). T. H. Topper, R. M. Wetzel and J. Morrow, "Neuber's Rule Applied to Fatigue of Notched Specimens," Journal of Materials, Vol. 4, March 1969, pp. 200-209.
- (5). K. N. Smith, P. Watson and T. H. Topper, "A Stress-Strain Function for the Fatigue of Metals," Journal of Materials, Vol. 5, December 1970, pp. 767-778.
- (6). H. S. Reemsynder, "Evaluating the Effect of Residual Stresses on Notched Fatigue Resistance," in "Materials, Experimentation, and Design in Fatigue - Proceedings of Fatigue 81," Westbury Press, Guildford, England, 1981, pp.273-295.
- (7). T. Seeger and P. Heuler, "Generalized Application of Neuber's Rule," Journal of Testing and Evaluation, Vol. 8, 1980, pp. 199-204.
- (8). J. M. Barsom and R. C. MacNicol, Fracture Toughness and Slow-Stable Cracking, ASTM STP 559, 1974, pp. 183-204.

- (9). G. R. Yoder, L. A. Cooley, and T. W. Crooker, "Observations on a Fracture Mechanics Approach to Fatigue Crack Initiation in Ti-6Al-4V," Fracture Mechanics: 60th Symposium, ASTM STP 868, 1985, 392-405.
- (10). C. Bathias, M. Gabra and D. Aliaga, "Low Cycle Fatigue Damage Accumulation of Aluminum Alloys," International Symposium on Low Cycle Fatigue, FIRMINY, France, ASTM STP 770, 1980, pp.23-44.
- (11). M. Gabra and C. Bathias, "Fatigue Crack Initiation In Aluminum Alloys Under Programmed Block Loading," Fatigue Engng. Mater. Struct., Vol. 7, No.1, 1984, pp. 13-27.
- (12). H. J. Gough, Am. Soc. Test. Mater. Proc., Vol. 33, pt. 2, 1933, pp.3-114.
- (13). W. A. Wood, Phil. Mag., 3, 1958, p.692.
- (14). S. S. Manson and M. H. Hirshberg, US Nat. Aeronaut. Space Admin. Rep. (NASA Tn 3146), 1967.
- (15). N. E. Dowling, ASTM STP 677, 1979, p.247.
- (16). R. E. Peterson, Stress Concentration Factors, Wiley, NY, 1974.
- (17). N. F. Frost, K. J. Marsh, and L. P. Pook, Metal Fatigue, Oxford, 1974.
- (18). J. A. Collins, Failure of Materials in Mechanical Design, Wiley, 1981.
- (19). R. Bagheri, Master Thesis, Lehigh University, 1991.
- (20). W. M. Murray, Fatigue and Fracture of Metals, MIT Press, 1952.
- (21). H. Neuber, Theory of Notch Stress, J. W. Edwards, Ann Arbor, Mich., 1946.

- (22). R. E. Peterson, "Notch Sensitivity," Chapter 13 in "Metal Fatigue," G. Sines and J. L. Waisman, Editors, McGraw-Hill, NY, 1959.
- (23). L. F. Coffin, *Advances in Fatigue Science and Technology*, Kluwer Academic Publishers, 1989, pp. 417-444.
- (24). A. R. Jack and A. T. Price, *Int. J. of Frac. Mech.*, 6, No. 4, 1970, p.401.
- (25). H. S. Reemsnyder, *Society for Automotive Engineers Transactions*, 88, 1979, p.1905.
- (26). C. Massonnet, *Proc. Am. Soc. Test. Mater.*, 56, 1956, p.954.
- (27). ASM, *Metals Handbook*, 8th ed., Vol. 1, Properties and Selection of Metals, ASM, Novelty, OH, 1961, p.217.
- (28). G. A. Miller, D. H. Avery, and W. A. Backofen, *Transactions of the Metallurgical Society of AIME, TMSAA*, Vol. 236, 1966, pp.1667-1673.
- (29). J. C. Grosskreutz, *Metallurgical Trans.*, Vol. 3, May 1972, pp. 1255-1262.
- (30). A. W. Thompson and W. A. Backofen, *Acta Met.*, Vol. 19, July 1971, pp. 597-606.
- (31). R. G. Forman, *Engineering Fract. Mech.* Vol. 4, No. 2, 1971, pp. 333-345.
- (32). W. G. Clark, *ASTM STP 559*, American Society for Testing and Materials, Philadelphia, 1974, pp. 205-224.
- (33). S. T. Rolfe and J. M. Barsom, *Fracture and Fatigue Control in Structures*, 2nd ed., Prentice-Hall, Englewood Cliffs, NJ, 1987, pp. 272-274.

- (34). S. T. Rolfe, R. A. May, A. Stuber, in WRC Bulletin No. 243, Welding Research Council, NY, Nov. 1978, pp.1-26.
- (35). B. L. Braglia, R. W. Hertzberg, and R. Roberts, in Fracture Mechanics, ASTM STP 677, American Society for Testing and Materials, Philadelphia, 1979, pp. 290-302.
- (36). K. Saanouni and C. Bathias, Eng. Frac. Mech., Vol. 16, No. 5, 1982, pp. 695-706.
- (37). T. A. Prater and L. F. Coffin, ASTM STP 801, American Society for Testing and Materials, Philadelphia, 1983, pp.423-444.
- (38). S. R. Novak, ASTM STP 801, American Society for Testing and Materials, Philadelphia, 1983, pp.26-63.
- (39). G. R. Irwin, in Structural Mechanics: Proc. of the First Symp. on Naval Structural Mechanics, J. N. Goodier and N. J. Hoff, Eds., Pergamon Press, NY, 1960, pp. 557-594.
- (40). M. Creager, Master of Science Thesis, Lehigh Univ., Bethlehem, PA, 1966.
- (41). S. T. Rolfe and J. M. Barsom, Fracture and Fatigue Control in Structures, 2nd ed., Prentice-Hall, Englewood Cliffs, NJ, 1987, p. 254.
- (42). W. K. Wilson, Journal of Pressure Vessel Technology, Nov. 1974, pp. 293-298.
- (43). A. Baus, H. P. Lieurade, G. Sanz and M. Truchon, ASTM, Stp 631, American Society for Testing and Materials, 1977, pp. 96-111.
- (44). T. H. Topper, B. I. Sander, and JoDean Morrow, Journal of Materials, JMLSA, Vol. 4, No. 1, March 1969, pp. 189-199.

- (45). F. V. Lawrence, Jr., R. J. Mattons, Y. Higashida, and J. D. Burk, "Estimating the Fatigue Crack Initiation Life of Welds," ASTM STP 648, American Society for Testing and Materials, 1978, pp. 134-158.
- (46). A. L. Snow, B. F. Langer, and W. G. Gibbons, *Journal of Materials*, JMLSA, Vol. 5, No. 3, Sept. 1970, pp. 719-737.
- (47). H. Neuber, "Theory of Stress Concentration for Shear- Strained Prismatic Bodies with Arbitrary Nonlinear Stress- Strain Law," *Transactions of the ASME*, Dec. 1961, pp. 544-550.
- (48). S. S. Manson, *Exp. Mech.*, Vol. 5., No. 7, 1965, p.193.
- (49). S.S. Manson and M. H. Hirschberg, "Fatigue: An INterdisciplinary Approach," Syracuse Univ. Press, Syracuse, NY, 1964, p.133.
- (50). G. E. Dieter, *Mechanical Metallurgy*, McGraw- Hill, 3rd ed., 1986, p. 392.
- (51). F. Lorenzo and C. Laird, *Mater. Sci. Eng.*, Vol. 62, 1984, pp. 206-210.
- (52). T. H. Topper, B. I. Sander and JoDean Morrow, "Cumulative Fatigue Damage Under Cyclic Strain Control," *Journal of Materials*, Vol. 4, No. 1, March 1969, pp. 189-199.
- (53). M. M. Hammouda, R. A. Smith, and K. J. Miller, *Fatigue of Eng. Materials and Structures*, Vol. 2, 1979, pp. 139-154.
- (54). D. Socie, "Variable Amplitude Fatigue Life Estimation Models," SAE Paper No. 830689, Society for Automotive Engineers, Warrendale, PA, 1982, pp.133-151.
- (55). H. S. Reemsnyder, "Constant Amplitude Fatigue Life Assessment Models," SAE Paper No. 820688, Society for Automotive Engineers, Warrendale, PA, 1982, pp. 119-132.



- (56). ASTM E112-85, "Standard Methods for Determining the Average Grain Size," Annual Book of ASTM Standards, Vol. 03.03, 1985.
- (57). ASM, Metals Handbook Ninth Edition, American Society for Metals, 9th ed., Vol. 9, 1985.
- (58). ASTM E8-87a, Annual Book of ASTM Standards, 1987.
- (59). ASTM E399-83, Annual Book of ASTM Standards, 1983.
- (60). A. Saxena, and S.J., Hudak, and W. K. Wilson, "Engineering Methods for the Design and Selection of Materials Against Fracture," DDC Report AD-801001, Defence Documentation Center, 1966.
- (61). US Dept. of Defense, Military Standardization Handbook, "Metallic Materials and Elements for Aerospace Vehicle Structures," Vol. 1, 1983.
- (62). P. C. Paris, Fatigue— An interdisciplinary Approach, Proceedings, 10th Sagamore Conference, Syracuse Univ. Press, Syracuse, NY, 1964, p.107.
- (63). R. W. Hertzberg, Deformation and Fracture Mechanics of Engineering Materials, Wiley & Sons, 3rd ed., 1989, p. 528.
- (64). L. E. Murr, Interfacial Phenomena in Metals and Alloys, Techbooks, 1975.
- (65). P. C. J. Gallagher, "The Influence of Alloying, Temperature, and Related Effects on the Stacking Fault Energy," Metallurgical Transactions, Vol. 1, Sep. 1970, pp. 2429-2461.
- (66). S. S. Manson: Int. J. of Frac. Mech. Vol.2, 1966, pp. 327-363.
- (67). S. S. Manson, and M. H. Hirschberg: NASA TN D-3146, Washington, 1967.
- (68). S. S. Manson, and M. H. Hirschberg: 1st. Int. Conf. On Fract., Vol. I, 1966, pp. 479-498.

(69). K. Yamaguchi, K. Kanazawa: Metallurgical Transaction, Vol. 10A, 1979, pp. 1445-1451; 11A, 1980, 2019-2027.

(70). C. Levillant: " Approche me'tallographique," These d' etat, UTC, 1984.

(71). A. Pineau, " Fatigue at High Temperature," R. P. Skelton, Ed., Appl. Sci. Publ., London, 1983, pp. 305-364.

(72). K. J. Miller, K. P. Zachariah, J. Strain Anal., Vol. 12, 1977, p. 262.

(73). K. J. Miller, M. F. E. Ibrahim, Fatigue Engng. Mater. Struct., Vol. 4, 1981, pp.263-277.

## APPENDIX

### •Strain Measurements

In order to evaluate the quantity  $\frac{K_{td} \cdot S}{2E}$  as a measure of strain at distance "d" ahead the notch, the Moire-fringe technique was utilized\* to measure the distribution of the principal strain( the strain in the loading direction) in the vicinity of the notch. These measurements were performed on two copper and two brass specimens with both blunt and sharp notches. The specimen grating for strain measurement had a frequency of 1200 lines/mm and was produced from a photographic mold by replication. The specimen was then placed in a portable loading frame at zero load. A spectra physics model 127-25 mW was used as a source of Helium-neon laser light. The interference pattern emerging from the specimen was accumulated by a CCD video camera that was connected to a PC-based digital image processor. The apparatus and specimen were adjusted for proper optical alignment and orientation. Several optical parameters were checked to ensure that laser beams were projected along correct angles. Actually, some deviations from ideal setting existed in practice. This resulted in an initial pattern of relatively few fringes(at null or zero load). Also, in this case, residual stresses left from machining the notch influenced the initial pattern. Moreover, there are always a few fringes at the edge of adhesive due to surface tension effects. In the present study, this influenced the initial pattern since we had to deal with the edge of adhesive placed at the notch root. However, the initial pattern did not affect the final displacement results because it was subtracted from the next pattern, obtained at load, to determine the load induced displacements.

After the zero-load pattern(null field) had been recorded, the specimen was loaded to desired load and the pattern was recorded. In order to measure the applied load, the notch opening displacement was recorded using a digital voltmeter and a 0.4 inch clip gage being attached to knife edges machined in the mouth of the notch.

---

\* Moire fringe measurements were made with the assistance of Professor A. S. Voloshin and Mr. P. H. Tsao.

The readings then were compared with Crack Opening Displacement COD measurements previously performed on similar specimens. After different patterns related to five different loads(including zero load) were obtained, an image processing software was used to analyze the patterns and to evaluate displacements at selected areas around the notch root. However, since the displacements dealt with in this study were rather large and were beyond the software sensitivity limit, displacements were simply measured over a given number of fringes and at several distances ahead of the notch. Then, strains were determined from the strain-displacement relations as follows:

$$\epsilon_y = \frac{\partial V}{\partial y} \quad (I)$$

The results for copper with blunt and sharp notches and for brass with sharp notch are shown in Figure 1 through Figure 3. In the case of brass with a blunt notch, the grating was far from the notch root and therefore, no data was obtained. As would be expected, in sharply notched specimens, the strain decreases sharply as the distance from notch root increases, and the slope is lower for the blunt keyhole notch. As mentioned, at a given load and at a given distance from the notch, strain was measured over a distance of about 100  $\mu\text{m}$  above and below X-axis and in Y-direction. Then the value was regarded as strain at the given distance. This assumption may introduce a large error, particularly for sharp notches where strain gradient is large. However, this assumption introduces less error for blunt notched specimens. Figure 4 shows measured strain versus calculated strain for copper with blunt notch at three nominal stress levels  $S=140, 200, \text{ and } 350 \text{ MPa}$ , and at a distance  $d=160 \mu\text{m}$  ahead the notch root. As can be seen, as load increases, calculated strain increases more than the measured strain. The first reason is that as local plasticity occurs, the stress gradient sharply decreases whereas, in contrast, strain gradient increases sharply. Therefore, if part of the distance over which strain is measured has already plastically deformed while the other part is still elastic, the average strain over the distance will be less than the absolute value of the strain. Second reason lies in the fact that as load increases, number of fringes increases and thus, the accuracy of measurements drops. Figure 5 through Figure 7 show the Moire pattern for copper V-notched specimen at three different loads.

In summary, when the Moire fringe technique is used, the absolute values of strain must be measured rather than the average values, particularly for sharp notches. A grating frequency of 1200 lines/mm appears to be unsuitable where the strain magnitude is large. In fact, it is too sensitive. In cases such as this study where strain is to be measured at the notch root, the effect of residual stresses and the effect of the adhesive edge must be accounted for.

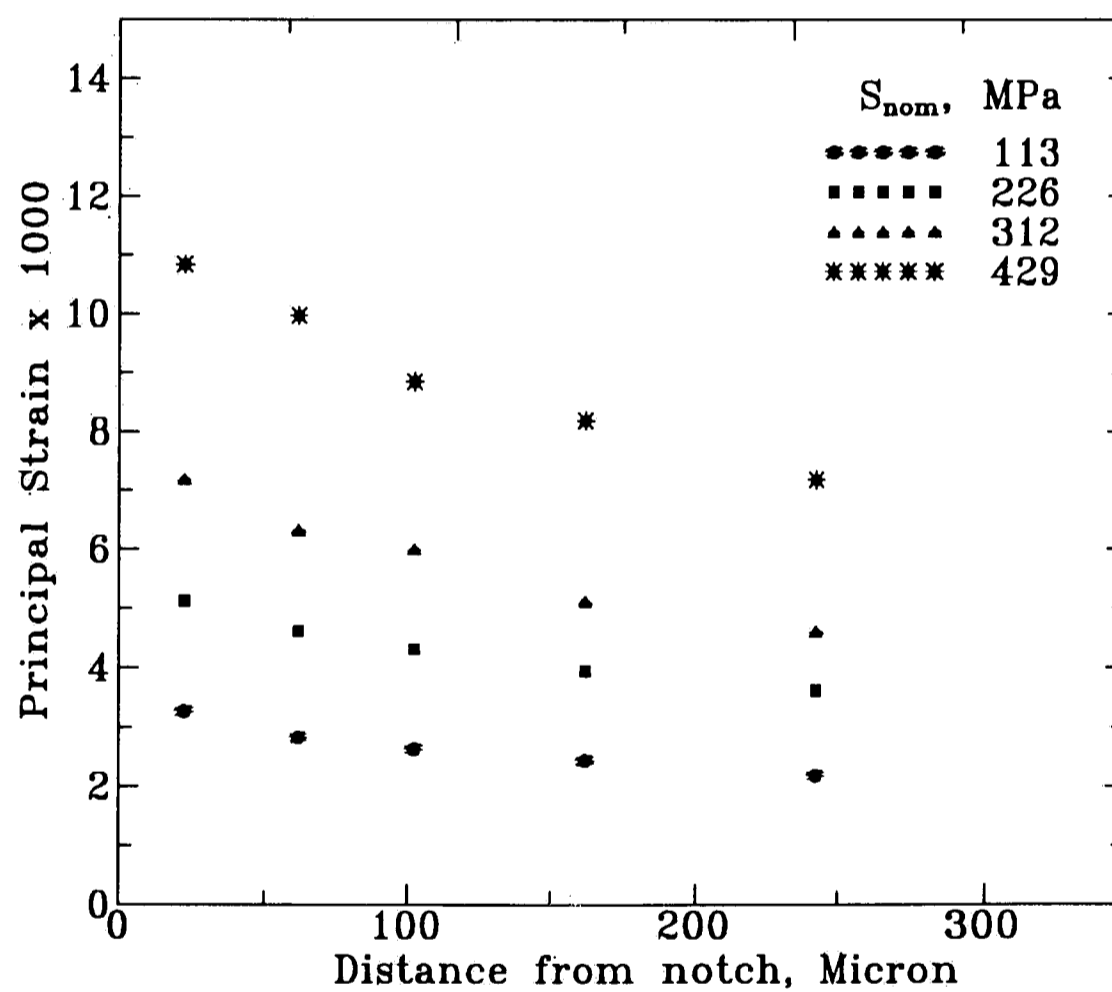


Figure 1. Distribution of the strain in the loading direction and at the vicinity of the notch for copper with blunt-keyhole notch.

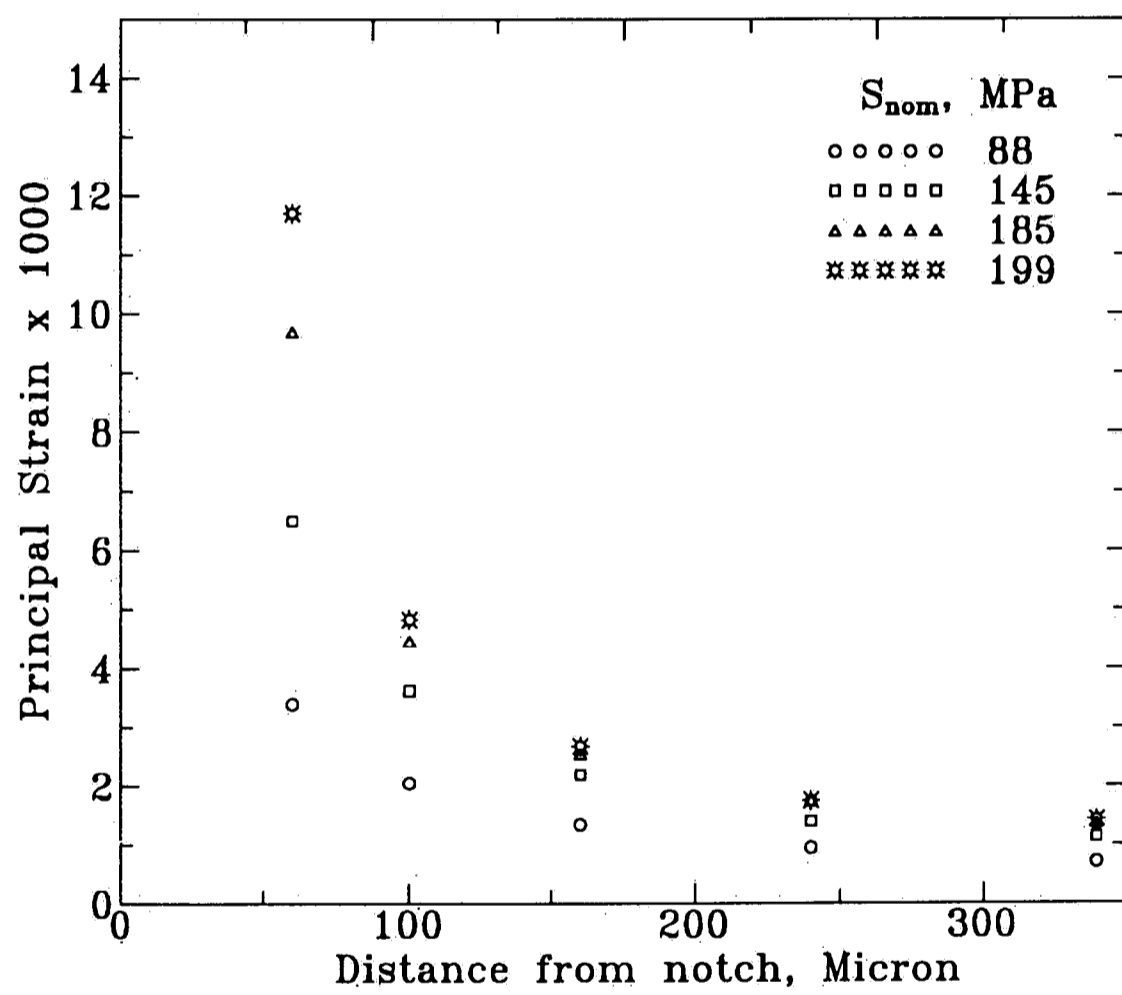


Figure 2. Distribution of the strain in the loading direction and at the vicinity of the notch for copper with sharp-v notch.

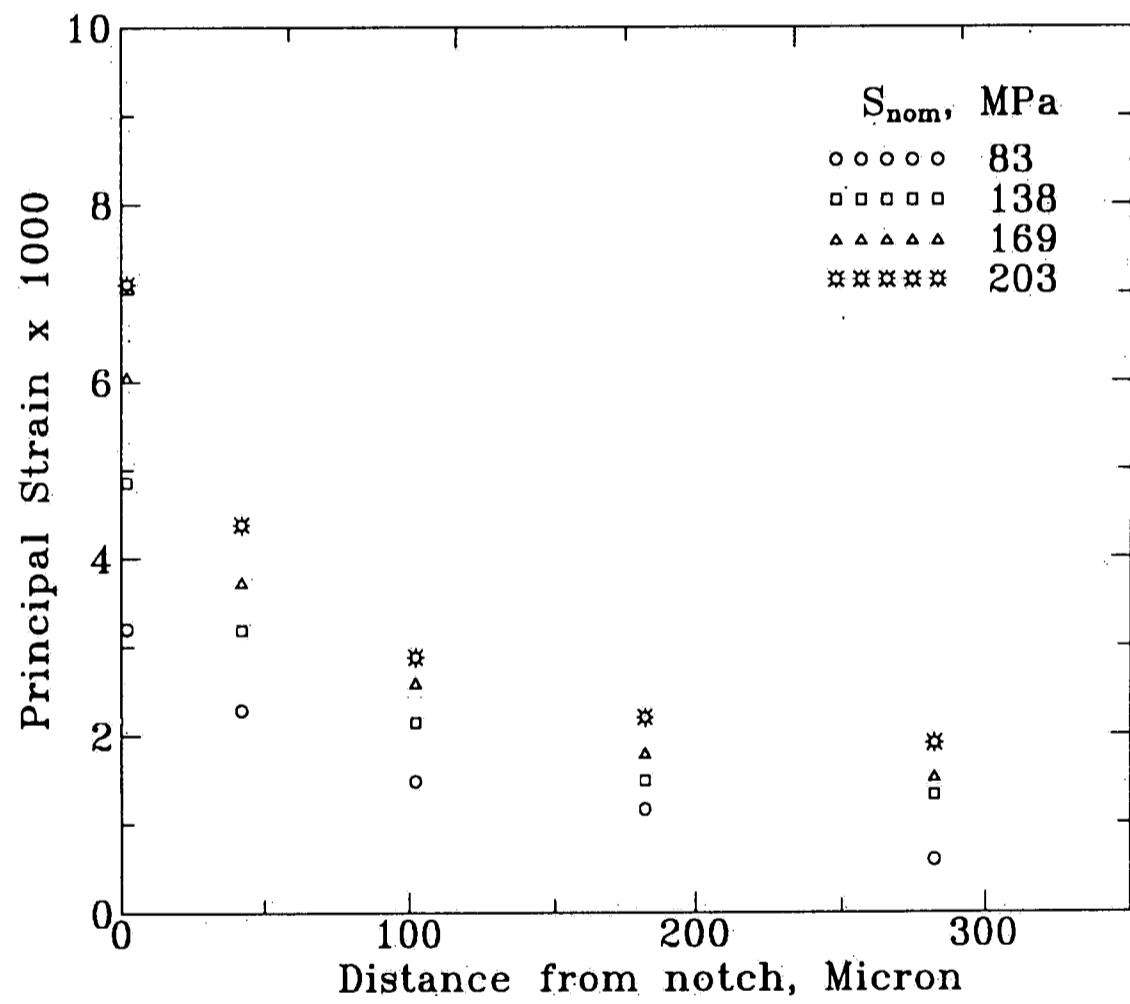


Figure 3. Distribution of the strain in the loading direction and at the vicinity of the notch for brass with sharp-v notch.

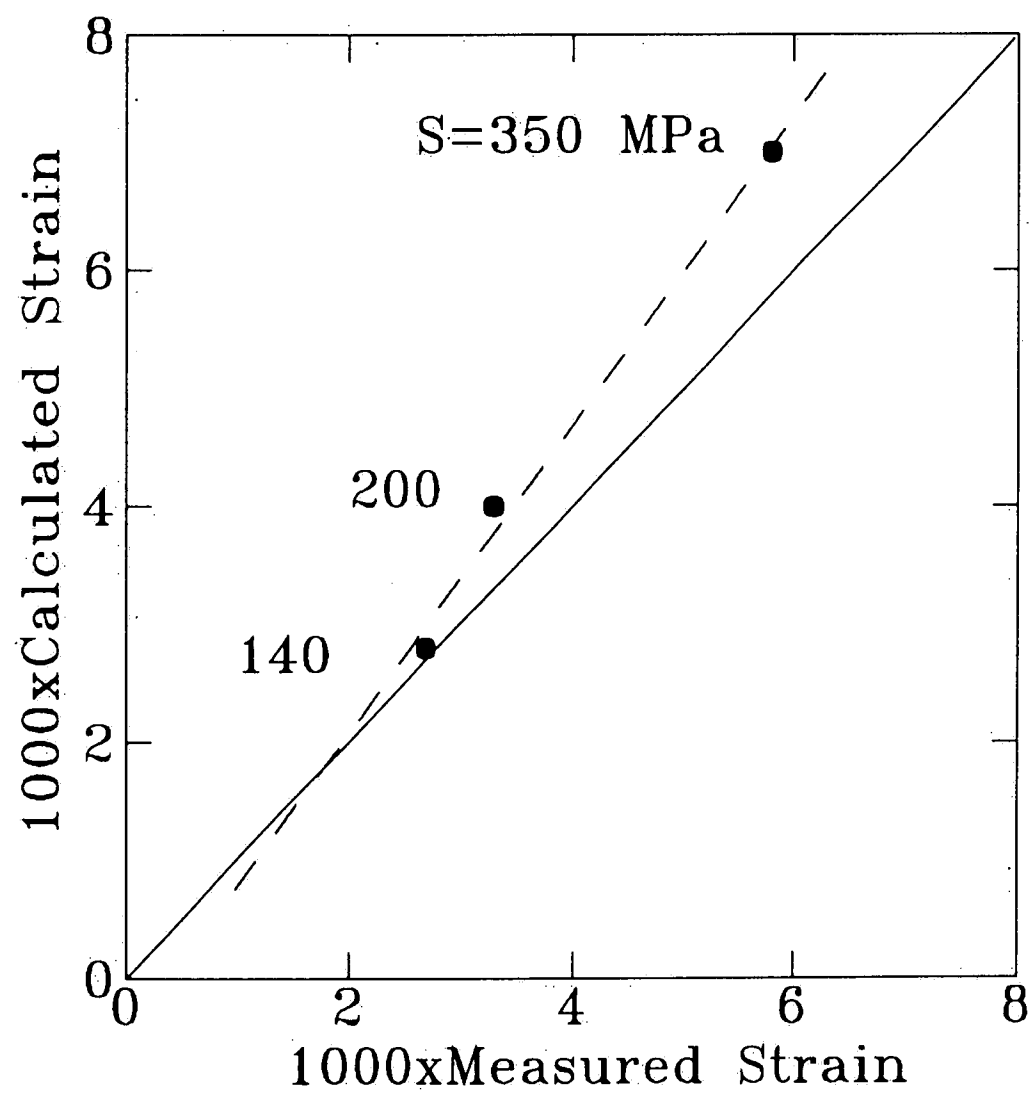


Figure 4.- Estimated strain using the parameter  $K_{td}S/2E$  versus measured strain from Moire fringe technique for copper with blunt keyhole-notch at distance  $160 \mu\text{m}$  far from the notch root.



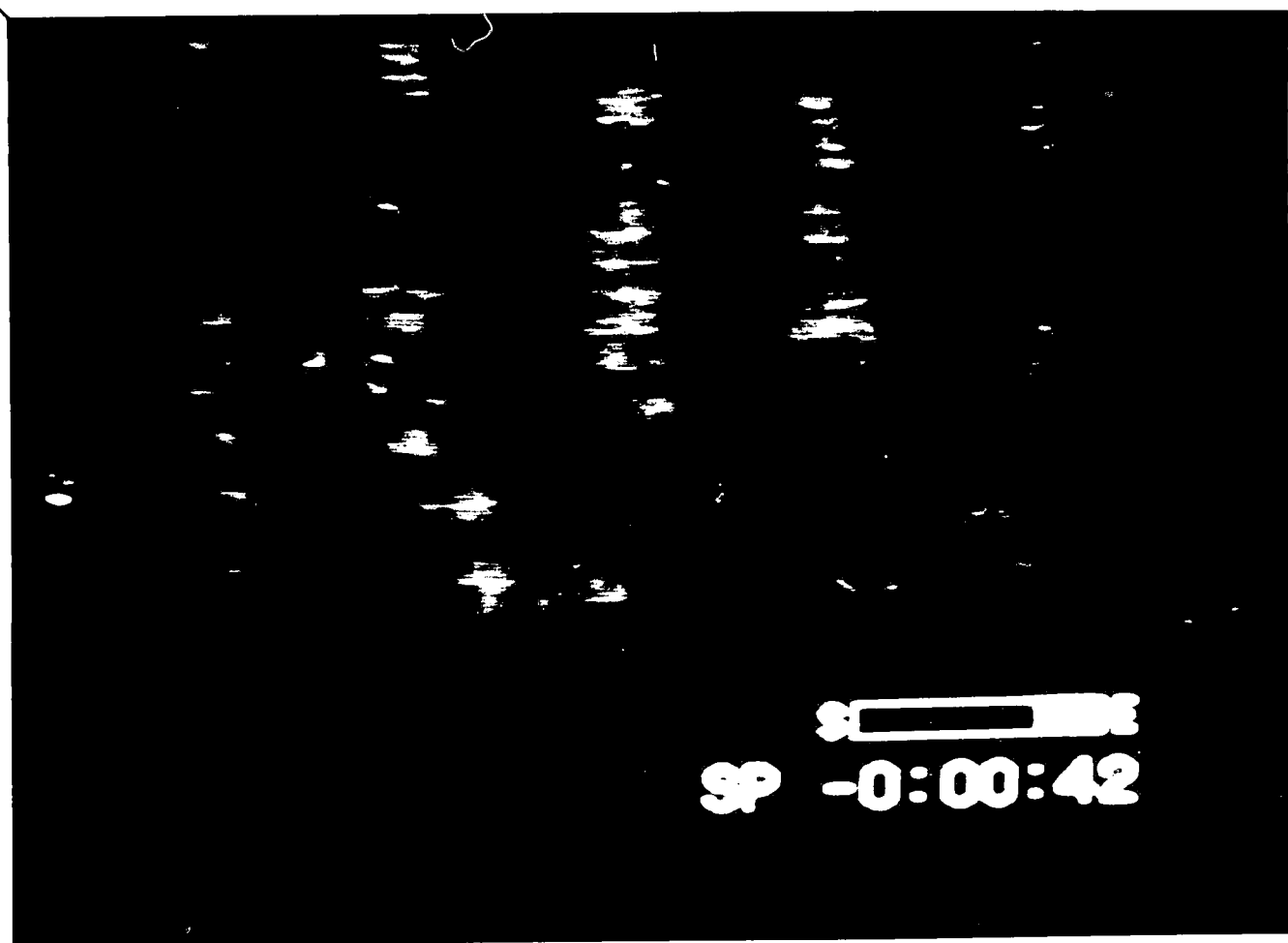


Figure 5. Moire pattern for copper specimen with sharp-v notch and at zero load.

INTENTIONAL SECOND EXPOSURE

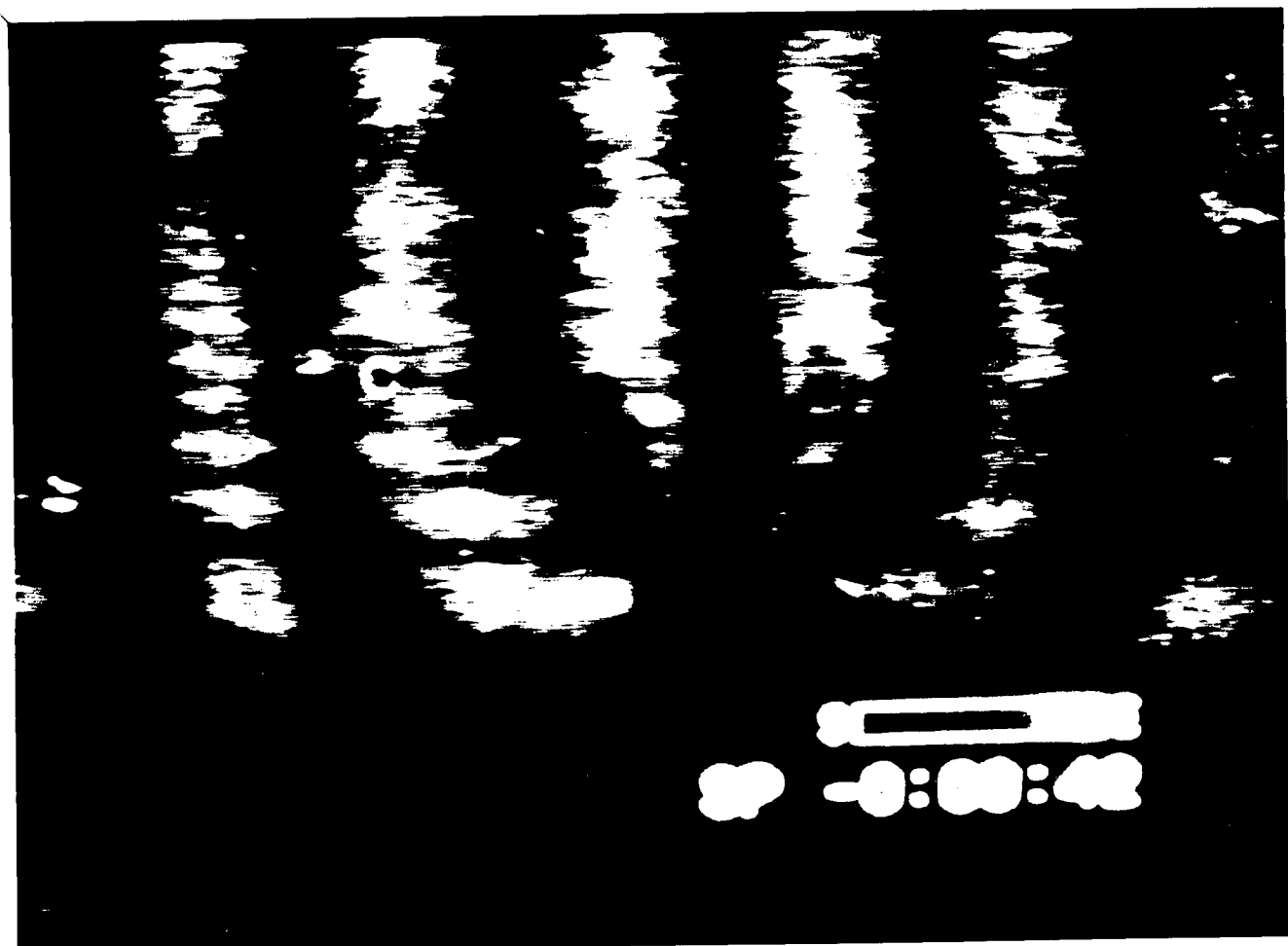


Figure 5. Moiré pattern for copper specimen with sharp notch and at zero load



Figure 6. Moiré pattern for copper specimen with sharp-v notch and at nominal stress  $S = 138$  MPa.

INTENTIONAL SECOND EXPOSURE



Figure 6. Mode pattern for copper specimen with sharp V notch and at nominal stress  $S = 138$  MPa.

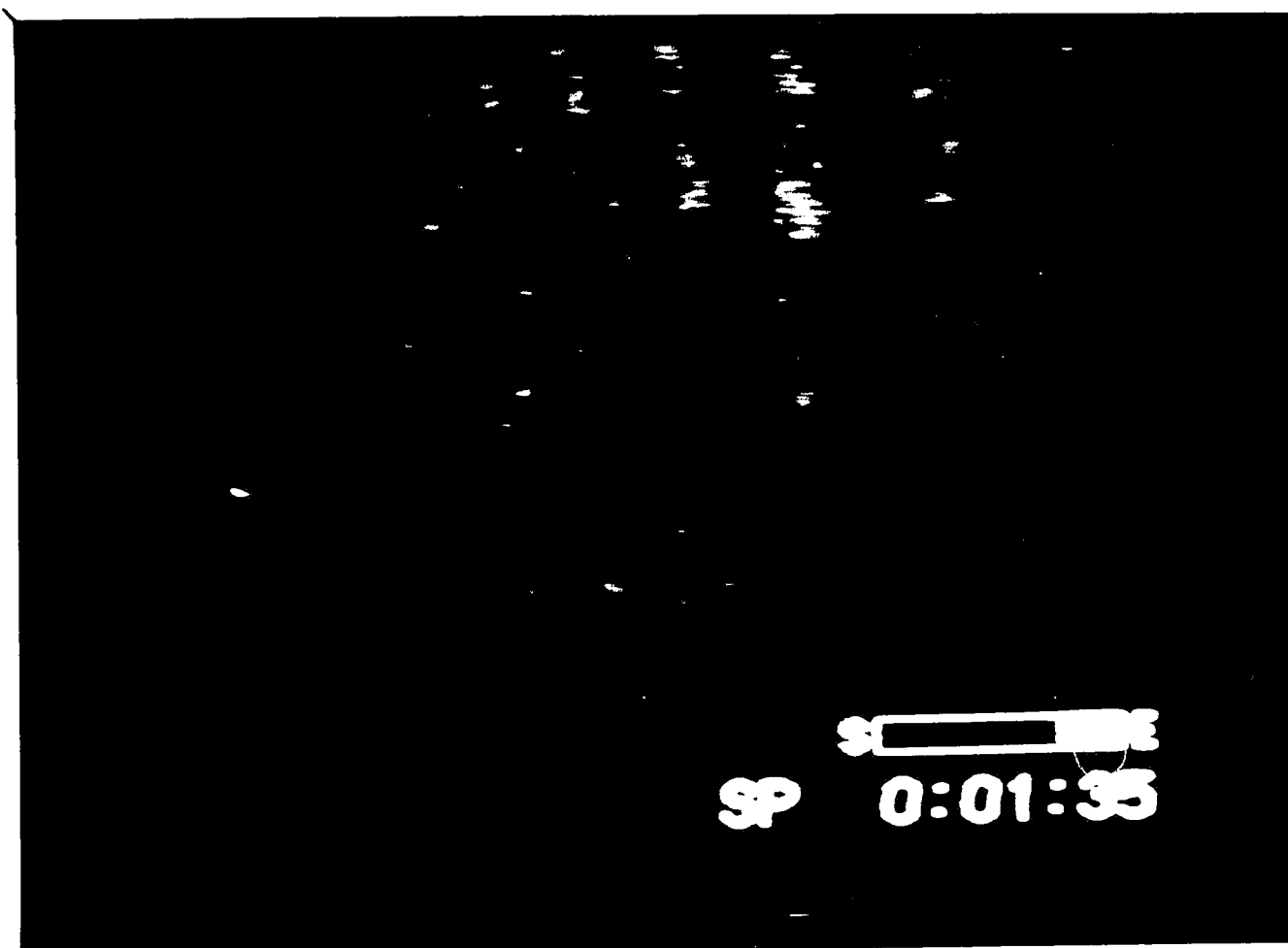


Figure 7. Moiré pattern for copper specimen with sharp-v notch and at nominal stress  $S = 209$  MPa.

INTENTIONAL SECOND EXPOSURE

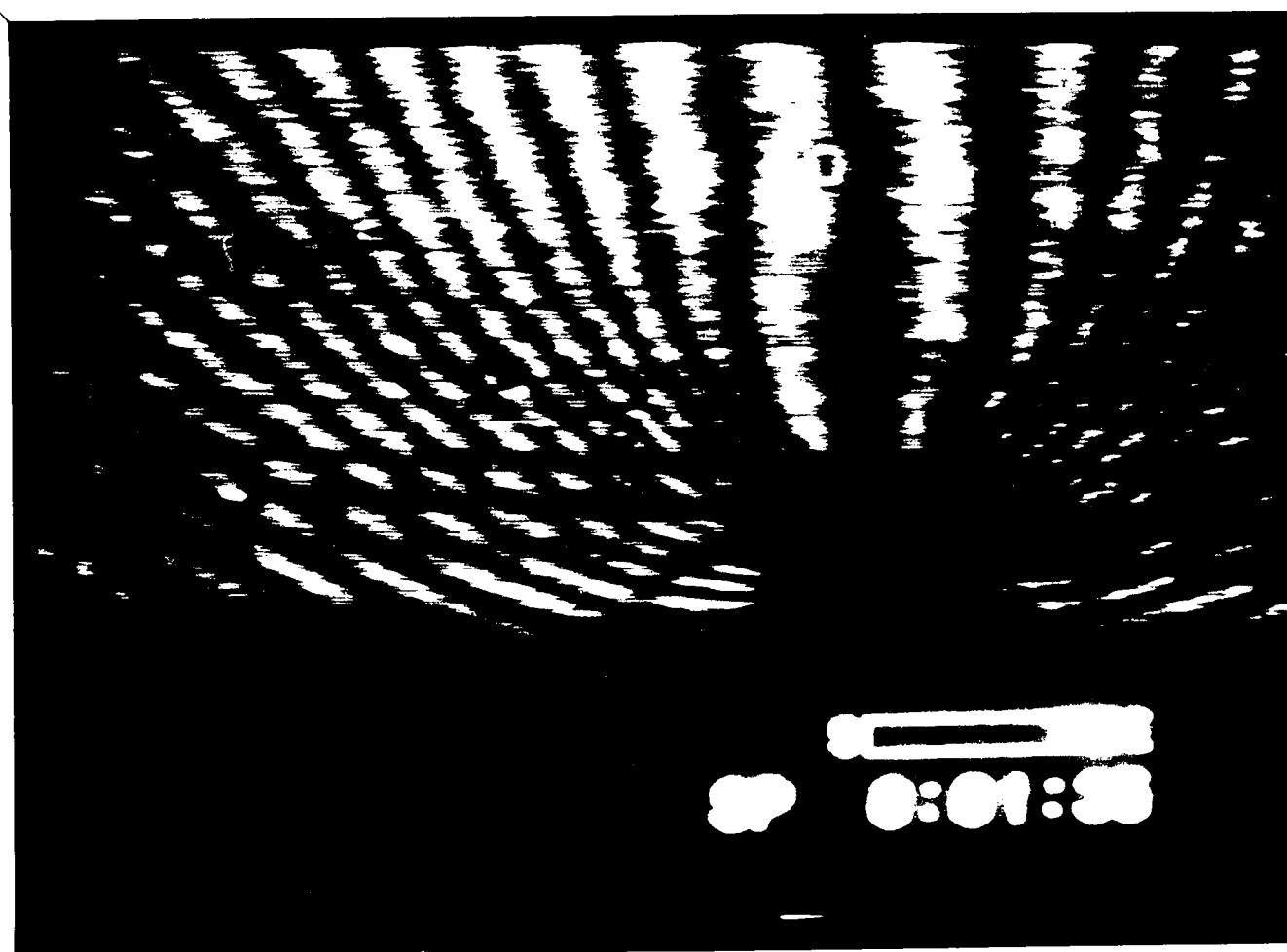


Figure 7. Moiré pattern for copper specimen with sharp notch and at nominal stress  $S = 209$  MPa.

## VITA

Hamid R. Azimi was born to Fatemeh and Hosseingholi Azimi on September 23, 1960 in the village of Taherabad, Kashan, Iran. He graduated from Kharazmi-2 High School in June of 1979 and entered Sharief University of Technology in Tehran.

After receiving his B. S. degree in Metallurgical Engineering in January of 1987, he was employed by the Department of Metallurgical Engineering of Sharif University as a research engineer for more than two years. In January of 1990, he began his graduate studies in the Materials Science and Engineering Department at Lehigh University and under the guidance of Dr. Gary A. Miller.